Targeting aspartyl–tRNA synthetase as novel mode of action to fight *Mycobacterium tuberculosis*

By

BOGDAN M. DUMA

A thesis submitted to the University of Birmingham

for the degree of

DOCTOR OF PHILOSOPHY

School of Chemistry
College of Engineering and Physical Sciences
University of Birmingham

August 3, 2018

Declaration

The work presented in this thesis has been carried out under the supervision of Dr L. R. Cox and Prof. G. S Besra from The University at Birmingham. Work was carried out in the School of Biosciences at the University of Birmingham, UK, B15 2TT during the period August 2014 and December 2015, and then at GSK Tres Cantos, PTM C/Severo Ochoa, 2, 28760, Spain during the period December 2015 and July 2017. The work in this thesis is original except where acknowledged by reference. No part of the work is being, or has been submitted for a degree, diploma or any other qualification at any other University.

Bogdan M. Duma

August 3rd, 2018

Abstract

Tuberculosis is an infectious bacterial disease caused by *Mycobacterium tuberculosis*. Commonly affecting the lungs, tuberculosis has been ranked by the World Health Organization as a leading cause of death worldwide, causing 1.7 million fatalities in 2016 alone. Moreover, a daunting 10.4 million people are estimated to have been infected with tuberculosis in the same year.

To overcome this issue we have explored targeting aspartyl–tRNA synthetase an enzyme that to the best of our knowledge has not been researched so far against *M. tuberculosis*, as a possible target. Using an enzymatic assay developed in our research group combined with the results of a screening campaign performed using known tuberculosis inhibitors released by GSK as part of the GSK TB set, we have identified a novel class of compounds that target *M. tuberculosis* AspRS. This work contains the results of a structure–activity relationship study performed on this family of compounds as well as additional studies exploring the biological hit–enzyme interaction. These latter studies were performed attaching biotin and diazirine probes at specific positions of the initial hit. In addition, in the last chapter this work additional molecular structures able to interact with and inhibit aspartyl–tRNA synthetase are evaluated.

Overall, although the structure–activity relationship study was inconclusive, the biotin probe employed in this work indicates that this was not because of the possible promiscuity of this family of compounds. Meanwhile, the ongoing analysis employing the diazirine probe is expected to help determine the binding mode of these compounds and the enzyme. This sets a path for the future exploration of this enzyme in targeting *M. tuberculosis* by either further exploring our initial family of compounds or through compounds coming out of new screening campaigns.

This thesis is dedicated to my parents.

Acknowledgments

Firstly, I would like to thank my academic supervisors, Dr. L. R. Cox and Prof. G. S. Besra for their support and continued guidance throughout the duration of my PhD. I am also greatly indebted to my industry supervisors, Dr. Mónica Cacho–Izquierdo and Dr. Joel Lelièvre for always offering their expertise, advice and continued support during my stay at GSK Tres Cantos.

Secondly, I would like to extend my gratitude to Dr. Natacha Veerapen for her advice, continued support and friendship. I am also very grateful to everyone in Prof. Besra's Research Group for a great work atmosphere, continuous support and helpful discussions. So thank you Padraic, Monika, Szilvia, Panchali, Asma, Cristian, Perla, Patrick and Katherine. I want to specially thank Giacomo for his friendship and support during these years.

I would also like to thank to everyone at GSK Tres Cantos, chemists and biologists alike. Very special thanks to Dr. Beatriz Rodríguez and Dr. Esther Pérez for their teachings and assistance performing the biology experiments. I am fortunate to have worked with so many great people and be able to consider them my friends.

I am grateful to the Marie Curie Programme for funding and all my colleagues in the Marie Curie Network CooperaTB for valuable science discussions and other enjoyable times.

Last but not least, I would to like to thank my family and friends, especially my parents for the continuing love and support that I can always rely on.

Contents

Abbreviations

Abbreviation	Name
A	Adenine
aaRS	Aminoacyl–tRNA Synthetase
Ac	Acetyl/Acyl
Ala	Alanine
AMP	Adenosine Monophosphate
Arg	Arginine
Asn	Asparagine
Asp	Aspartic Acid (Aspartate)
ATP	Adenosine Triphosphate
BCG	Bacillus Calmette–Guérin
C	Cytosine
CLND	Chemi–Luminescent Nitrogen Detection
Cys	Cysteine
DIBAL–H	Diisobutylaluminium Hydride
DNA	2–Deoxyribonucleic Acid
DMF	*N,N*–Dimethylformamide
DMSO	Dimethyl Sulfoxide
EF	Elongation Factor
EMA	European Medicines Agency
Et	Ethyl
FDA	U.S. Food and Drug Administration
G	Guanine
GDP	Guanosine Diphosphate
Gln	Glutamine
Glu	Glutamic Acid (Glutamate)
Gly	Glycine
GTP	Guanosine Triphosphate
GSH	Glutathione
His	Histidine
HIV	Human Immunodeficiency Virus
HTS	High–Throughput Screening
IF	Initiation Factor
Ile	Isoleucine
Leu	Leucine
LG	Leaving Group
Lys	Lysine
Me	Methyl
Met	Methionine

Abbreviation	Name
MIC	Minimum Inhibitory Concentration
MIDA	*N*–methyliminodiacetic acid
mRNA	Messenger RNA
MRSA	Methicillin–resistant *Staphylococcus aureus*
Ms	Methanesulfonyl
NMR	Nuclear Magnetic Resonance
OE	Over–expressor
PAGE	Polyacrilamide Gel Electrophoresis
PCC	Pyridinium Chlorochromate
Phe	Phenylalanine
P_i	Inorganic Phosphate
PMB	*p*–methoxybenzene
Pro	Proline
RF	Release Factor
RNA	Ribonucleic Acid
SAR	Structure–Activity Relationship
SDS	Sodium Dodecyl Sulfate
Ser	Serine
T3P	Propylphosphonic Anhydride
TB	Tuberculosis
TETD	Tetraethylthiuram Disulfide
TFA	Trifluoroacetic Acid
TLC	Thin Layer Chromatography
Thr	Threonine
tRNA	Transport RNA
Trp	Tryptophan
Tyr	Tyrosine
U	Uracil
Val	Valine
WGS	Whole–Genome Sequencing
WHO	World Health Organisation
XRD	X–Ray Diffraction

Chapter 1

Introduction

1.1 Protein Biosynthesis

Proteins are high molecular weight organic polymers that play most of the functional roles in cells.[1,2] They are made up of α–amino acids linked together by peptide bonds, and are biosynthesised following a similar series of processes to those involved in the biosynthesis of other biopolymers such as DNA and RNA. The process through which proteins are biosynthesised is known as translation.

Translation is the process through which the sequence of nucleic acids in DNA, coded in the four–letter alphabet corresponding to the four DNA bases, is translated into the alphabet of proteins, formed from the twenty letters corresponding to each amino acid. Translation takes places inside ribosomes, where tRNA, mRNA, the ribosome itself and many other proteins are involved in a number of complex processes, the outcome of which is the synthesis of polypeptidic chains.

The three main stages of the translation process are initiation, elongation and termination. Additionally, in a pre–initiation stage, the precursors are activated, whilst after termination, *i.e.* when the full protein sequence has been assembled, the nascent structure undergoes a post–synthetic processing stage. Both pre– and post–synthetic stages play a paramount role in guaranteeing the fidelity of the biosynthesis and the correct role of the new protein.[2,3]

At its core, the translation process is fundamentally the same in prokaryotic and eukaryotic cells, the only significant difference being that in eukaryotes the number and type of proteins involved is larger, which adds complexity to the system at each stage.

Activation

Incorporating new amino acids into a polypeptidic chain requires the carboxylic acid group of each amino acid to be first activated in order to promote the formation of the new peptide bonds. This activation stage occurs in the cytosol, where a class of enzymes known as aminoacyl–tRNA synthetases (aaRSs) first activate each specific amino acid and subsequently catalyse the formation of an aminoacyl–tRNA conjugate. The formation of this aminoacyl–tRNA conjugate is essential, since a connection has to be established between each amino acid and the mRNA encoding the corresponding nucleotide sequence in order that the amino acids can be incorporated into the growing polypeptide according to this sequence. The link between amino acids and mRNA is the tRNA.[3]

Initiation

The following stage in protein biosynthesis is known as initiation. This stage is rate–limiting in protein biosynthesis and also the most regulated. The bacterial 70S ribosome, which is composed of two subunits, the larger 50S and the smaller 30S, dissociates into its two components upon binding of initiation factors 1 (IF–1) and 3 (IF–3) (Figure 1.1). After this dissociation step, initiation factor 2 (IF–2), mRNA and fMet–$tRNA_f^{Met}$, the aminoacylated and formylated initiator tRNA, bind to the 30S subunit of the ribosome in a currently unknown order.[4] This process leads to the formation of the 30S preinitiation complex (Figure 1.2), which is composed of the 30S ribosomal subunit, mRNA, the three initiation factors and fMet–$tRNA_f^{Met}$ bound in a codon–independent fashion. This unstable preinitiation complex then undergoes a rate–limiting change in its conformation to form the 30S initiation complex, which now includes a codon–anticodon interaction with fMet–$tRNA_f^{Met}$ (Figure 1.3).

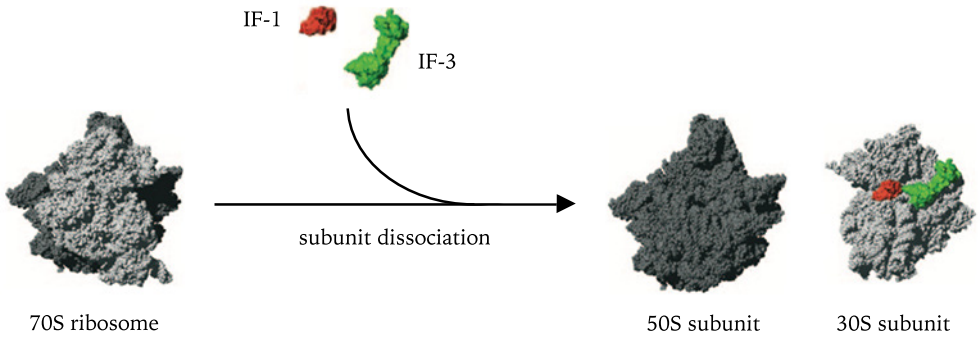

Figure 1.1: **Dissociation of the 70S bacterial ribosome.**[4]

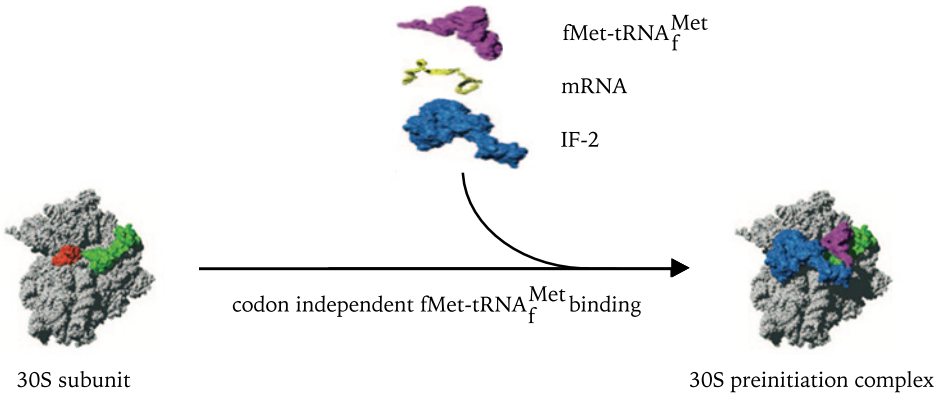

Figure 1.2: **Formation of the 30S preinitiation complex.** [4]

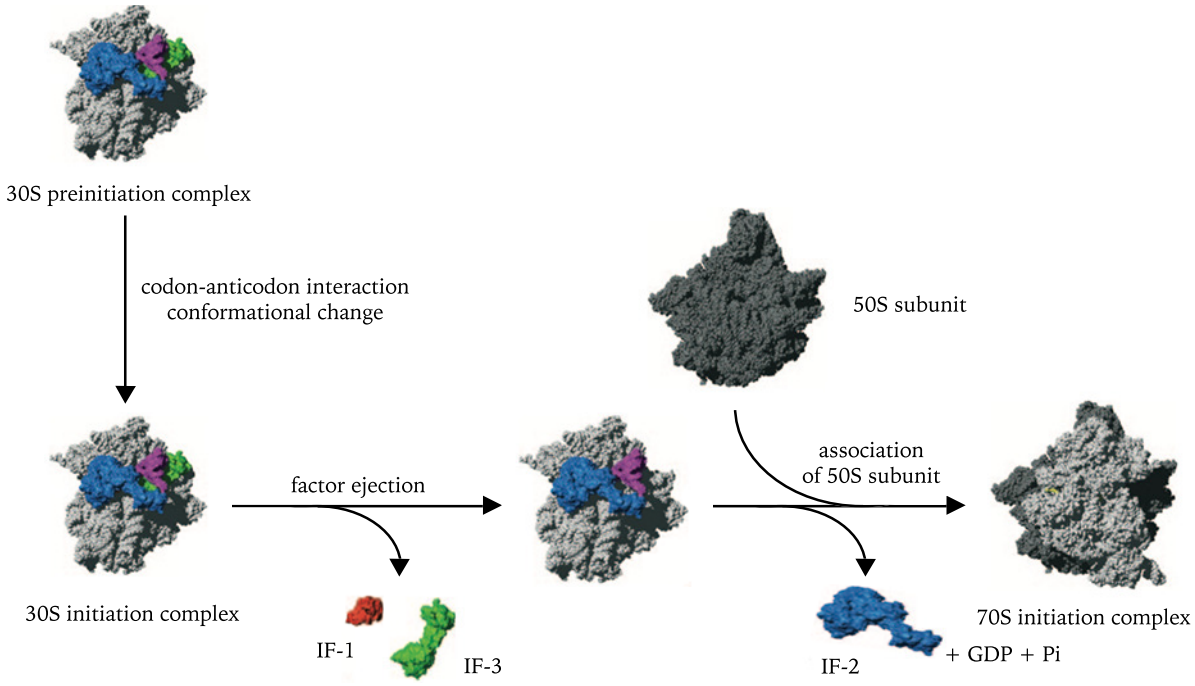

Figure 1.3: **Formation of the initiation complex.** [4]

After this step, initiation factors IF–1 and IF–3 are expelled, leaving IF–2, which promotes association with the 50S ribosomal subunit. IF–2 is released in a subsequent step during which GTP bound to IF–2 is hydrolysed to GDP and P_i giving way to the 70S initiation complex.

Elongation

The newly formed 70S initiation complex proceeds to the third stage of protein synthesis, namely elongation. During this stage (Figure 1.4) the nascent polypeptidic chain is extended through the formation of new peptide bonds between the amino acids conveyed to the ribosome by their tRNA in the form of aminoacyl–tRNA conjugates. Each aminoacyl–tRNA conjugate accurately positions the amino acids in the ribosome through anti–codon/codon pairing with the mRNA. This process is assisted by a class of proteins known as elongation factors (Tu and Ts), which similarly to the aforementioned initiation factors, provide energy through a series of GTP–GDP hydrolysis reactions.

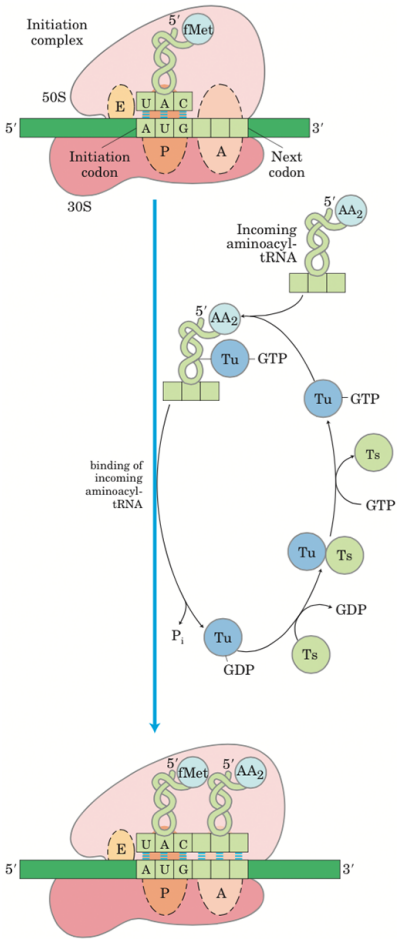

Figure 1.4: **Elongation stage of protein synthesis.**[3]

Termination

During the fourth stage of protein biosynthesis, termination, the newly assembled polymer is released from the ribosome with the cooperation of proteins known as release factors (RF) (Figure 1.5). Termination of the polypeptidic chain is triggered by the presence of a termination codon in the mRNA. Upon detection of this termination sequence, binding of a release factor induces the hydrolysis of the amino acid–tRNA bond. Finally, the components (release factors, mRNA and tRNA) leave and the 70S ribosome disassembles into its 30S and 50S subunits.

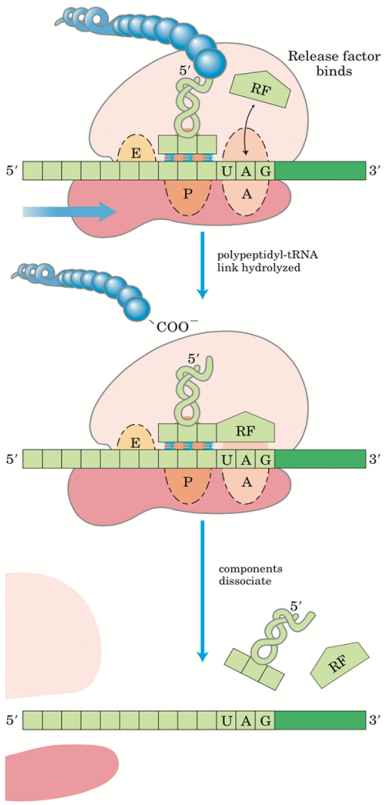

Figure 1.5: **Termination stage of protein synthesis.** [3]

Post–translational modifications

The fifth and final stage of protein biosynthesis involves folding and post–translational processing. The biologically active form of the new protein is attained through folding into its correct three–dimensional conformation. The new polypeptide can also be subjected to enzymatic processing at this stage, which may involve the removal of amino acids, addition of functional groups to an individual amino acid, and the addition or proteolytic cleavage of prosthetic groups or oligosaccharides.

1.2 Transfer RNA

Transfer RNAs are molecules acting as adaptors in the translation of the alphabet of nucleic acids into the alphabet of proteins. They bind to a specific codon contained in the mRNA and bring with them an amino acid which is incorporated into the polypeptidic chain. tRNAs are relatively small in molecular mass[a], and consist of a single strand of RNA that when drawn in two dimensions forms a four–armed structure resembling a cloverleaf. Longer tRNAs have a short, fifth arm or extra arm (Figure 1.6A). In three dimensions, tRNAs resemble a twisted L (Figure 1.6B) with the anti–codon loop at one end of the L and the CCA terminus (Figure 1.7), which accommodates the amino–acid attachment site, at the opposite end.[2,3]

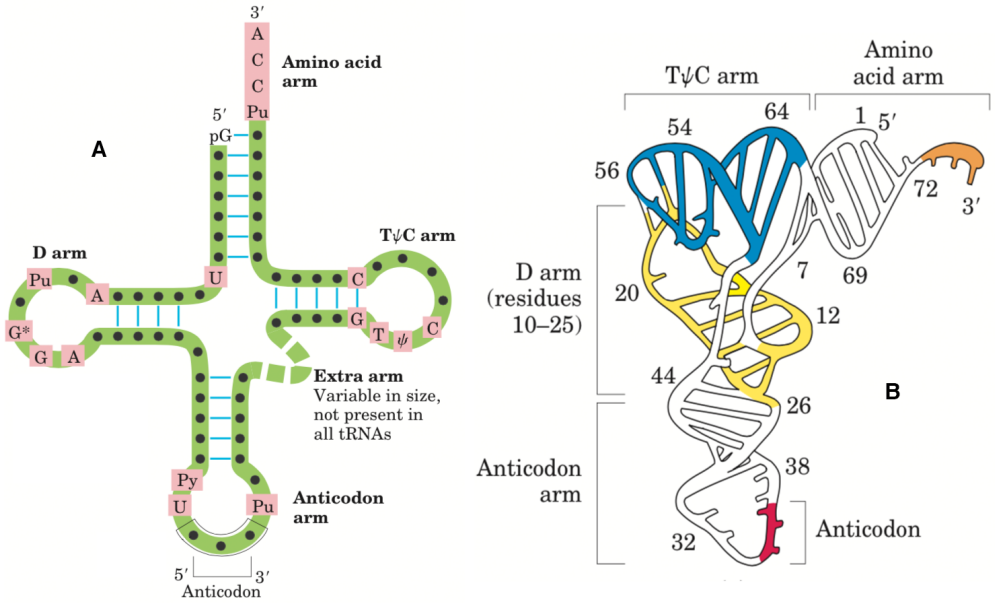

Figure 1.6: **A) Cloverleaf structure of tRNA.** The black dots represent nucleotide residues and the blue bars base pairs. Pink colour denotes characteristic residues common to all tRNAs. Modified nucleotides are represented as follows: pseudouridine (ψ), ribothymidine (T), purine (Pu), pyrimidine (Py), guanylate (G*). **B) Yeast tRNA$^{\mathbf{Phe}}$ three–dimensional representation.** The different arms depicted in panel A are highlighted in different colours.[3]

[a]Bacterial tRNAs and the tRNAs in the cytosol of eukaryotes usually consist of 73 to 93 nucleotides.

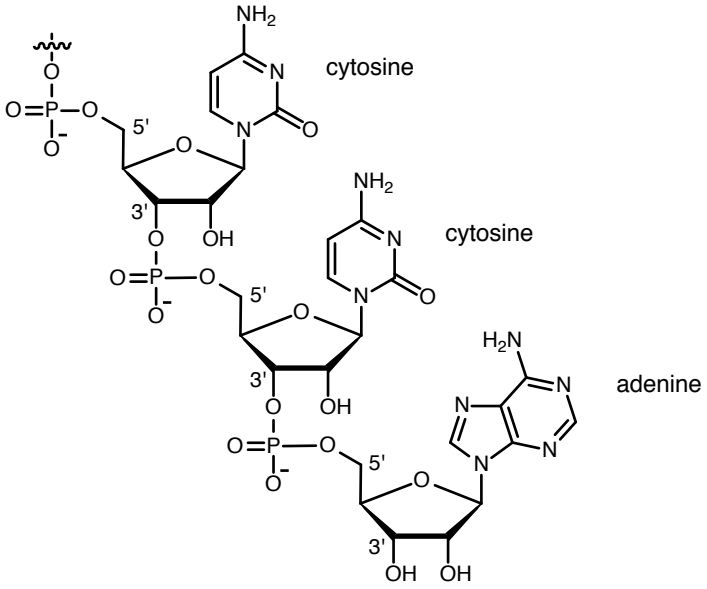

Figure 1.7: **Chemical structure of the CCA sequence at the 3'– end of tRNA.**

Two of the four arms present in a tRNA molecule play key roles in its function as an adaptor. The anticodon arm of the tRNA molecule incorporates the anticodon, which recognises the codon encoded in the mRNA, whilst the amino–acid arm acts as a transporter of amino acids. To achieve this function, the carboxylic acid residue of the amino acid is first attached through an ester bond to the 2'– or 3'–hydroxyl group of the A residue, which is located at the 3' end of the tRNA molecule (Figure 1.7).

The other two arms of the tRNA molecule are the D and the TψC arms. The D arm contains the atypical nucleoside dihydrouridine **1** (D) (Figure 1.8) and together with the TψC arm has a significant role in interactions that produce the observed folding of the tRNA molecule. The TψC arm contains the uncommon ribothymidine **2** (T) and pseudouridine **3** (ψ) nucleosides. This arm is also involved in the translation process through its interaction with the large 50S subunit of the ribosome.[3]

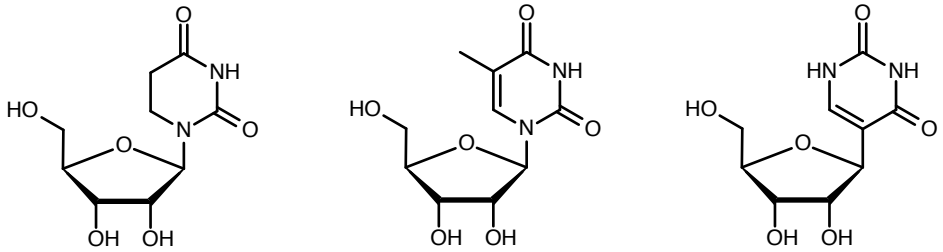

Figure 1.8: **Chemical structure of ribonucleosides dihydrouridine 1 (D), ribothymidine 2 (T) and pseudouridine 3 (ψ).**

1.3 Aminoacyl–tRNA Synthetases

1.3.1 Introduction

Aminoacyl–tRNA synthetases (aaRSs) (EC 6.1.1) play a fundamental role in the translation mechanism. They catalyse two back–to–back reactions: activation (through esterification) of the carboxylic acid moiety in the 20 natural amino acids and subsequently, the transfer of the resulting activated amino–acid residue to the cognate tRNA molecule. This second step results in the formation of specific aminoacyl–tRNA conjugates for each amino acid.[5] The majority of organisms have one aaRS for each amino acid. In the case of those amino acids that have two or more corresponding tRNAs, it is generally the selfsame enzyme which aminoacylates all of them.[3]

1.3.2 Classes of *aaRSs*

Aminoacyl–tRNA synthetases are found across the whole phylogenetic tree (eukarya, bacteria and archaea), which suggests they are among the oldest polypeptide families. Whilst they share a common structural scaffold, a diversity in their molecular masses, quaternary structures, mechanisms of reaction and amino–acid sequences has led to the division of these enzymes into two different classes, each comprising ten enzymes (Table 1.1).[6,7,8,9] The two classes of enzymes are the same in all organisms although there is no evidence pointing to a common ancestor for the two classes. Moreover, since the two classes of enzymes perform fundamentally identical processes, the evolutionary reasons for their divergence stand unresolved.[3,8]

Table 1.1: **Classification of aminoacyl–tRNA synthetases by class and subclass and their subunit structure in *E. coli*.[3,8,10]**

Class I		Class II	
1a		2a	
Leu (α)	Ile (α)	Ser (α_2)	Thr (α_2)
Val (α)	Arg (α)	Ala (α, α_4)	Gly (α_2, $\alpha_2\beta_2$)
Cys (α)	Met (α, α_2)	Pro (α_2)	(His α_2)
1b		2b	
Glu (α)	Gln (α)	Asp (α_2)	Asn (α_2)
Lys–I (α)		Lys–II (α_2)	
1c		2c	
Trp (α_2)	Tyr (α_2)	Phe ($\alpha_2\beta_2$)	

Class I enzymes are commonly monomeric (Table 1.1) and present two short distinctive motifs, namely signature peptidic sequences HIGH (His–Ile–Gly–His) and KMSKS (Lys–Met–Ser–Lys–Ser); both are located in the active–site domain together with the also characteristic *Rossmann fold*[b]. In contrast, class II enzymes tend to be dimeric and do not possess either the HIGH or the KMSKS motifs or the *Rossmann fold*. The active–site domain of class II enzymes exhibits a characteristic fold composed of a six–stranded antiparallel β–sheet and three motifs containing somewhat less–conserved sequences, *i.e.* ...P... in the case of motif 1, ...FRXE... in the case of motif 2 and ...GXGXGXER... for motif 3.[12]

Enzymes from the two classes can be further differentiated by their binding to opposite sides of the acceptor stem of the tRNA molecule. In class I enzymes, the *Rossmann fold*, located in the catalytic region, binds the tRNA acceptor stem from the minor groove side, using the two aforementioned highly conserved sequences.[13] For class II enzymes, the antiparallel β–sheet in the active site binds the acceptor stem from the major groove side using three degenerate sequence motifs.[14] A direct consequence of these different interactions is the further subdivision of aaRSs into three subclasses (Ia,b,c and IIa,b,c), based on their binding mode to the tRNA acceptor stem (Table 1.1).[8]

The mode of binding to the tRNA acceptor stem and thus the class partition, can be further correlated with a major difference in the mode of action of these enzymes: the position where the amino acid is linked to the terminal adenosine. All class I aaRSs attach their amino acid to the 2'–hydroxyl group of the ribose of the terminal adenosine residue of tRNA. By contrast, class II aaRSs, with the exception of PheRS, attach the amino acid to the

[b] A Rossmann fold is an α,β structure containing a parallel β–sheet in the centre and an α–helix on both sides.[11]

3'–hydroxyl group of the ribose of the terminal adenosine.[3,7,14,15]

1.3.3 Mode of Action

Aminoacyl–tRNA synthetases catalyse two consecutive reactions which involve three different substrates: ATP, an amino acid and tRNA. In the first step, the amino–acid carboxylic acid group is activated by reaction with ATP in the presence of a Lewis acid (Mg^{2+}) leading to the formation of an aminoacyl–adenylate (or aminoacyl–AMP), which remains bound to the enzyme.[15,16] This activation step is proposed to take place through a nucleophilic attack by the carboxylic acid group of the amino acid on the α–phosphoryl group of the ATP molecule resulting in the formation of an anhydride linkage (Figure 1.9). Pyrophosphate (PP_i) is released as a by–product.[3,9] In the second step, the aminoacyl group contained in the aminoacyl–adenylate is transferred to the corresponding tRNA. In accord with their opposite approach to the tRNA acceptor stem, enzymes from class I and class II catalyse this step differently (Figure 1.9). Enzymes belonging to class I first transfer the aminoacyl group to the 2'–hydroxyl group of the 3'–terminal A residue and subsequently to the 3'–hydroxyl group through an intramolecular transesterification reaction. In contrast, enzymes belonging to class II transfer the aminoacyl group directly onto the 3'–hydroxyl group of the terminal adenylate.[8]

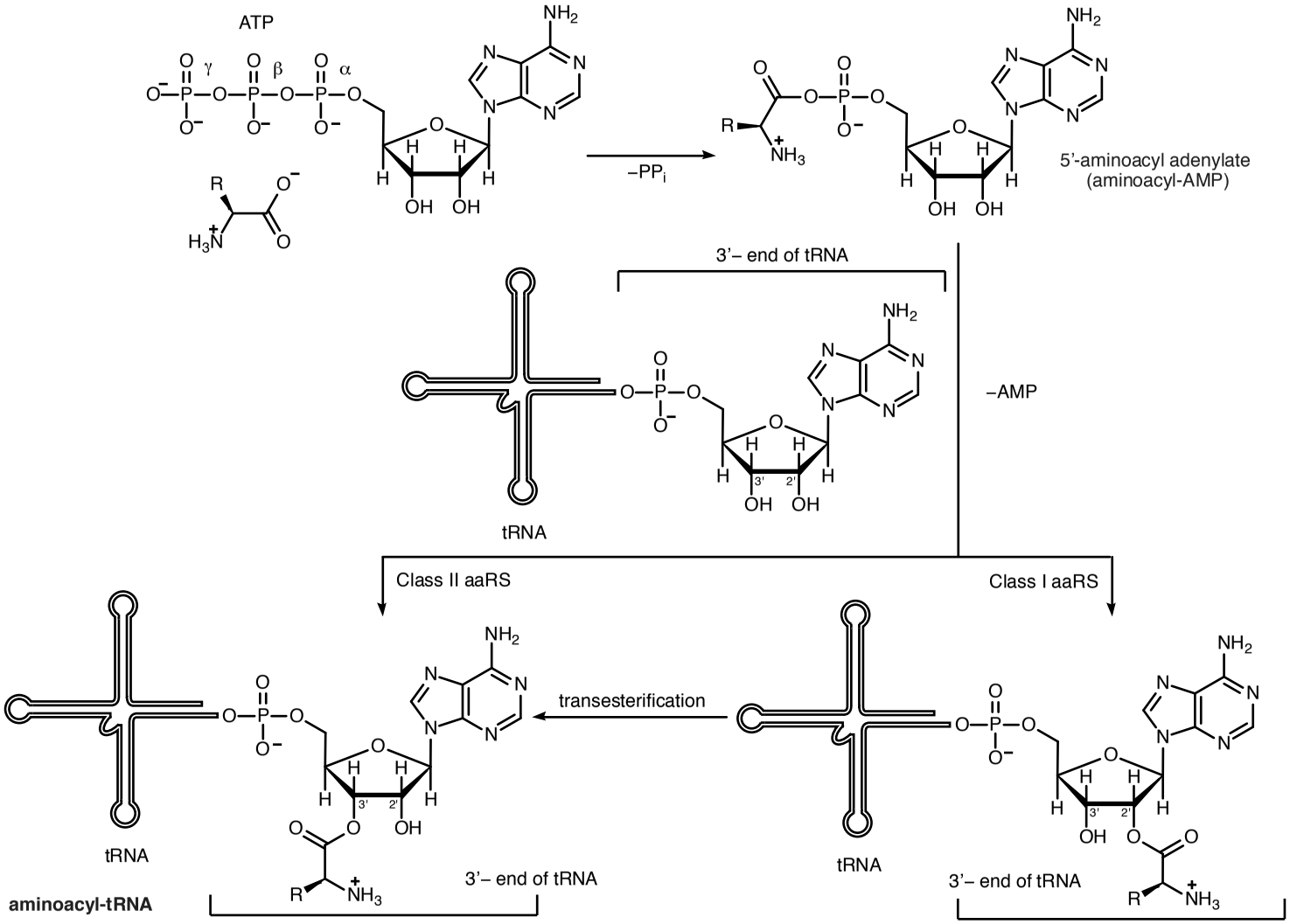

Figure 1.9: **Mechanism of aminoacylation of tRNA by aminoacyl–tRNA synthetases**

Particularly relevant to this work is aspartyl–tRNA synthetase (AspRS, EC 6.1.1.12), a class II enzyme found in organisms belonging to all three domains of cellular life, including *Homo sapiens* and *Mycobacterium tuberculosis*.[12,17] Using yeast as a homologue of *M. tuberculosis*[18] researchers have been able to obtain crystal structures of the functional complexes of this enzyme; these have shown that the aspartic acid binding site is located as an extension to the ATP binding site just after the α–phosphate binding pocket. The size and shape of the pocket are ideal to accommodate aspartic acid (and nothing else) in the correct orientation for reacting with the bound ATP. Access to this pocket is blocked when the ATP is bound, indicating that the binding events take place in a specific order, with the amino acid entering the active site first.

Based on the interactions observed in AspRS crystal structures, the amino–acylation reaction has been proposed to proceed following a specific pathway which is summarised in Figure 1.10.

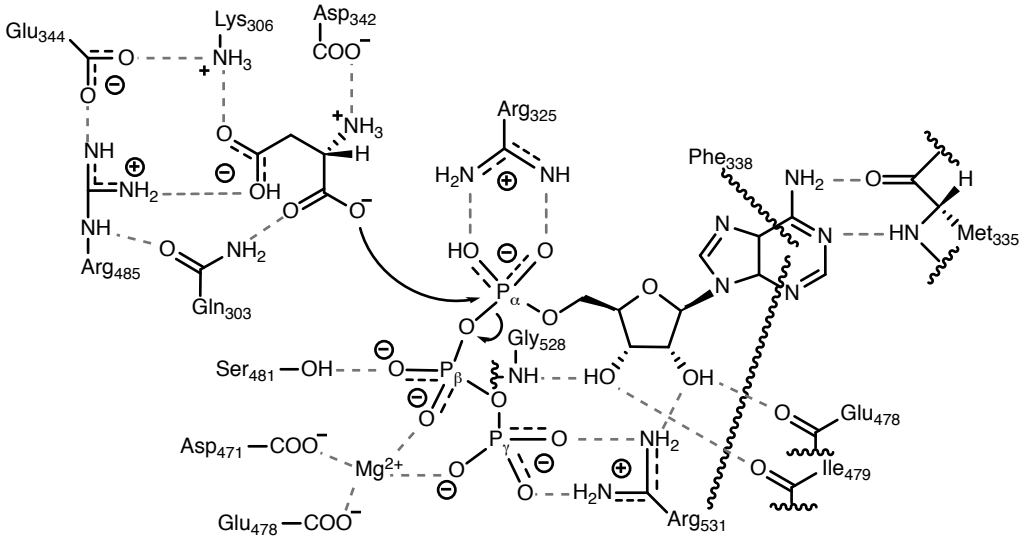

Figure 1.10: **The first step of the AspRS aminoacylation reaction.**[15]

Preceding the initial step of the chemical reaction, Asp and subsequently ATP attach to their respective binding sites. ATP assumes a bent conformation aiming its γ–phosphate towards Arg531. At this point, the aspartic acid substrate is somewhat shifted compared to the position observed in the aminoacyl–adenylate product.

It is suspected that the Asp342 residue plays an essential role in positioning the amino acid for the reaction through a direct interaction with the amino group. In addition, this interaction modifies the electron density in that region of the aspartic acid, presumably enhancing the nucleophilicity of the amino–acid carboxylate moiety. Meanwhile Lys306, Glu344, Arg485 and Gln303 residues are tasked with the precise orientation of the side–chain carboxylic acid group present in Asp (Figure 1.10) which ensures that the nucleophilic attack on the α–phosphate does not require a pronounced movement of either substrate. At this stage, Arg325, an invariant residue in all class II enzymes, is proposed to stabilise the penta–coordinated intermediate formed after the attack by locking the position of the α–phosphate. Finally, the release of the pyrophosphate is facilitated by the Mg^{2+} ion and Arg531.[15]

It is noteworthy that the amino acids previously mentioned, given their various roles in maintaining the local environment that is essential for activating the amino acid, are strictly conserved in AspRSs. Any mutation in most of these sites can completely inactivate the enzyme or at best drastically reduce its catalytic capability.[15]

The newly formed aminoacyl–adenylate, situated underneath the terminal ribose of tRNA, is ideally positioned for the second step of the reaction (Figure 1.11). In this step, the 3'–hydroxyl group of the sugar moiety undergoes a nucleophilic attack on the carboxylic group of the adenylate affording the final product of the enzymatic reaction.

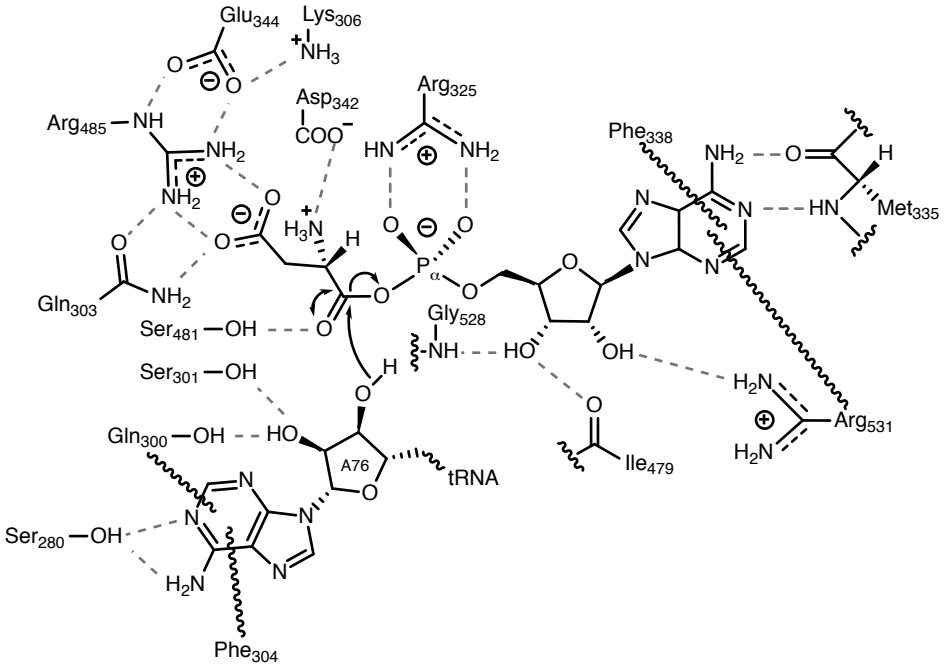

Figure 1.11: **The second step of the aminoacylation reaction in AspRS.**[15]

1.3.4 Process Accuracy

Achieving the high fidelity required in protein synthesis is critically dependent upon attaching the correct amino acid to its specific tRNA. Indeed, due to their high specificity for a particular amino acid, tRNA synthetases only incorporate an erroneous amino acid once every 10^4 or 10^5 reactions that they catalyse.[3] This degree of precision is achieved because every aaRS makes the most of the properties of its amino–acid substrate, utilising both its functional groups and its shape to prevent the attachment of an incorrect amino acid to its corresponding tRNA.[2,3]

In spite of these control mechanisms, given the structural similarity of certain amino acids, some aaRSs still risk recognising amino acids with similar structural characteristics to their own substrate more frequently than is desirable.[c] To minimise such mistakes, aaRSs have developed additional proofreading mechanisms to ensure the accuracy of their task. Given aaRSs can also catalyse the reverse reaction and hydrolyse the ester linkage between the amino acid and tRNA, some synthetases have a second active site at which incorrectly linked amino acids are removed by this means. The acylation active site generally doesn't accept larger amino acids than the true substrate due to a lack of room for them. The active site in charge of hydrolysing the bond between the amino acid and tRNA cleaves activated species which are smaller than the correct substrate. Interestingly, those aaRSs charged with activating amino acids that lack structurally similar alternatives, such as CysRS, show greatly reduced proofreading or completely lack this capability altogether. In these instances the catalytic site in charge of performing the aminoacylation is able to adequately differentiate the correct substrate from any erroneous amino acid.[2,3]

AaRSs need to be able to discriminate between dozens of tRNAs. This is as important towards achieving the aforementioned high fidelity as it is for these enzymes to discriminate between amino acids. A great majority of aaRSs (17 of the 20) are able to identify the amino acid and the anticodon of its cognate tRNA at the same time. Importantly, although the anticodon is an obvious differentiating feature in tRNAs, different parts of the tRNA molecule (*e.g.* the variable arm, the variable pocket and the acceptor stem) may also present characteristic recognition points which help aaRSs

[c] It should be noted the exception presented by several prokaryotes such as mycobacteria, which lack a specific synthetase for Asn and Gln. In these cases, a non–discriminating acylation is catalysed by AspRS to produce both $tRNA^{Asp}$ and $tRNA^{Asn}$ and by GluRS to produce $tRNA^{Glu}$ as well as $tRNA^{Gln}$.[17,19]

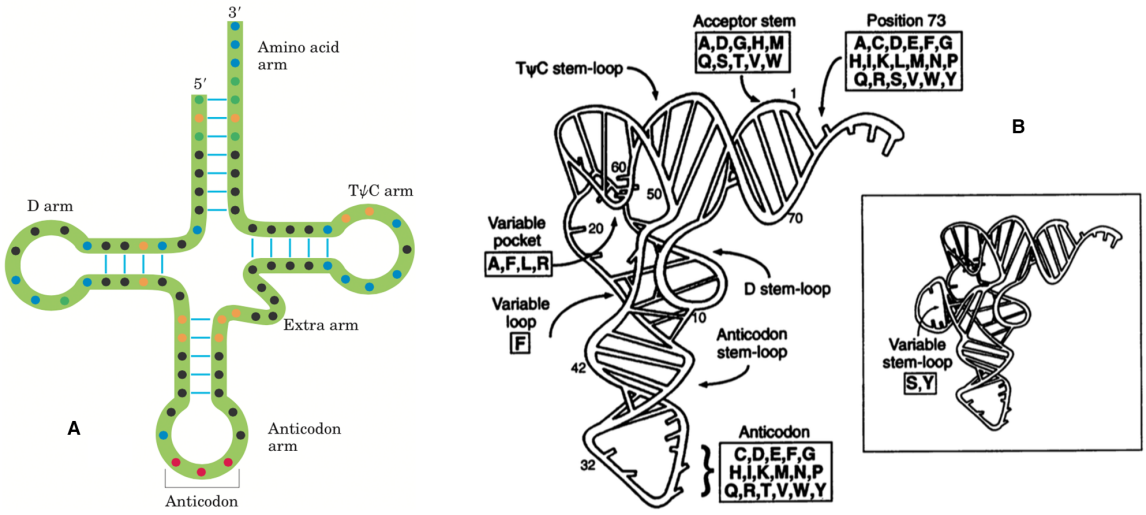

Figure 1.12: **tRNA nucleotide positions recognised by aaRSs.** A) Blue positions are equivalent in all tRNAs. Orange and green positions are known recognition points for aaRSs. B) Common locations of nucleotides that contribute to the recognition of amino acids in *E. coli*.[3,20]

to discriminate between different tRNAs (Figure 1.12). However, in a small number of cases (*e.g.* Ser and Ala), the tRNA anticodon is not identified by the synthetase, in which case the aaRS relies on other identity features in different places on the tRNA for its recognition.[3,9,20]

The high specificity of these enzyme–substrate interactions has been confirmed through sequencing and structural studies which have also demonstrated a correlation within the various subclasses of synthetases, as members of a particular subclass tend to have the same anticodon binding sequences. As an example, four of the class IIa synthetases (GlyRS, HisRS, ProRS and ThrRS) present a unique *C*–terminal anticodon binding sequence of approximately 100 residues that is not present in any other proteins. Similarly, class IIb synthetases AsnRS, AspRS and LysR, all closely related, contain a similar *N*–terminal anticodon binding sequence made up of approximately 100 residues.[9]

The overall error rate of protein synthesis is not quite as low as that of DNA replication. However, defects in the resulting proteins are obliterated when these molecules are degraded, and since they are not handed over to future generations, they lack the same biological relevance and impact of potential defects in DNA. Nevertheless, the level of fidelity achieved in protein synthesis is sufficient to guarantee that most proteins are not faulty. Moreover, having one malfunctioning protein tends not to be very important when it finds itself surrounded by many correct replicates of the same protein.[3]

1.4 Inhibition of Aminoacyl–tRNA Synthetases Enzymatic Activity

1.4.1 Introduction

The essential role that aaRSs play in protein synthesis has singled these enzymes out as promising targets for the development of antibiotics. Inhibiting the reactions this class of enzymes catalyse, either the first or the second step, causes the stockpiling of free tRNA molecules. This in turn leads to a situation where the excess tRNA binds to ribosomes, which provokes the interruption of the elongation process, halting the growth of the polypeptidic chain. This induces what is known as the *stringent response* by *rel*A[d], the result of which is the synthesis of guanosine tetra– and pentapeptides. These peptides block the activity of RNA polymerase and downregulate a number of processes including the synthesis of DNA, RNA, and proteins. This results in the halting of bacterial growth under *in vitro* conditions and a reduction

[d] *rel*A is an enzyme, also known as *stringent factor*, which under conditions of amino–acid starvation, binds to the ribosome and catalyses the formation of the nucleotide guanosine tetraphosphate using GTP and ATP as substrates.

of pathogenic virulence *in vivo*.[10,19]

1.4.2 aaRSs as Drug Targets

Aminoacyl–tRNA synthetases present several features underscoring their suitability as targets for drug discovery:[10,19]

- although they are universally distributed in cellular organisms, prokaryotic and eukaryotic[e] aaRSs present an evolutionary divergence that allows selective targeting of bacterial enzymes.

- each aaRS is phylogenetically conserved across different bacterial pathogens. Therefore antimicrobial agents targeting a specific bacterial aaRS can potentially be used to inhibit homologous enzymes present in other bacteria, increasing the prospects of discovering broad–spectrum antibiotics.

- the 20 different aaRSs found in most species (including bacteria) potentially constitute 20 different targets for discovering new drugs.

- aaRSs are easy to purify in large quantities. Moreover, they are soluble and stable in aqueous buffers, and can therefore be used in the routine assays required for HTS.

- X–Ray crystal structures of many aaRSs have already been solved, providing an essential base for rational drug design.

[e] As a rule, drug targets that have *no* human counterpart, *e.g.* those involved in cell–wall biosynthesis, are preferred. However, drugs whose bacterial target has an human counterpart have also proven to be efficient and have been approved by regulatory agencies. In the case of aaRSs, numerous studies have highlighted the evolutionary differences of these enzymes in eukarya (specifically *Homo sapiens*), bacteria and archaea and drugs targeting these enzymes, such as mupirocin (see Section 1.4.3.), have already been successfully marketed.[21,22,23,24]

1.4.3 Inhibition Mechanisms

Direct Inhibition

Currently the only clinically available aaRS inhibitor is mupirocin **4** (marketed as Bactroban, Figure 1.13). This antibiotic is a natural product of *Pseudomonas fluorescens* and selectively inhibits bacterial IleRS. It is currently the most widely used antibiotic in the world for the control of MRSA.

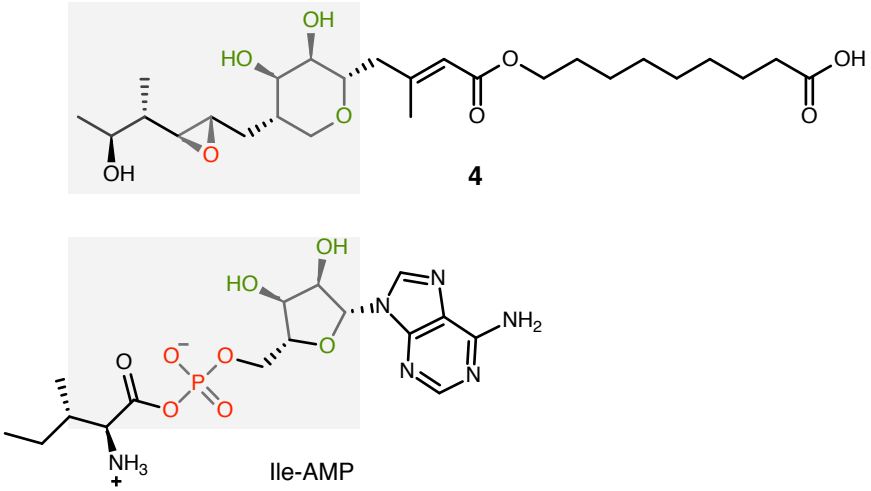

Figure 1.13: **The natural product mupirocin A.**

Mupirocin mimics the isoleucyl structure present in the isoleucyl–adenylate conjugate (Ile–AMP),[f] which enables it to bind to IleRS in the same region where Ile–AMP binds. Through the epoxide moiety (red), which occupies the same domain as the phosphate group of the Ile–AMP conjugate, mupirocin acts as an irreversible covalent inhibitor. Upon recognition by the enzyme, a covalent bond is formed when a nucleophilic residue of the enzyme opens the epoxide ring, which results in the permanent blocking of the enzymatic active site. This translates into the blocking of the function of the enzyme and ultimately of the protein biosynthesis pathway.

[f]The target of mupirocin has been confirmed after finding that the inhibition process is reversed when the concentration of Ile is increased, allowing the bacteria to synthesise proteins once again.[10,19]

In order to facilitate enzymatic recognition, the dihydroxytetrahydropyran ring (green) binds to the enzyme in a similar position as the ribose group in Ile–AMP, and the fragment which is structurally similar to the hydrophobic side–chain of Ile is recognised by the hydrophobic pocket which binds Ile.[10,19]

A number of other natural products have been identified as aaRS inhibitors (Figure 1.14). These include reveromycin A **5** (which also targets IleRS), borrelidin **6** (whose target is ThrRS), granaticin **7** (whose target is LeuRS), furanomycin **8** (whose target is IleRS), ochratoxin A **9** (whose target is PheRS) and cispentacin **10** (whose target is ProRS).[10,19] It is currently unclear whether or not these inhibitors represent useful lead compounds for antimicrobial drug discovery, as many also affect the counterpart human enzymes. Moreover, despite showing strong inhibition *in vitro*, due to their inability to penetrate efficiently the bacterial cell wall, their *in vivo* activity is severely undermined. Additionally, off–target activity against other enzymes seems to be relatively common for these molecules.[19,25]

Second–Step Inhibition

A separate group of aaRS inhibitors are analogues of the aminoacyl–adenylate reactive intermediate. The rationale behind this approach to inhibition is that analogues of reaction intermediates will most likely bind a specific synthetase in a similar fashion to the substrate, showing at the same time a high affinity for the target enzyme. In this way, it should be possible to obtain compounds that exhibit strong inhibition against the corresponding enzyme. The syntheses of these molecules have so far aimed at supplanting the relatively labile phosphate esters of aminoacyl adenylates with isosteric groups such as sulfamoyl linkages based on observations on the mode of

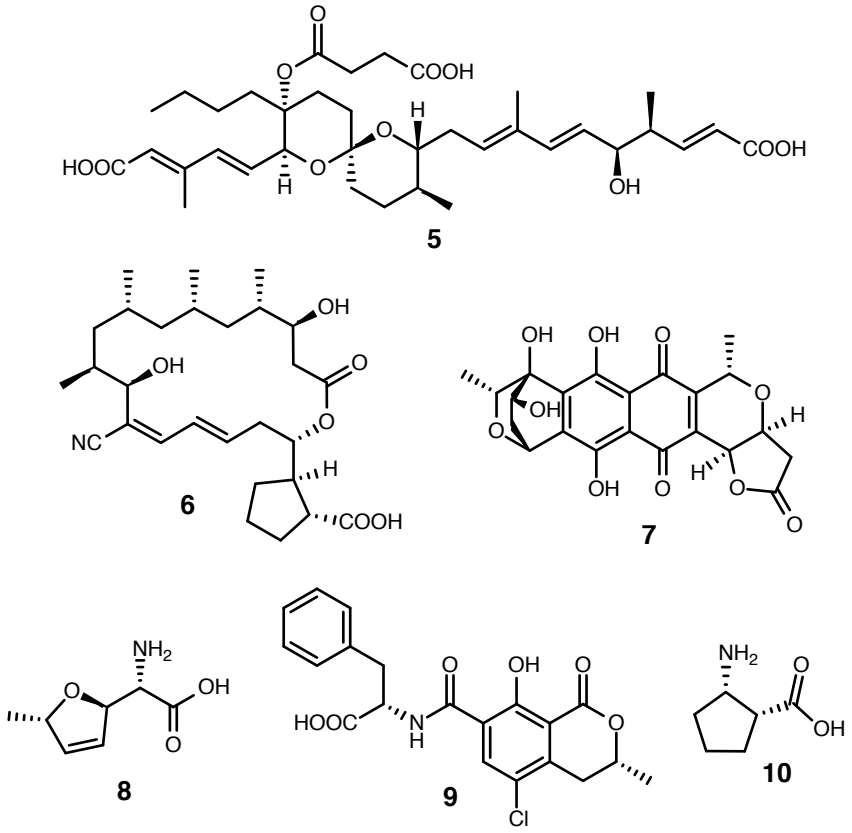

Figure 1.14: **Aminoacyl–tRNA synthetase inhibitors reveromycin (5), borrelidin (6), granaticin (7), furanomycin (8), ochratoxin A (9) and cispentacin (10).**[10,19]

action of antibiotics such as ascamycin (Figure 1.15). The introduction of these hydrolytically more stable moieties has led to the creation of families of compounds such as **11**, reported by Heacock *et al.*,[26] a prolyl adenylate analogue which is relatively stable towards hydrolysis by ProRS.

Although this type of inhibitor can be easily obtained synthetically, they tend to be rather inefficacious antibiotics owing to their potential ability to inhibit human aaRSs. Moreover, a great majority display little or no *in vivo* activity because they are unable to pass through bacterial cell membranes.

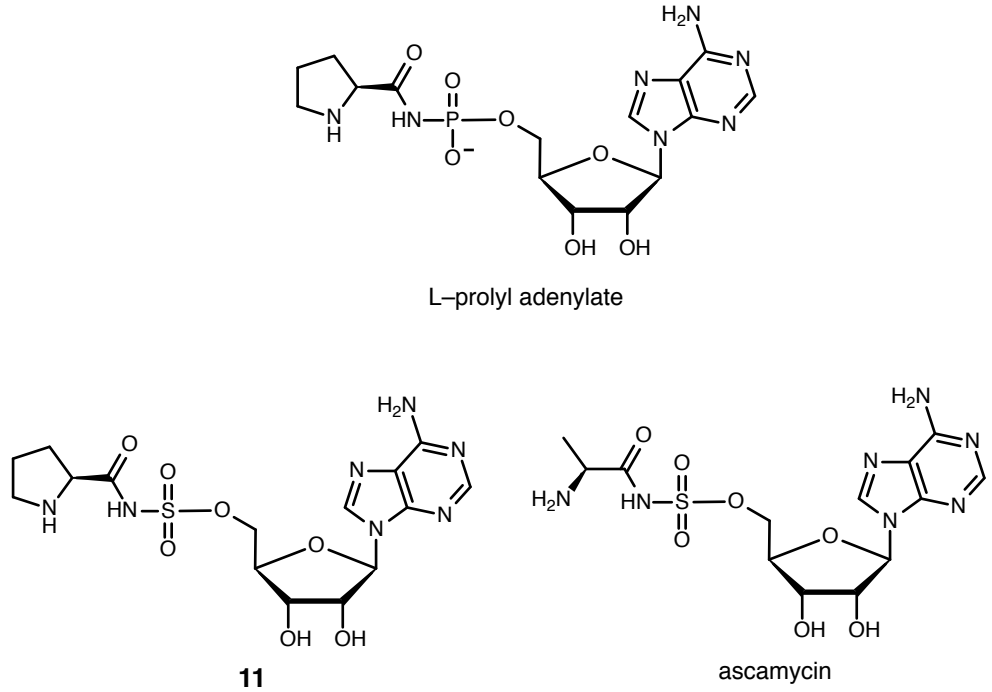

Figure 1.15: **Chemical structure of ProRS inhibitor 11, ascamycin and L–prolyl adenylate.**[27,26]

Trojan Horse Inhibition

Nature has cleverly overcome some of the limitations of some of the inhibitors described in the previous section through a tactic akin to the "Trojan horse" strategy. This strategy consists of covalently attaching the active fragment of the drug, in our case the aminoacyl–adenylate (the "Trojan horse"), to a specialised segment which promotes transport through bacterial cell walls. After reaching the cytoplasm, the "Trojan horse" segment is removed, releasing the active compound, which can then act as an inhibitor.[19] Several examples of natural antibiotics based on aminoacyl–adenylate analogues that take advantage of this strategy are known, among them (Figure 1.16 and Figure 1.17) are the LeuRS inhibitor agrocin84,[28] the SerRS inhibitor albomycin[29] and the AspRS inhibitor microcinC7 (Figure 1.17).[30]

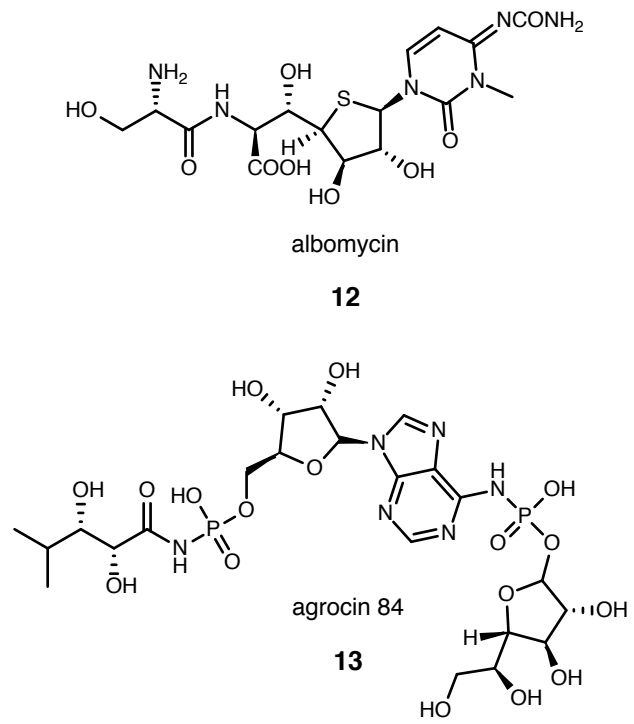

Figure 1.16: **Structure of albomycin (12) agrocin 84 (13).**

MicrocinC7 (**15**, Figure 1.17) is a heptapeptide containing a formyl group at the N–terminus and an adenylate bound through a phosphoramidate to the C–terminus. Following its biosynthesis, the heptapeptide is transported out of the cell of the producing organism and after recognition by specific active transporters, is taken up by sensitive bacterial strains. After reaching the inside of the target cell, microcinC7 undergoes a number of enzyme–mediated processes starting with the removal of the formyl group by the enzyme peptide deformylase. The molecule is subsequently further fragmented in a process progressing in the N to C direction through the action of various aminopeptidases. When the peptide bond linking the sixth (Ala) and seventh (Asp) amino acids in the peptide is broken, the active part of microcinC7 is set loose within the target cell. Removing the first six amino acids present in microcinC7 is essential for its antibiotic activity; their only role is to facilitate the transport of the antibiotic inside the target cells.[19]

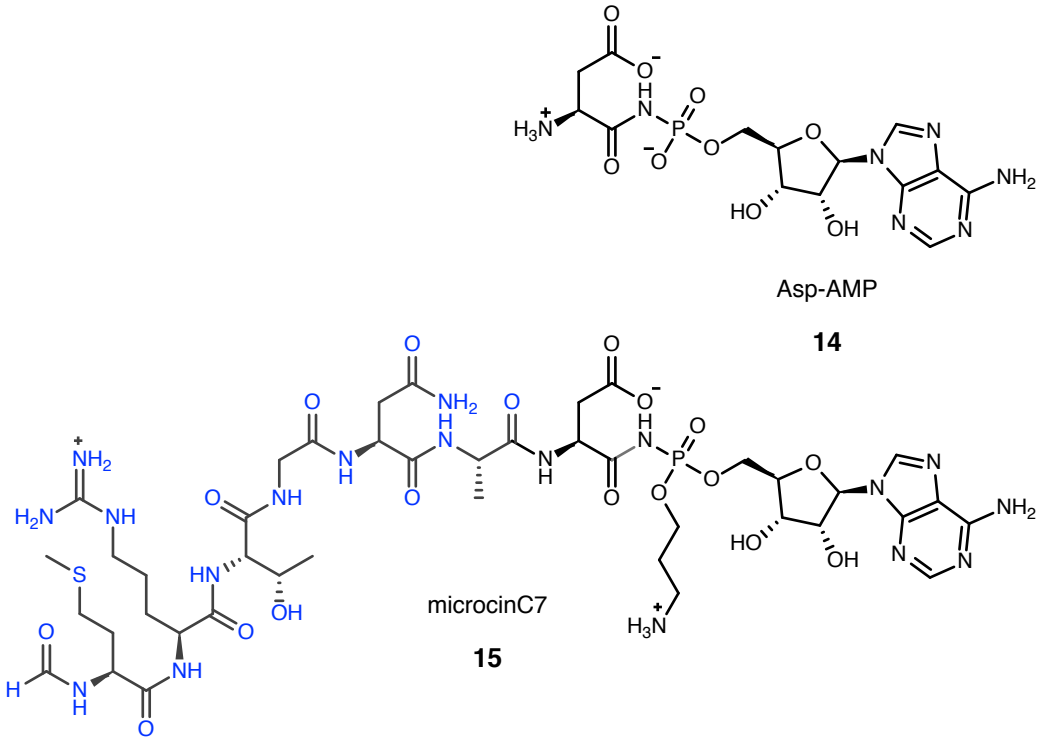

Figure 1.17: **Structure of microcinC7 (15) and its corresponding aminoacyl–adenylate (14).**

Inhibitors Identified by High–Throughput Screening)

Improvements in High–Throughput Screening (HTS) technology have accentuated the role of this approach as a pivotal tool for the discovery of small molecules that act against diverse targets, including aaRSs. Exploiting automation to swiftly assay the biological activity of a large number of drug–like molecules to identify active compounds, combined with the chemical optimisation of the resulting hits, has produced a myriad of pharmacophores which inhibit bacterial aaRSs. Among the most attractive contenders obtained to date are a series of quinolinone derivatives, described by GlaxoSmithKline (GSK), which inhibit the MetRS enzyme of *Staphylococcus aureus* through direct competition with methionine, its natural substrate. In particular, compound **16** (Figure 1.18) has been proven to selectively inhibit bacterial

MetRS (IC_{50} = 12 nM for *S. aureus* MetRS) and was shown to be potent against *S. aureus* (MIC_{90} = 1 μg mL^{-1}) and *Enterococcus* spp. (MIC_{90} = 0.25 μg mL^{-1}).[10,31]

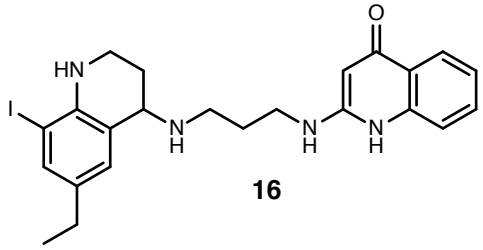

16

Figure 1.18: **Structure of GlaxoSmithKline's racemic quinolone MetRS inhibitor 16.**[10]

1.5 Tuberculosis

In spite of the lack of media attention in most of the developed world, tuberculosis (TB) is ranked by the WHO, alongside HIV, as a leading cause of death worldwide, affecting most of the poorest places of our planet. In 2016, 1.7 million people died because of TB (1.3 million HIV–negative and 0.4 million HIV–positive)[g] (Figure 1.19).[34] A daunting 10.4 million people were estimated to have been infected with TB in 2016. Of these, 90% were adults, 65% were male, and 10% of the total were also diagnosed with HIV.[34]

[g]Patients co–infected with HIV and TB suffer a faster progression of HIV due to a shorter replication period.[32] Furthermore, HIV infection is the most significant factor associated with a heightened susceptibility to TB, increasing the lifetime risk of developing active TB from the latent form of the disease from 1 in 10 to 1 in 3.[33]

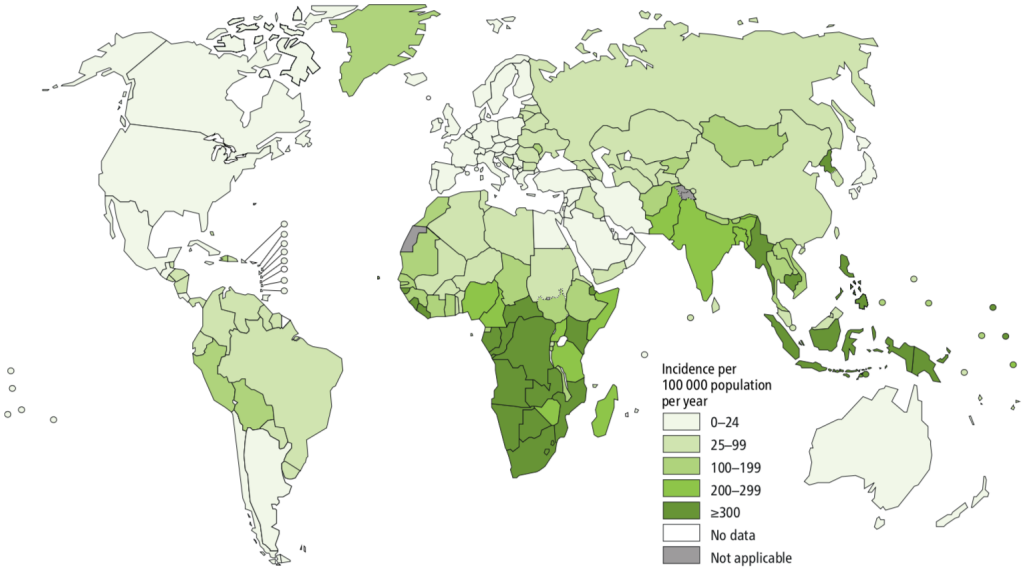

Figure 1.19: **Estimated TB incidence rates in 2016.** Adapted from the WHO Global Tuberculosis Report 2017.[34]

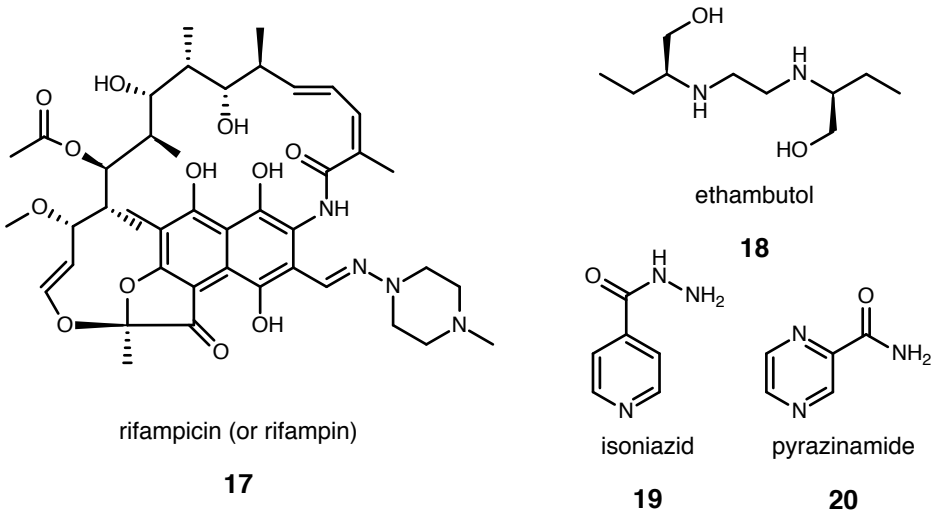

Figure 1.20: **Drugs used in a combination in the treatment of TB following the DOTS protocol.**

TB can be successfully treated. However, the current multidrug therapy programme (Figure 1.20) recommended by the WHO [known as Directly Observed Therapy Short–Course (DOTS)] is becoming increasingly less efficient in battling *M. tuberculosis*, the bacterium that causes TB. Although naturally occurring spontaneous mutations can confer drug resistance, the

increase in bacterial resistance to the WHO recommended drugs is considered to be primarily a consequence of the lack of patient compliance with the DOTS therapy. This, in turn, has flatlined and even created spikes in the number of yearly infections and deaths. A notable example are HIV co–infected patients, in which not only is TB diagnosis much more difficult,[32] but co–therapy with antiretroviral agents significantly increases the pill burden. This, in turn, creates overlapping toxic side–effects that are a primary cause of low patient compliance with the treatment. Additionally, subtherapeutic concentrations of antitubercular drugs caused by malabsorption or drug interactions[35] increase the treatment period, putting an additional burden on those affected by the disease.[32,36,37,38]

A combination of the factors mentioned above has led to the emergence of multidrug–resistant, extensively drug–resistant, and in some cases, totally drug–resistant TB. And whilst the past 10 years have witnessed a noticeable shift towards developing novel drugs that can kill *M. tuberculosis* (Figure 1.21), out of the six new compounds reaching phase II and III clinical trials, only two molecules (bedaquiline **19** and delamanid **20**, Figure 1.22) have been conditionally approved by the FDA and EMA for use in extreme situations.[39] Therefore, given the current situation in which one can easily imagine a future in which it becomes increasingly difficult to cure the disease, it remains of paramount importance to develop new drugs that can overcome the growing bacterial resistance to the existing treatment regimen in order to tackle the disease efficiently.

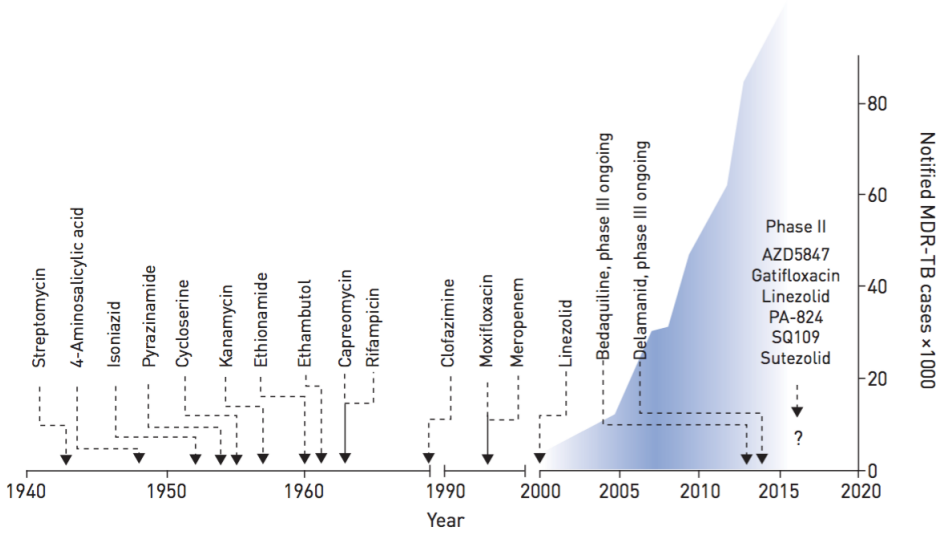

Figure 1.21: **Discovery of novel drugs against TB and number of reported multidrug–resistant TB cases worldwide.** Adapted from the work by Olaru *et. al.*[39]

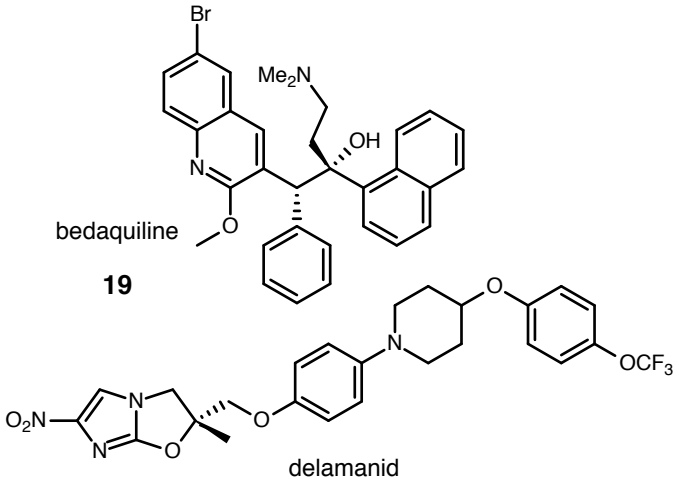

Figure 1.22: **New drugs granted conditional approval for the treatment of multidrug–resistant TB.**

One way of tackling bacterial resistance is to develop drugs with different mechanisms of action. Combining such drugs with existing or novel drugs with a range of mechanisms of inhibition means that even if resistance does develop against one mechanism, the other drugs in the treatment regimen will eventually kill the microorganism. In this sense, since there are currently no

drugs in the clinic that target *M. tuberculosis* tRNA synthetases, this project aims to establish the validity of AspRS as a potential druggable target for TB and to set the basis for future research based on its outcome.

Chapter 2

Synthesis of Inhibitors Targeting AspRS

2.1 Introduction

Aiming to fight *M. tuberculosis* by engaging novel targets within the bacterium, this project has its roots in a number of hit molecules. These were obtained through an HTS campaign combined with whole–genome sequencing (WGS) of resistant isolates. Maddry *et al.* carried out the screening campaign against *M. tuberculosis* in 2009, employing the National Institute of Health (NIH) Small–Molecule Rejapository (SMR)[a]. This compound screen provided a total of 2500 active compounds of wide structural variety. Out of these, and particularly relevant to this project, was the identification of a cluster of four 2,5–disubstituted thiazolidin–4–ones, of which compound **23** (Figure 2.1) was the most active (IC_{90} = 3.6 μM).[40]

[a]The Small–Molecule Repository of the NIH contained 215110 different compounds at the time of the screening.

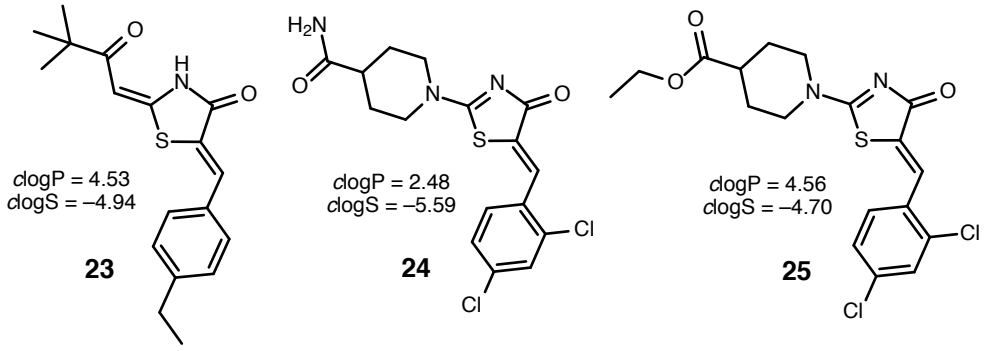

Figure 2.1: **2,5–Disubstituted thiazolidin–4–ones that were active against *M. tuberculosis*.**

Subsequent work carried out by Ioerger *et al.* on compound **24** (Figure 2.1), a structural analogue of **23**, provided additional evidence to support the anti–tubercular activity of this class of compounds. This compound was active in a whole–cell screening against *M. tuberculosis* H37Rv with an MIC_{99} = 0.7 μM. When resistant mutants of the H37Rv strain were isolated and submitted for WGS, a comparison of the genomes of the parental strains and the resistant isolates identified mutations in the gene expressing AspRS.[18]

It is worth noting at this point that human and bacterial AspRS are different in their amino acid sequence due to the evolutionary divergence between the different kingdoms; however, the regions associated with their binding site and catalytic activity are highly conserved between species.[12] Therefore, compounds such as **24**, which inhibit the enzymatic activity of AspRS in bacterial cells could potentially cause the same effect in human AspRS. As a consequence, establishing the mode of action of compound **24** would be a crucial step towards designing a suitable inhibitor that can target selectively *M. tuberculosis* AspRS in the presence of human AspRS.

Initial efforts in our group were directed towards fully characterising the interaction of compound **24** with *M. tuberculosis* AspRS, with the aim of developing tools which would allow the design of a more potent and potentially selective inhibitor. After growing resistant AspRS mutants using *Mycobacterium smegmatis*[b] and comparing their nucleotide sequence with the original AspRS sequence, it was possible to identify those amino–acid residues (Thr565, Asp174 and Phe521 in *M. smegmatis* corresponding to Thr570, Asp179 and Phe526 in *M. tuberculosis*) with which inhibitor **24** might be interacting in order to block the activity of the enzyme. At the same time, an *in vitro* activity assay was developed[17] that allowed the measurement of the IC_{50}[c] values. Significant effort was also invested in obtaining crystal structures of *M. smegmatis* AspRS bound to inhibitor **24** and similar analogues, as these would provide more meaningful information on the enzyme–inhibitor interaction. These efforts resulted in a crystal structure of *M. smegmatis* AspRS (Figure 2.2), which revealed this enzyme to be a dimeric protein with a three–domain architecture made of an N-terminal, β–barrel–like domain, a central catalytic domain and an insertion domain. Unfortunately, attempts to co–crystallise the protein and inhibitor **24** have been unsuccessful. We hypothesised that the most likely causes for this are the low aqueous solubility of compound **24**, a low affinity between the protein and the inhibitor, or a combination of both.

The difficulty in obtaining inhibitor–protein co–crystals highlighted solubility as a particular issue for compounds of similar structure to inhibitor **24**, an issue which would need to be addressed through the synthesis of more soluble analogues. A different potential problem was noticed in the

[b] *M. smegmatis* is a non-pathogenic microorganism commonly used as a model for mycobacterial species. It shares more than 2000 homologues with *M. tuberculosis* as well as its unusual cell–wall structure.[41]

[c] IC_{50} is defined as the concentration resulting in a 50% inhibition of enzymatic activity.

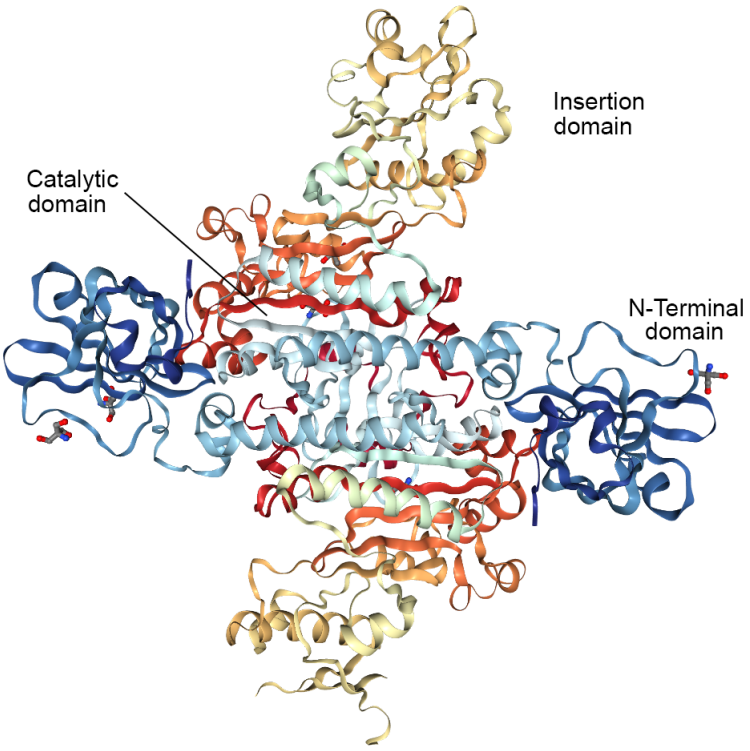

Figure 2.2: **Crystal structure of *M. smegmatis* AspRS.** Adapted from the work of Gurcha *et al.*[17]

presence of rhodanine as the core of inhibitor **24**. Compounds based on thiazolidinone or rhodanine cores such as **24** are often considered Pan Assay INterference compounds or PAINS.[42] These types of molecules have been shown to be promiscuously active in a multitude of HTS campaigns and carry the reputation of being difficult to optimise against specific targets.[17] As a consequence, attempts are being made to eliminate this class of compounds from screening libraries and increase the scrutiny of literature reports which identify these compounds as hits from screening campaigns.[42] Nonetheless, it is important to highlight that despite these problems, there are a number of drugs that incorporate this type of scaffold, for example ralitoline **26** (an anti–convulsant), etozoline **27** (anti–hypertensive agent) and pioglitazone **28** (treatment of diabetes) (Figure 2.3). Moreover, information obtained by our group so far indicates that compounds such as **24** display specific activity

against AspRS, as mutations have been observed specifically for this protein at concrete locations in the genome of resistant mutants. This result stands in contrast to promiscuous compounds that have multiple targets, for which identifying a unique target through the generation of resistant mutants is not possible.[17]

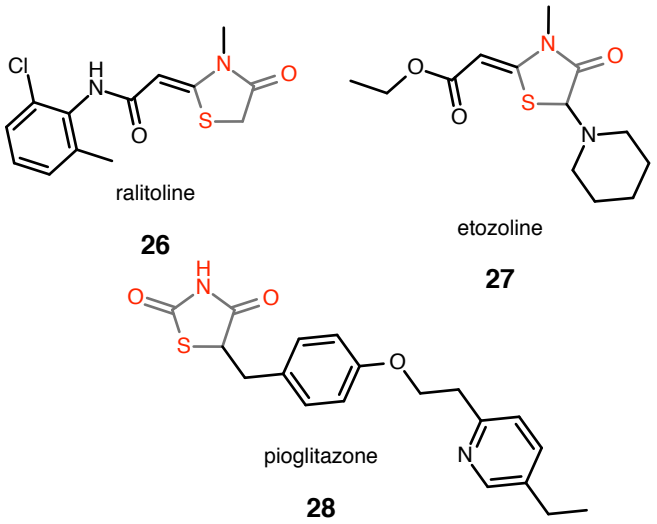

Figure 2.3: **Marketed drugs containing a rhodanine–based core.**

2.2 Synthesis

The main goal of this work was to attempt to correlate the structure of inhibitor **24** with its anti–tubercular activity by synthesising analogues and comparing their activity with that for the original structure, with the aim of rationalising how structural changes to hit **24** impact on activity. Therefore, the first step was to perform a retrosynthetic analysis of **24** in order to devise a synthetic plan that would allow the preparation of analogues through the introduction of diverse structural changes and functionalities (Scheme 2.1).

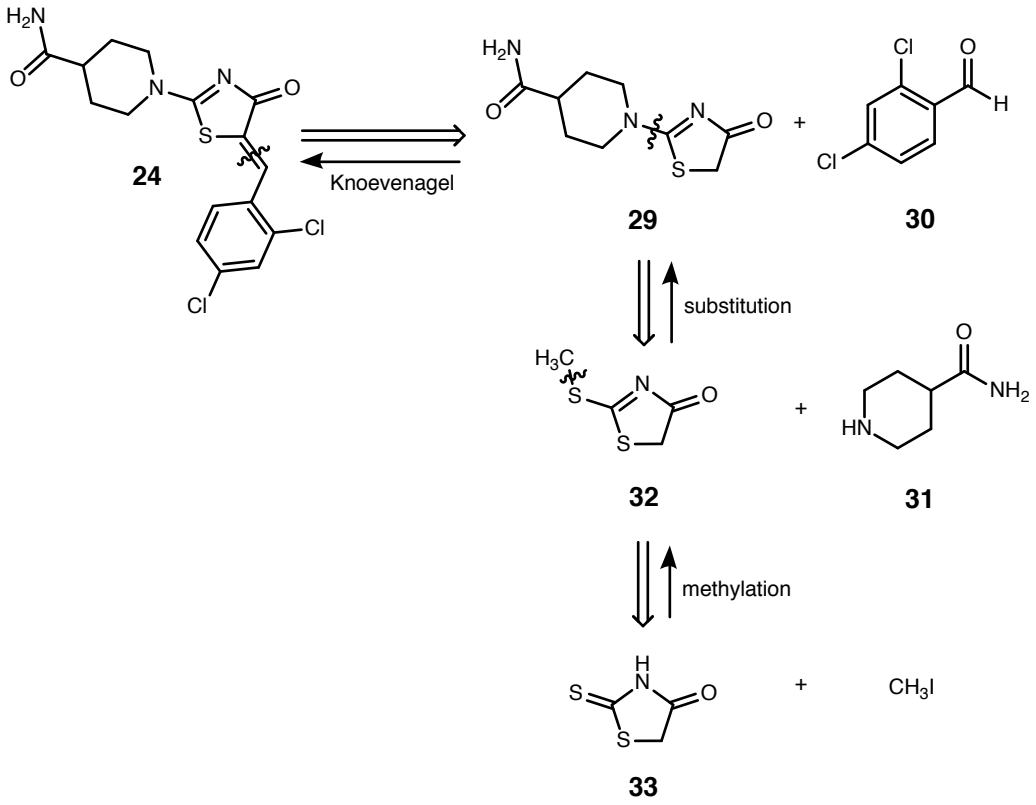

Scheme 2.1: **Retrosynthetic analysis of inhibitor 24.**

We envisaged that by breaking the exocyclic double bond in compound **24** (Scheme 2.1), which could be installed through a Knoevenagel condensation,[43] we would be able to introduce variability in this region of the molecule in the last step of the synthesis by employing a diverse range of aldehydes and potentially ketones too. In turn, breaking the C–N bond between the piperidine ring and the rhodanine core would allow us to introduce further diversity by employing different amines (and potentially other nucleophiles) in a substitution reaction[44] on thiazolidinone **32**, a molecule easily accessible from rhodanine **33**, a commercially available and well–known heterocycle in medicinal chemistry.[45]

This retrosynthetic plan has the attractive feature that the order in which the exocyclic double–bond or the C–N bond are introduced allows an alternative retrosynthetic approach depicted in Scheme 2.2. Using this retrosyn-

thesis we can introduce variability on the piperidine side of the rhodanine core of inhibitor **24** in the final step of the synthesis. In this way, by carefully selecting aldehydes and amines, and through judicious choice of the order in which these groups are introduced, we postulated that we would be able to efficiently explore a large array of analogues of inhibitor **24**.

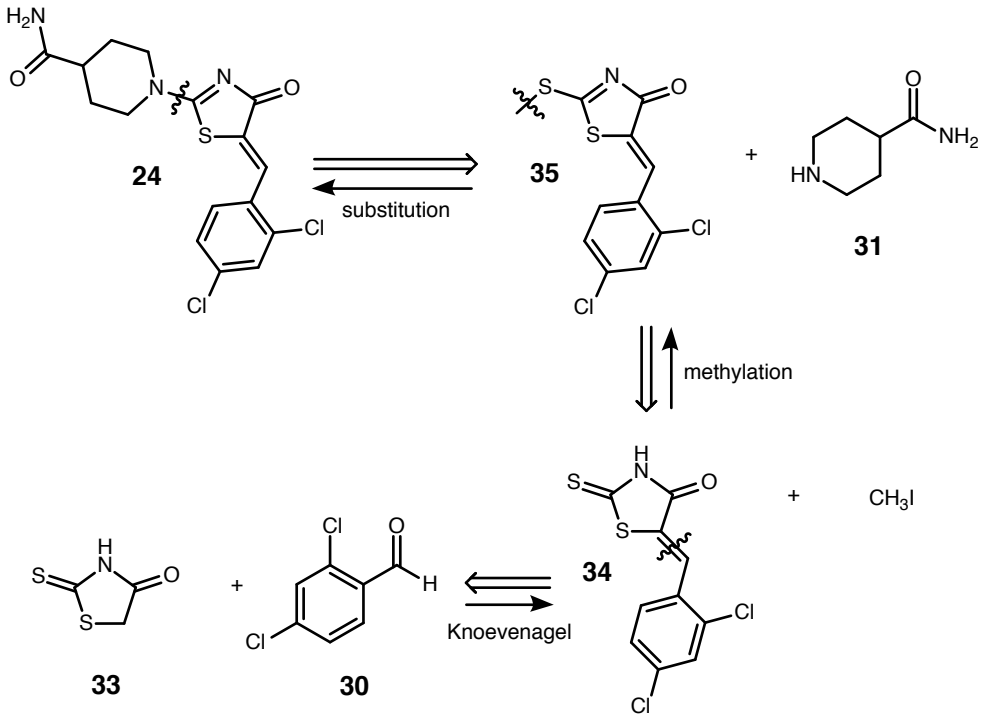

Scheme 2.2: **Alternative retrosynthetic analysis of inhibitor 24.**

Following our first strategy outlined in Scheme 2.1, the synthesis of hit compound **24** started with the chemoselective methylation of rhodanine **33** to give compound **32** (Scheme 2.3).[46] A subsequent displacement of the thiomethyl group using piperidine **31** provided thiazolinone **29**,[47] which subsequently underwent a completely stereoselective Knoevenagel condensation with aldehyde **30** to provide hit **24**.[48] Reversing the steps to allow the introduction of an amine in the final step, inhibitor **24** was also accessed starting with a stereoselective Knoevenagel condensation between benzaldehyde **30** and rhodanine **33**, followed by chemoselective methylation of the

condensation product **34** to provide sulfide **35** (Scheme 2.4). Finally, substitution of the thiomethyl group by amine **31** provided inhibitor **24**.

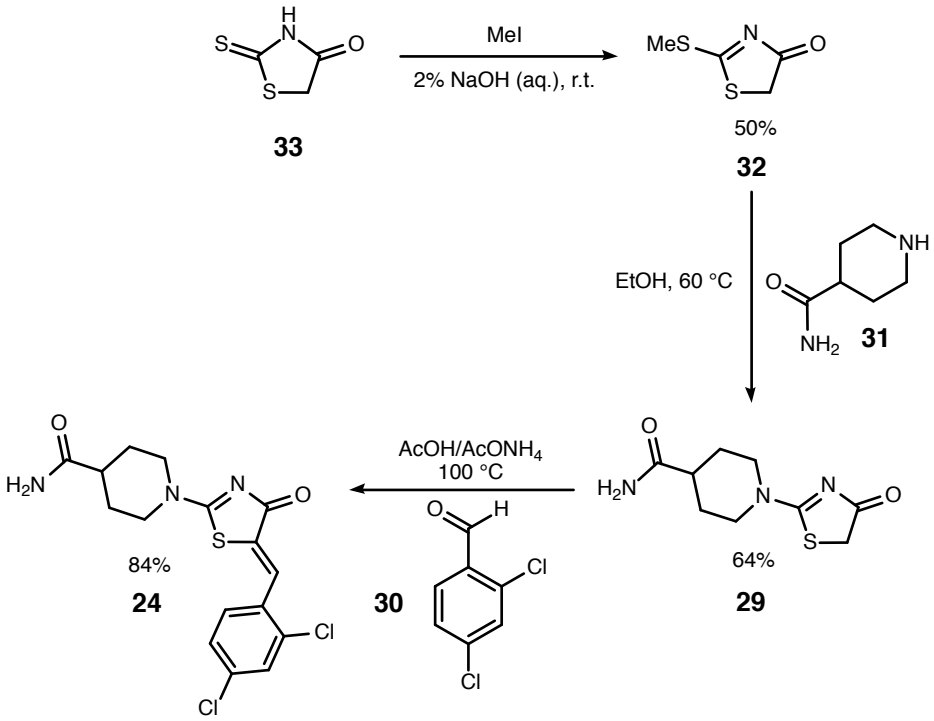

33 **32** **31** **29** **30** **24**

Scheme 2.3: **Synthesis of inhibitor 24.**

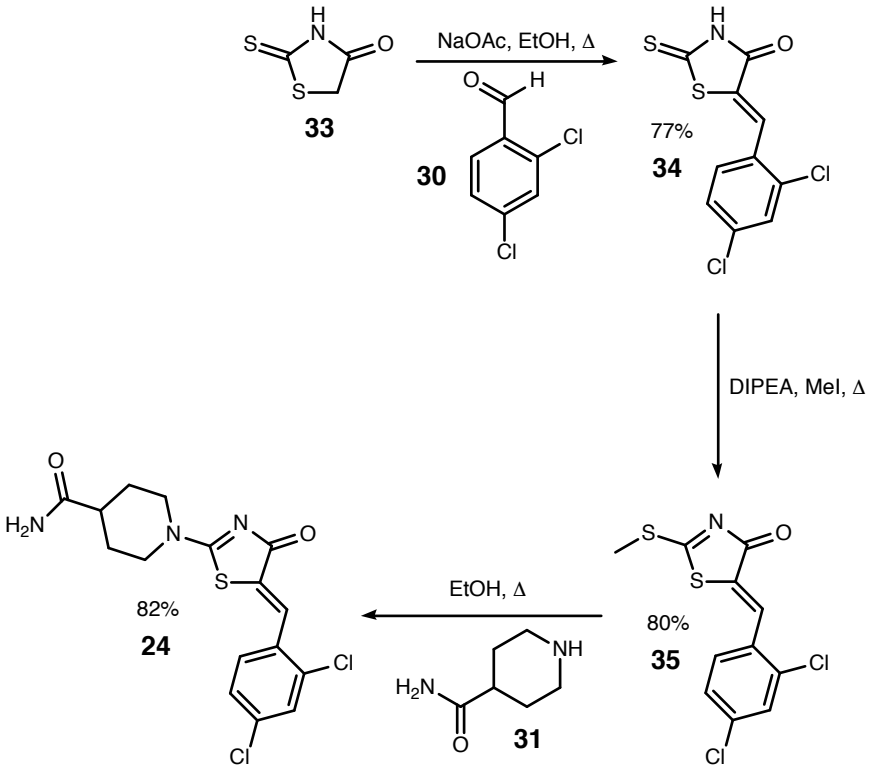

Scheme 2.4: **Alternative synthesis of inhibitor 24 undertaken by our GSK collaborators.** This synthesis was also performed at the University of Birmingham. The molecules described in the experimental section were characterised after being synthesised at the University of Birmingham. Yields described here were obtained at GSK.

Focused on introducing variability around the aromatic ring of hit **24**, this inhibitor was synthesised at the University of Birmingham according to Scheme 2.3. Meanwhile, our colleagues at GSK, aiming to introduce variability on the piperidine side of the compound, synthesised hit **24** following the procedure outlined in Scheme 2.4. The synthesis according to Scheme 2.3 provided hit **24** in an overall yield of 27% over the three steps. The limiting step was the methylation of rhodanine **33** to obtain sulfide **32**, where the best yield achieved was 50%. Although small amounts of unreacted starting material were detected when the reaction was stopped, competing methylation occurs, albeit to a lesser extent, on the N atom in rhodanine, requiring careful chromatography to separate the two regioisomers. The following two

steps proceeded with no particular issues, the only limitations in terms of scalability being the chromatography step in the isolation of thiazolinone **29** and the recovery of hit **24**, which was best achieved by crystallisation. Following the alternative route (Scheme 2.4), the overall yield achieved was 50%. The limiting steps affecting the overall yield of this synthesis were the first two steps. The Knoevenagel condensation on rhodanine **33** does not proceed as efficiently as on thiazolinone **29**, with unreacted starting material being recovered even after 24 hours of reaction. Additionally, the methylation of Knoevenagel product **34** to provide sulfide **35** was a particularly burdensome experimental step, requiring time–consuming washing and precipitation steps prior to purification by chromatography, both causing significant product loss. It should be mentioned that none of the steps described in the two synthetic approaches were extensively optimised. Aiming to obtain only a few milligrams of each analogue, the routes were deemed adequate for this purpose; optimisation would be the focus of a later stage of the project depending on its evolution.

Given the literature precedents in the synthesis of similar molecules, especially the extensive study performed by Ohishi *et al.*,[49] we expected the *Z* double–bond configuration to be the more thermodynamically stable olefin geometry for compound **24**. However, the molecular structure provided by the supplier (ChemBridge) of the initial screening, depicted inhibitor **24** as the *E* stereoisomer. In order to ascertain whether the commercially supplied inhibitor and the inhibitor we had synthesised following literature protocols possessed the same geometry, it was necessary to determine definitively the olefin configuration of the newly synthesised hit **24**. To this end, we focused on the NMR spectroscopic data registered for our synthesised compound. Vogeli *et al.*[50] reported that the coupling constant between the carbonyl

C(1)–atom and the C(3) H–atom (Figure 2.4) of analogous molecules (Figure 2.5, **26**) presents a ${}^3J^{cis}_{C-H}$ value of approximately 5.3 Hz, whereas a ${}^3J^{trans}_{C-H}$ coupling constant should have an approximate value of 11.5 Hz. Our experimental determination for ${}^3J_{C(1)-H(3)}$ was 5.5 Hz, which is in close agreement with the expected value for a *Z* (*cis*) configuration of the double bond. In a different study, for exocyclic double–bonds of 2,4–thiazolidinediones and related heterocycles (Figure 2.5, **27**), Momose *et al.*[51] reported a ^{1}H NMR chemical shift of $\delta_H \approx 7.9$ ppm for the *Z* (*cis*) alkene and of $\delta_H \approx 7.4$ ppm for its *E* (*trans*) stereoisomer. The chemical shift for the olefinic hydrogen in our synthesised compound **24** was $\delta = 7.97$ ppm. Taken together, these data support the *Z* configuration for the alkene in compound **24**. Finally, given the physicochemical and biochemical properties of the compound **24** used in the initial screening campaign and the compound synthesised in our laboratory were the same, we concluded that the alkene configuration for the commercial inhibitor was wrongly assigned and all data measurements had been made all along on the thermodynamically more stable *Z*–isomer. The same stereoisomer of hit **24** was obtained using both synthetic approaches (Scheme 2.3 or Scheme 2.4); testing the compound obtained at the end of each synthetic route provided the same results.

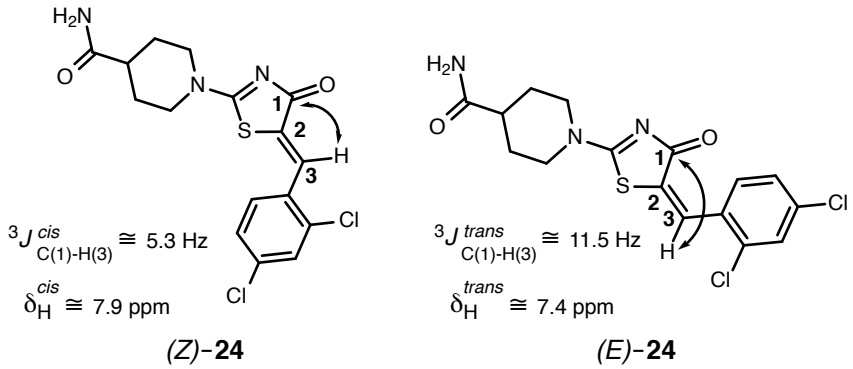

Figure 2.4: **The two possible double–bond geometries for hit 24.**

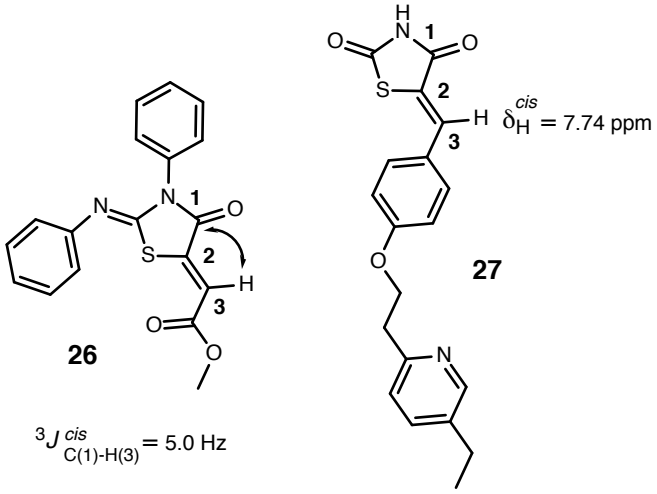

Figure 2.5: **Examples of the molecules used in the spectroscopic studies of Vogeli *et al.* (left) and Momose *et al.* (right).**

Having confirmed the double–bond geometry in the compound prepared through a Knoevenagel condensation (Scheme 2.3), we synthesised a range of analogues of inhibitor **24** with the aim of generating more potent inhibitors with improved physicochemical and pharmacokinetic properties. The structures of the analogues synthesised can be found in Table 2.1 and Table 2.2. Compounds included in Table 2.1 were synthesised at the University of Birmingham as part of this project, while compounds included in Table 2.2 were synthesised independently by our colleagues working at GlaxoSmithKline's Diseases of the Developing World Open Lab centre. $IC_{50}(\mu M)$ values contained in Table 2.1 and Table 2.2 were measured at the University of Birmingham by Ramón Soto using the assay developed by Gurcha *et al.*[17] Measurements were performed in duplicates and are shown as average values. Predicted cLog P, cLogD and cLogS values listed in Table 2.1 and Table 2.2 were calculated using ChemAxon Marvin/JChem 18.11.0.

Table 2.1: Analogues of inhibitor **24** synthesised at the University of Birmingham.

Compound	Structure	$IC_{50}(\mu M)$	clogP	clogD	clogS
36	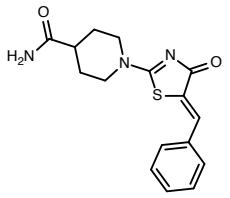	83	1.27	1.27	–4.21
37	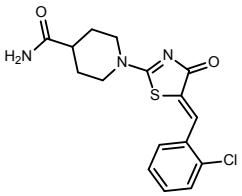	52	1.88	1.88	–4.91
38	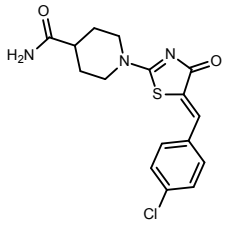	51	1.88	1.88	–4.91
24	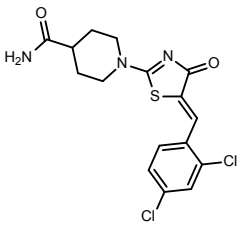	85	2.48	2.48	–5.59
39	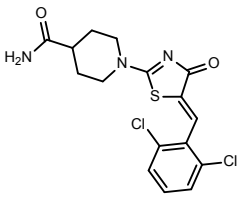	89	2.48	2.48	–5.59
40	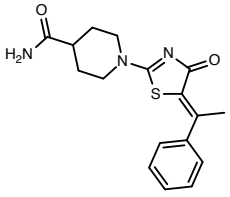	357	1.57	1.57	–4.17

Compound	Structure	$IC_{50}(\mu M)$	clogP	clogD	clogS
41	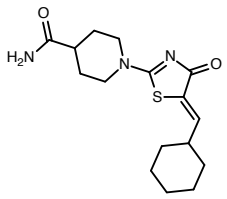	1250	1.66	1.66	–4.94
42	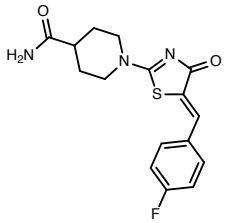	106	1.42	1.42	–4.48
43	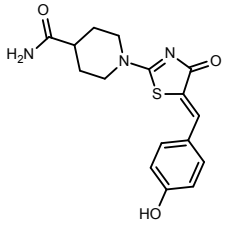	76	0.97	0.96	–3.77
44	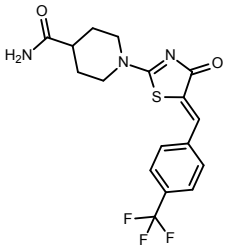	133	2.15	2.15	–5.18
45	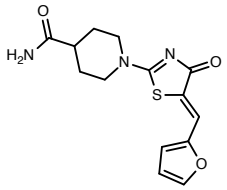	81	0.33	0.33	–3.65
46	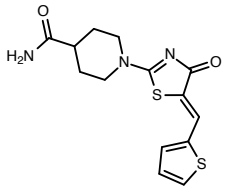	91	1.19	1.19	–4.21

Compound	Structure	$IC_{50}(\mu M)$	clogP	clogD	clogS
47	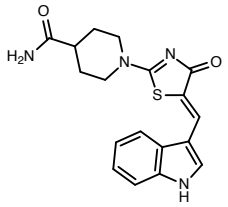	68	1.37	1.37	–4.97
48	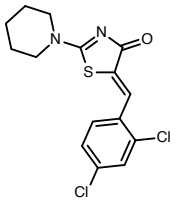	94	4.07	4.07	–6.05
49	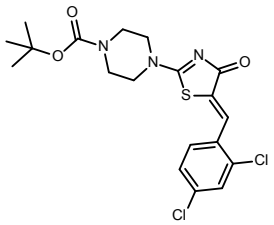	55	3.96	3.96	–6.46
50	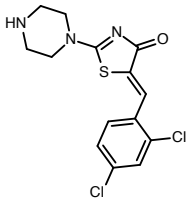	63	2.68	1.34	–3.80
51	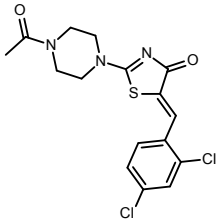	89	2.29	2.29	–5.72
52	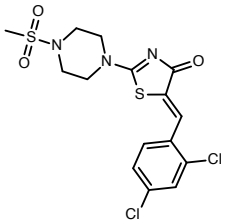	128	1.78	1.78	–5.33
53	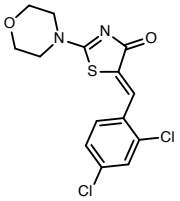	238	3.00	3.00	–5.54

Table 2.2: Analogues of inhibitor **24** synthesised at GSK.

Compound	Structure	$IC_{50}(\mu M)$	clogP	clogD	clogS
54	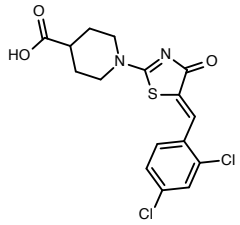	83	3.29	0.07	–2.89
55	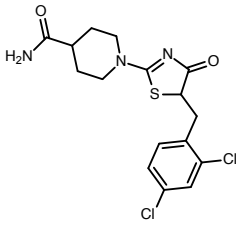	–	2.58	1.61	–3.65
56	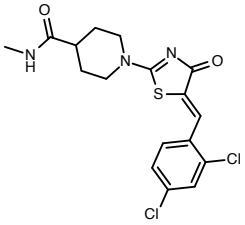	78	2.71	2.71	–5.56
57	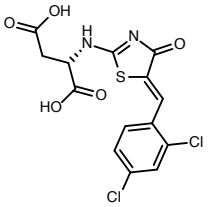	86	2.36	–3.56	0.00
58	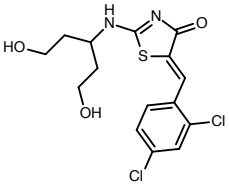	51	1.75	1.75	–4.84
59	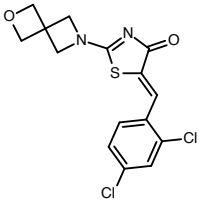	54	2.68	2.68	–5.62
60	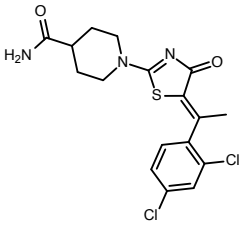	411	2.78	2.78	–5.53

Compound	Structure	$IC_{50}(\mu M)$	clogP	clogD	clogS
61	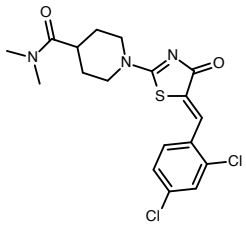	76	2.93	2.93	–5.55
62	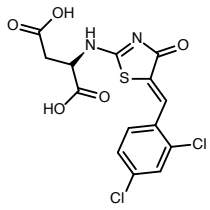	57	2.36	–3.56	0.00
63	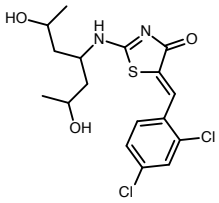	70	2.59	2.59	–5.47
64	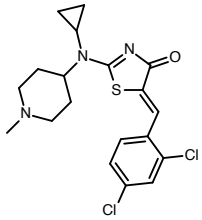	82	3.71	3.38	–5.34
65	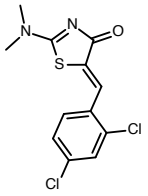	85	3.22	3.22	–5.08
67	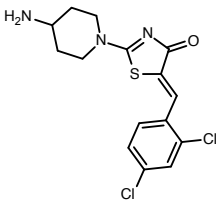	88	2.43	0.57	–3.89
68	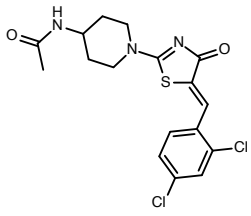	86	2.25	2.25	–6.08

All of the analogues listed in Table 2.1 and Table 2.2 were synthesised as described in Scheme 2.3 or Scheme 2.4, and were obtained in moderate or good overall yields in all cases except for analogues **40** and **41**. In the case of tetrasubstituted alkene **40**, the acetophenone starting material for the Knoevenagel condensation proved to be much less reactive than any of the aldehydes that had been employed before, and the condensation proceeded with a very low 4% yield. Alongside compound **40**,[d] unreacted starting material and uncharacterised decomposition products were also recovered. Nonetheless, the 5 mg of **40** obtained using this unoptimised method was sufficient for characterisation and biology tests. In the case of cyclohexyl analogue **41**, the Knoevenagel condensation conditions described in Scheme 2.3 were unsuccessful. These reaction conditions yielded a complex mixture of compounds among which the mass peak of the desired product was detected; however, the product could not be isolated despite several chromatography attempts. A literature search provided a different set of conditions (Scheme 2.5) employed on similar starting materials[52] that allowed us to finally obtain the desired analogue, albeit with a low yield of 12%. In this case the main obstacle was adapting and understanding the conditions from a 1920s publication that was written in German. Anyhow, despite the unoptimised conditions, alongside unreacted starting material, sufficient analogue **41** was isolated for our purposes from the reaction mixture.

[d] The stereochemistry of the product not determined; it was assigned based on previous literature examples.[50,51]

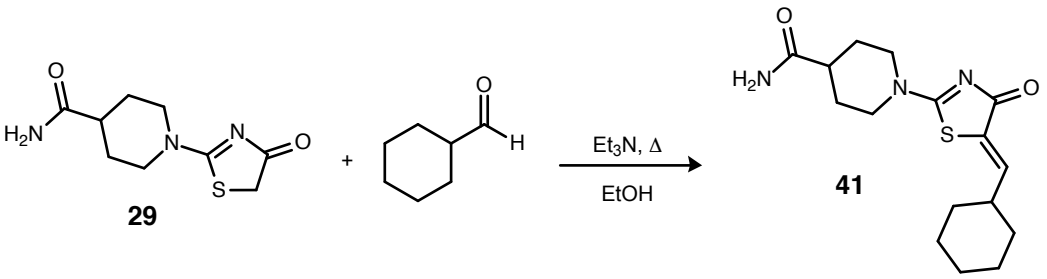

Scheme 2.5: **Final step in the synthesis of inhibitor 41.**

2.3 Discussion

In order to help establish a structure–activity relationship (SAR) between the molecules synthesised during the first stages of the project (Table 2.1 and Table 2.2) we took advantage of the enzymatic assay that had been previously developed in our group. This *in vitro* test, described in detail by Gurcha *et al.*,[17] measures the % of inhibition of *M. tuberculosis* AspRS using a concentration of 100 μM of compound and allows the determination of the IC_{50}, the concentration required to reduce the catalytic activity of the enzyme by 50%.

Analysing the properties of hit **24** summarised in Figure 2.6, the MIC_{90} and the lipophilicity as measured by Chrom logD fell within the range of values considered acceptable by GSK for a molecule at this point of a drug discovery project.[e] Therefore we initially directed our study towards improving the two properties where there was significant scope for improvement, namely IC_{50} and aqueous solubility. For these we set out target values of $IC_{50} < 1$ μM and solubility between 2.5–25 mM.

[e]GSK, similarly to other biopharmaceutical companies, utilises sets of standard parameters against which molecular properties are assessed at different stages of drug discovery projects. Those properties that fall within the expected parametric range are colour–coded as green, those outside the range but close to its limits are colour–coded orange and those properties showing divergence from the parametric range are colour–coded red.

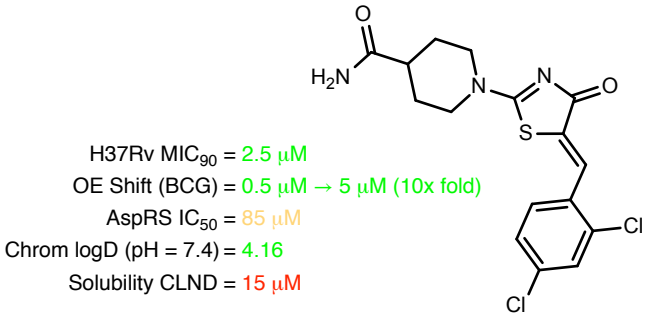

Figure 2.6: **Selected physicochemical and biological data for hit 24.**

We started by attempting to establish the importance of the chloro substituents in the aromatic ring of inhibitor **24** on its activity. To this end, analogues **36**, containing no substituent, **37**, containing just a 2–chloro substituent, and **38**, containing just a 4–chloro substituent, were examined (Figure 2.7). Of these three analogues of hit **24**, compounds **37** and **38** were the most potent, both reducing by almost 40% the concentration required to achieve the same inhibitory effect as hit **24**. It is notable that analogue **36** is just as potent as hit **24**, with an $IC_{50} = 83\ \mu M$ compared with $IC_{50} = 85\ \mu M$ for **24**, suggesting that the 2,4–dichloro substitution offers no advantages in terms of potency compared to the unsubstituted ring, although interestingly a single chloro substitution at either the *ortho* (**37**) or the *para* (**38**) position does improve potency.

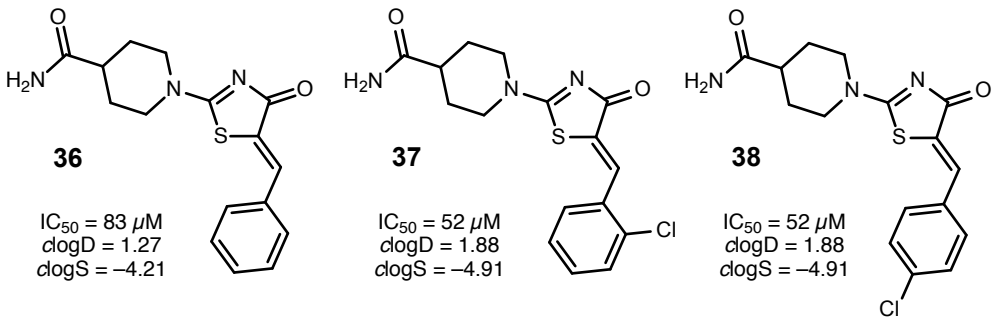

Figure 2.7: **Analogues of 24 used to probe the effect of chloro substitution on potency.**

Given the improvement in potency observed for the 4–chloro–substituted analogue **38**, we next explored whether there was any correlation between potency and the electron density around the aromatic ring as affected by chloro substituents in different positions. We modelled the electron density around the aromatic ring of hit **24** when different substitutions are made (Figure 2.8), and focused on the synthesis of further two 4–substituted analogues, specifically 4–fluoro–substituted analogue **42** and 4–hydroxy analogue **43**. Compound **42**, containing F, a smaller and more electronegative substituent than Cl, shows a similar electron density pattern around the aromatic ring as analogue **38**. On the other hand, analogue **43**, containing the hydroxy substituent, a more electronegative group than Cl but not as strong as F, presents a different electron density pattern around the aromatic ring, more similar to analogue **37** than **38**.

Analogues **42** (IC_{50} = 106 μM) and **43** (IC_{50} = 76 μM) showed lower potency than **38** (IC_{50} = 51 μM), indicating that introducing a potential hydrogen–bond donor (OH) or a smaller fluoro substituent did not strengthen the interactions between these inhibitors and the enzyme.

Next, we targeted analogues in which we altered the size of the aromatic ring and its electron density distribution by substituting the benzene ring in hit **24** with a furan (**45**, IC_{50} = 81 μM), a thiophene (**46**, IC_{50} = 91 μM) or an indole (**47**, IC_{50} = 68 μM) (Figure 2.9). Both five–membered rings present the same electron density distribution around the aromatic ring as compound **37**, our second most potent analogue (IC_{50} = 52 μM). However, the changes in the size of the aromatic ring did not produce a significant effect on the potency of the compounds, with both compounds exhibiting IC_{50} values in the same range as that of hit **24** (IC_{50} = 85 μM). Only indole analogue **47**, with a similar electron density distribution pattern around the

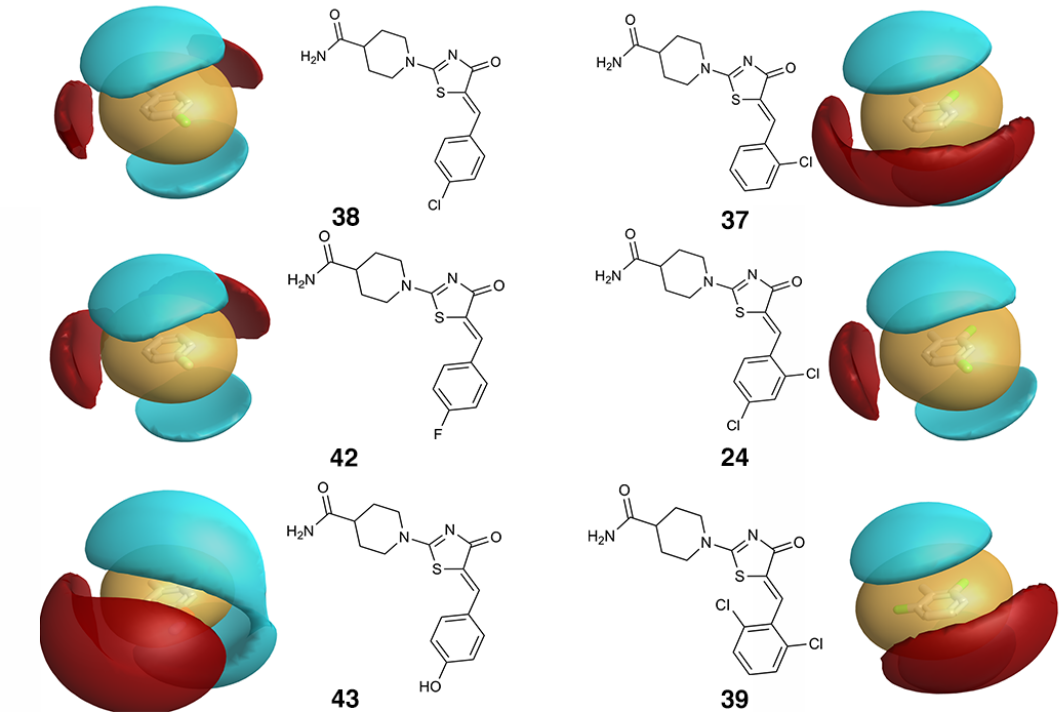

Figure 2.8: **Variation in the electron density field around the aromatic ring of hit 24 and analogues 37, 38, 39, 42 and 43.** Simulation performed using Cresset Torch Lite 10.5. The red surface symbolises the positive field around the molecule, the blue surface the negative field and the yellow surface the lipophilicity field.

aromatic ring as analogue **39**, showed a small increase in potency. However, no clear trend could be established based on the variation of the aromatic ring size and the IC_{50} values.

As discussed previously, in addition to trying to improve the potency of our hit, we also considered its other properties, and focused in particular on analogues with the aim improving aqueous solubility. This physicochemical property is especially relevant given these molecules must cross the highly lipophilic *M. tuberculosis* cell membrane, which has been a problem for other TB drug–discovery projects.[53] We hypothesised that modifications to both sides of the rhodanine core of the molecule, such as changes in functional groups, the degree of aromaticity and the size of aromatic rings colud help to

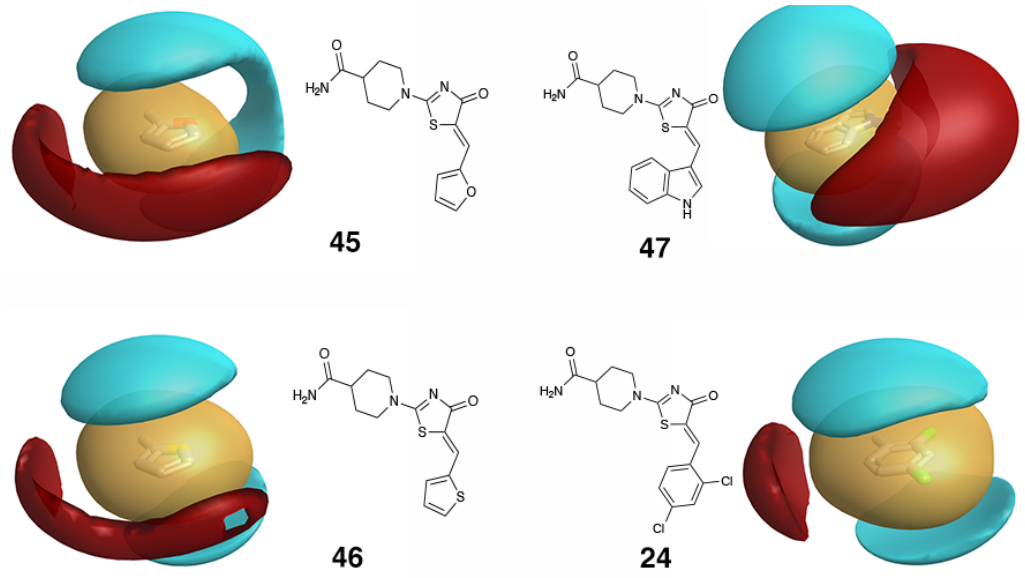

Figure 2.9: **Variation in the electron density field around the aromatic ring of hit 24 and analogues 45, 46 and 47.** Simulation performed using Cresset Torch Lite 10.5. The red surface symbolises the positive field around the molecule, the blue surface the negative field and the yellow surface the lipohilicity field.

improve the aqueous solubility. We postulated that one of the reasons behind the poor aqueous solubility of hit **24** is the planarity of the molecule due to extensive conjugation, which could lead to significant π–stacking interactions in its crystalline form and explain its high melting point: 254–255 ℃. With this in mind, we targeted analogue **39** (Figure 2.10), on the premise that positioning two bulky substituents in positions 2 and 6 of the aromatic ring would force a rotation of the aromatic ring with respect to the plane of the rhodanine core (Figure 2.11). This break in the planarity of the molecule should impede its stacking as a crystalline structure and consequently improve its solubility.[54] Although our calculated solubility (logS, Table 2.1) is the same for both compounds **24** and **39**, this is due to software limitations in interpreting the three–dimensional shape of the molecules. However, the measured melting point of **39** is 227–230 ℃, approximately 25 ℃ lower than that of hit **24**. This can be correlated with aqueous solubility through the

Yalkowsky[55] General Solubility Equation:

$$logS_w = -0.01(m_p - 25) - logP + 0.5$$

Applying this equation, logS for compound **24** is -4.28 whereas logS for analogue **39** is -4.03. This indicates that the lower melting point value observed for **39** could be caused by a weaker crystalline packing, which in turn correlates with the improved solubility calculated with the aforementioned equation. Overall, this supports our hypothesis that the solubility of hit **24** can be improved through the selective positioning of ortho substituents in the aromatic ring.

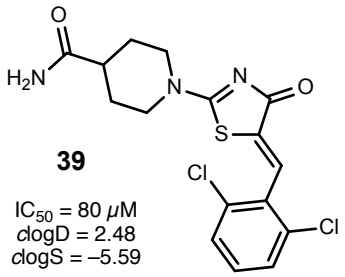

Figure 2.10: **Analogue 39 with a 2,6–dichloro substitution.**

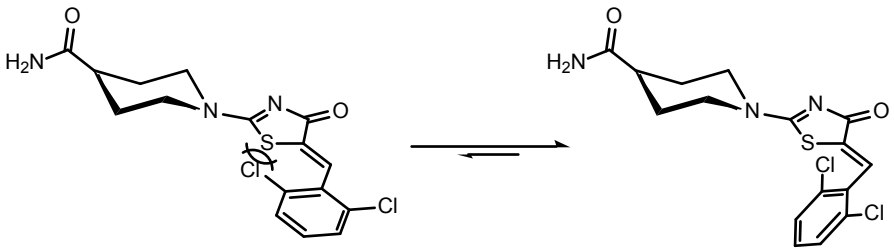

Figure 2.11: **Views of analogue 39 from the plane of the rhodanine core.**

Encouraged by this observation, we used analogue **39** in a trial to obtain AspRS–inhibitor co–crystals. Previous attempts at obtaining a co–crystal between hit **24** and the enzyme had proven unsuccessful, and we hypothesised that in part this was caused by the low solubility of our hit. The attempt to use analogue **39** proved unsuccessful as well, and no inhibitor–enzyme co–crystals were obtained. This led us to hypothesise that given the similarity of the IC_{50} measured for analogue **39** (IC_{50} = 89 μM) to that of hit **24** (IC_{50} = 85 μM), the difficulty in obtaining co–crystals might not be related to the solubility of either analogue **39** or hit **24**. It could be instead caused, among other reasons, by the low binding affinity of these compounds for the enzyme, rendering them unable to bind to the enzyme target under the crystallisation conditions. It should be noted though that if our hypothesis holds true and the equilibrium depicted in Figure 2.11 takes place, this could affect the inhibitor–enzyme interactions in the binding pocket, and even the ability of the analogue to reach this pocket, which in turn could be a reason for not obtaining the desired co–crystals. An additional observation on the IC_{50} value for **39** is that it supports our observations with analogues **36** and **37**/**38**, which suggest substitution is only effective in improving potency at specific locations in the aromatic ring; thus having 2,4– or 2,6– di–substitution does not improve potency.

A similar line of thought was followed in proposing the synthesis of analogue **41** (Figure 2.12), where the aryl ring was replaced with a cyclohexyl group with the idea that increasing the C_{sp^3} ratio of the molecule would increase its solubility.[56] Although both the calculated solubility and partition coefficient for analogue **41** (clogS = –4.94, clogD = 1.66) show values closer to the desired range established by GSK than hit **24** (clogS = –5.59, clogD = 2.48), the IC_{50} value measured for **41** (IC_{50} = 1250 μM) showed a steep

reduction in potency. This result was interpreted as a requirement for an aromatic moiety in that position of the molecule in order to interact with the enzyme, and as a result no additional aliphatic analogues were investigated.

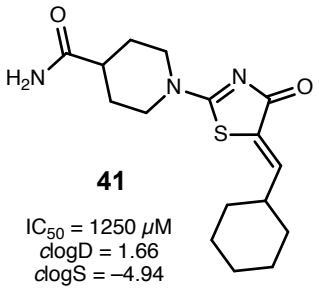

Figure 2.12: **Structure of analogue 41.**

At this point we had explored two different analogues, namely **39** and **41**, in an attempt to improve solubility by altering the planarity of hit **24**. However, although both analogues showed an improvement in this physicochemical property, neither compound demonstrated increased inhibitory activity against our target enzyme. Therefore we next focused on the substituted piperidine part of hit **24** in an effort to improve the solubility of our analogues. Our hypothesis in this case was to test whether possible hydrogen bonding interactions involving the primary amide group were at least in part responsible for the high melting point of hit **24**, and therefore indirectly responsible for its low solubility. To this end, we first assessed the corresponding secondary (**56**, clogS = –5.56, clogD = 2.71) and tertiary (**61**, clogS = –5.55, clogD = 2.93) methyl amides (Figure 2.13). The predicted solubility and partition coefficient values for these two compounds are in the same range as **24** (clogS = –5.59, clogD = 2.48), while their potency showed a small increase, with IC_{50} values of 78 μM and 76 μM, respectively.

A more promising result was observed when polar groups such as hydroxyl or amino substituents were introduced through analogues **50** (clogS = –

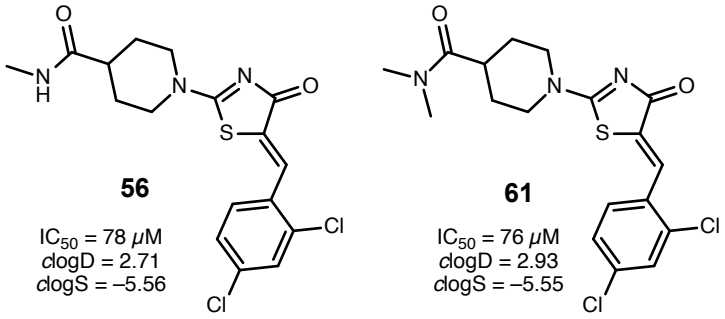

Figure 2.13: **Structures of analogues 56 and 61.**

3.80, clogD = 1.34), **58** (clogS = –4.84, clogD = 1.75), **59** (clogS = –5.62, clogD = 2.68) and **62** (clogS = 0.00, clogD = –3.56) (Figure 2.14). All of these analogues show similar or better solubility and lipophilicity values than hit **24** (clogS = –5.59, clogP = 2.48), supporting our hypothesis that introducing polar groups in the piperidine region of the molecule should result in more soluble compounds. In addition, all of these analogues displayed an improvement in potency: **50** (IC_{50} = 63 μM), **58** (IC_{50} = 51 μM), **59** (IC_{50} = 54 μM) or **62** (IC_{50} = 57 μM). These results suggest that introducing polar moieties into the piperidine part of hit **24** not only has a positive impact on solubility, but also provides a mechanism for introducing functional groups that strengthen the interaction between these compounds and the target enzyme.

This idea is further supported by analogues **48** (IC_{50} = 94 μM) and **65** (IC_{50} = 85 μM) (Figure 2.15), in which the carbonyl functionality in hit **24** has been removed, resulting in a decrease in potency compared with the molecules in Figure 2.14. We therefore hypothesise that a functional group that can participate in hydrogen bonding interactions with the enzyme such as the amide of hit **24** makes important interactions with the enzyme, as evidenced by the improvement in potency observed with the introduction of hydroxy groups in compounds **58** or carboxylate groups in **62**.

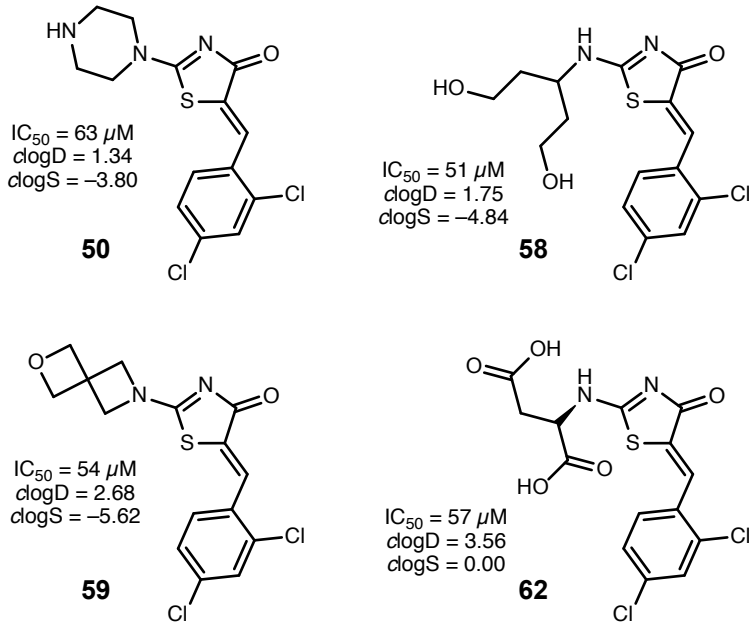

Figure 2.14: **Structures of analogues 50, 58, 59 and 62.**

However, the presence alone of polar groups in the piperidine side of the rhodanine core of hit **24** does not guarantee a more potent compound. Comparing structurally similar analogues, we see similar values of solubility and lipophilicity for **50** (IC_{50} = 63 μM, clogS = –3.80, clogD = 1.34) and **67** (IC_{50} = 88 μM, clogS = –3.89, clogD = 0.57) or **58** (IC_{50} = 51 μM, clogS = –4.84, clogD = 1.75) and **64** (IC_{50} = 82 μM, clogS = –5.34, clogD = 3.38) but a disparity in the IC_{50} values. Those compounds such as **67** and **64** where the C_{sp^3} ratio has increased, together with the introduction a polar group, exhibit lower potency. This indicates that perhaps a size threshold has been reached beyond which that part of the molecule no longer fits properly into the binding pocket of the enzyme and consequently the potency decreases.

At this point in the project we found ourselves analysing an unclear SAR; the series of analogues analysed thus far had provided no clear path towards making further structural changes to improve potency. More concerning, when our GSK collaborators reduced the exocyclic double bond of hit **24**

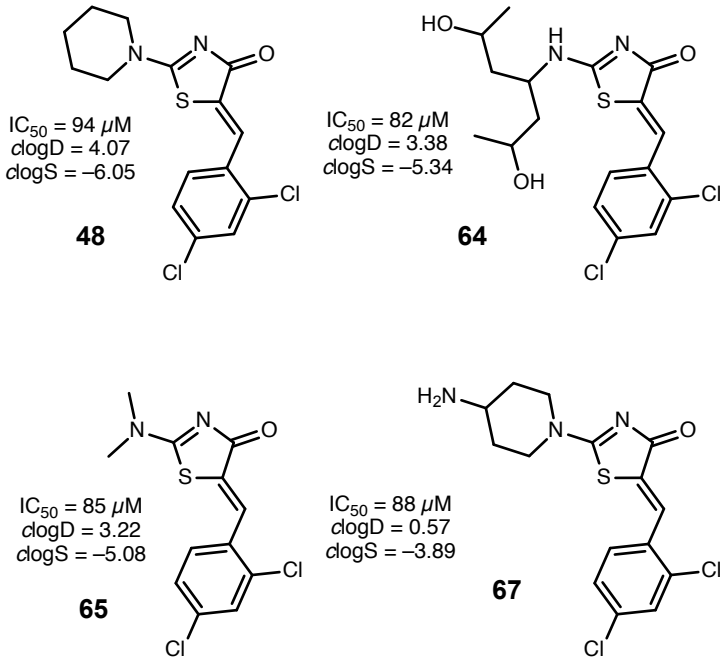

Figure 2.15: **Structure of analogues 48, 64 (meso starting material), 65 and 67.**

to a single bond in analogue **55** (Figure 2.16), this molecule proved to be completely inactive.

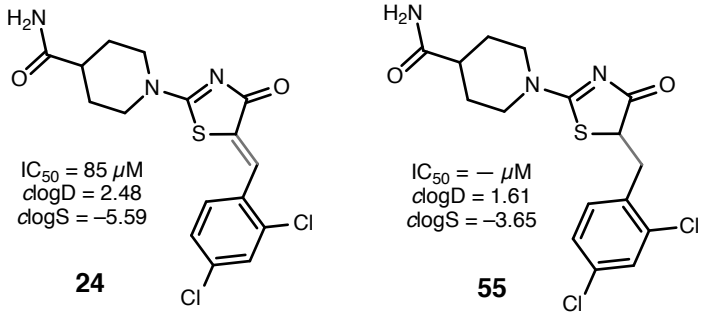

Figure 2.16: **Structure of analogue 55.**

This result was unexpected. We had chosen to reduce the double bond in hit **24** in order to increase the flexibility of the molecule. Based on the calculated properties of **24** (clogS = –5.59, clogD = 2.48) and **55** (clogS = –3.65, clogD = 1.61), we expected to observe an increase in the solubility of the molecule whilst not necessarily having a dramatic affect on activity.

However, the complete inactivity of analogue **55** made us consider the possibility that the exocyclic double bond might be acting as a Michael acceptor in our *in vitro* assays.[57] If so, this would represent a potential liability for the further development of this series of compounds, as these compounds could potentially react with the organism before reaching the target enzyme, AspRS.

Given the literature precedent for similarly conjugated double bonds acting as Michael acceptors[57] we decided to investigate blocking this hypothetically reactive site through steric hindrance. To this end we synthesised analogue **40** (Figure 2.17), postulating that the tetrasubstituted alkene would be less susceptible to nucleophilic addition. The drop in the potency of analogue **40** (IC_{50} = 357 μM) would support this hypothesis, although there are other possible explanations. In order to probe this behaviour further, we synthesised analogue **70**, in which the double bond would be maintained in a similar position to the alkene in hit **24** but its potential electrophilicity would now be blocked through its incorporation into an aromatic ring (Figure 2.18).

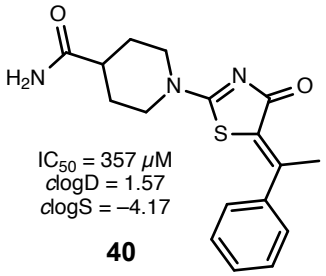

Figure 2.17: **Structure of analogue 40.**

Changing the core of the molecule from a rhodanine to a pyridine–thiazole required a different synthetic strategy for this analogue. Our retrosynthetic analysis of **70** is outlined in Scheme 2.6. By breaking first the piperidine–thiazole C–N bond, we could potentially introduce variability in the last step of the synthesis. Next, breaking the C–C bond between the phenyl ring and

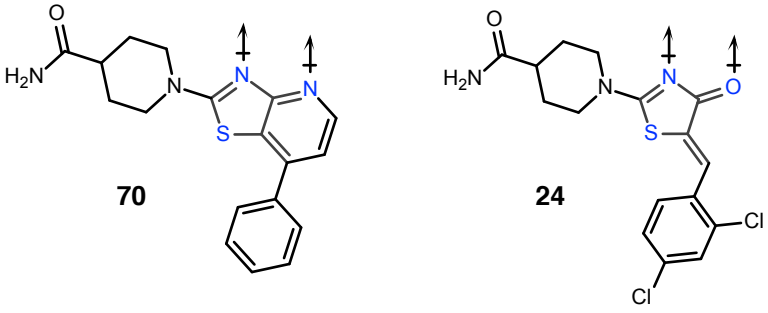

Figure 2.18: **Similarities between the rhodanine–based core in 24 and the alternative pyridinethiazole–based core in 70.** Hydrogen–bond acceptor sites are annotated with arrows.

the thiazole moiety would lead us to a halogenated pyridine–thiazole, which we postulated could in turn be synthesised from a halogenated 2–amino–pyridine.

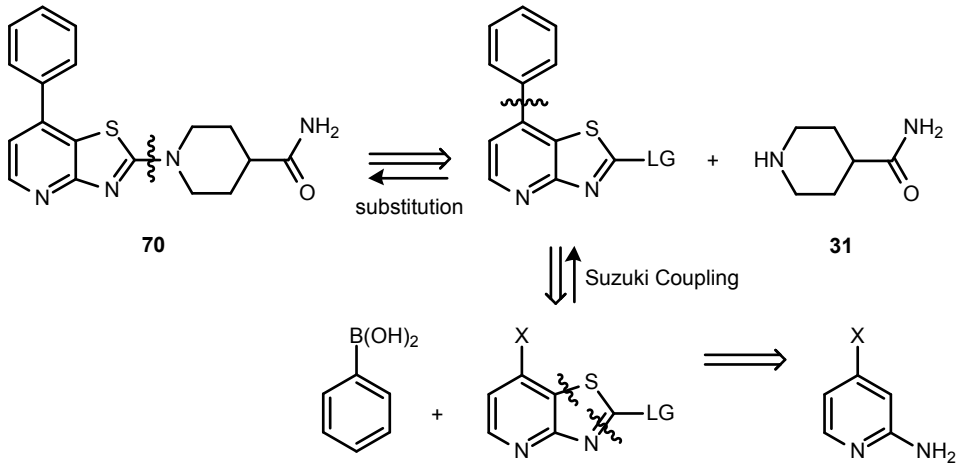

Scheme 2.6: **Retrosynthetic analysis for the pyridinethiazole–based analogue 70.**

A literature review of the various methods that have been reported for synthesising pyridine–thiazoles identified a procedure developed by Bethge *et al.*[58] starting from amino–pyridine **71** (Scheme 2.7). Thus, our synthesis began with a low–yielding Suzuki coupling between chloropyridine **71** and phenylboronic acid, which provided the biaryl skeleton for subsequent modifications. The amino group in the biaryl product was next acylated

to afford the corresponding pivaloyl amide in a yield of 95%. Dithiocarbamate **72** was synthesised in 78% yield in a one–pot two–step reaction involving *ortho*–lithiation followed by reaction of the lithiated intermediate with tetraethylthiuram disulfide (TETD). Cyclization of amide **72** under basic conditions provided pyridine–thiazole **73** in 41% yield. Under these conditions the amide is first hydrolysed. The resulting free amine attacks the dithiocarbamate moiety. Methylation of pyridine–thiazole **73** to obtain sulfide **74** (88% yield) created the same leaving group used in the the synthesis of **24**, which in this case was displaced with piperidine **31** under microwave irradiation to obtain pyridine–thiazole analogue **70** in a yield of 77%.[59] Overall the synthesis proceeded with good yields, except for the initial Suzuki coupling, where we suspect that the presence of the free amine in the starting material, capable of poisoning the Pd catalyst, was the main reason for the low yield. We hypothesised that if necessary, inverting the initial steps, *i.e.* pivaloyl protection followed by Suzuki coupling, could be an alternative to try if additional analogues were necessary.

Analogue **70** proved inactive against AspRS, which provided further support that the exocyclic double bond in hit **24** plays an active role in the mechanism of action of our inhibitor family. At the same time as this last synthesis was being performed, analysts at GSK tested inhibitor **24** and analogue **55** in an assay against glutathione (GSH) reactivity. In this assay, compounds **24** and **55** were each incubated in human–liver microsomes supplemented with GSH, followed by LC/MS analysis of the metabolites formed during the incubation. In the case of hit **24**, the GSH–addition adduct was detected in the analysis, whereas no GSH–addition adduct was observed for analogue **55**. To confirm this observation and in order to produce the conjugate addition product in sufficient quantities to allow full characterisation,

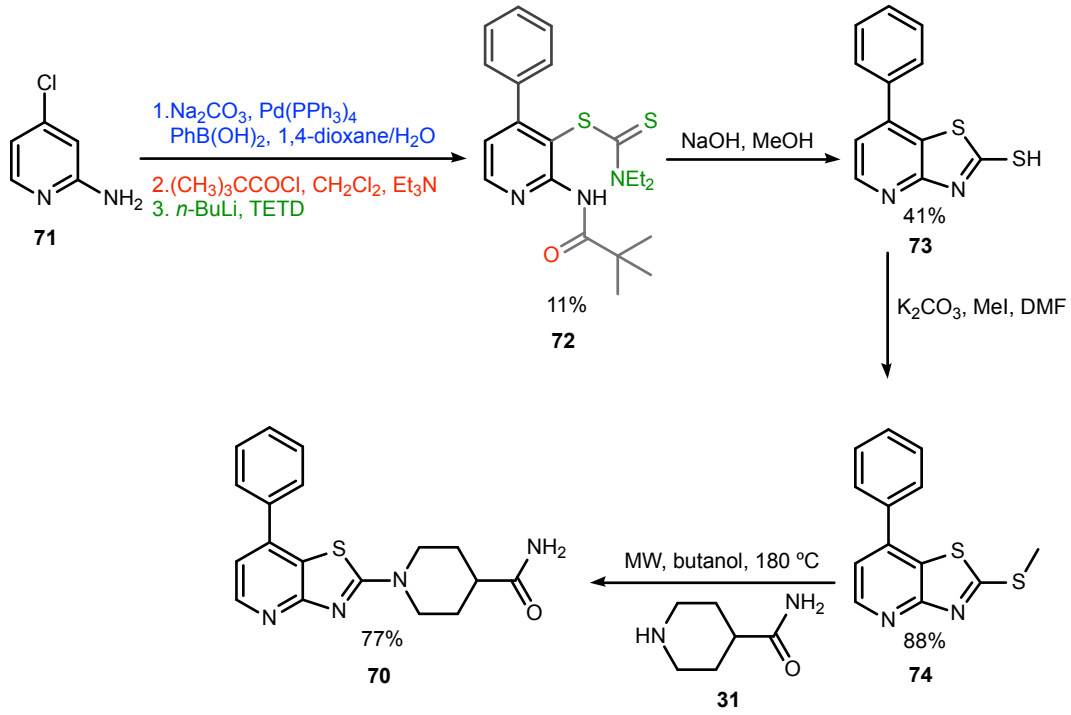

Scheme 2.7: **Synthesis of pyridinethiazole–based analogue 70.**

we tried to experimentally replicate the conjugate addition of GSH to hit **24** under the same buffer conditions used in the assay performed at GSK. However, we observed no trace of product formation. Whilst at odds with the result obtained in the GSH assay, it should be noted that under the assay conditions, the enzymes contained within the liver microsomes could potentially facilitate this reaction, which more closely mimics a real *in vivo* case than an experiment using only chemical reagents. Based on the GSH assay results performed at GSK, it was concluded that hit **24**, and presumably its analogues, could react with GSH in the liver through its exocyclic double bond, thus leading to potential hepatotoxicity issues if administered in humans. These issues would be especially relevant for long term treatments as is the case with TB. After consultation with our GSK collaborators, it was decided to halt the development of hit **24** from a medicinal chemistry perspective.

At this stage of the project it was clear that our SAR study had been unsuccessful in providing a clear path towards developing inhibitors with improved potency and physicochemical properties. We had designed a flexible synthetic procedure that had allowed us to explore a wide range of molecular variability around the hit, and most compounds had been synthesised with reasonably good yields. However, we did not achieve a significant improvement in potency and the results obtained in the biological assays when the exocyclic double bond was reduced raised a clear alert regarding the viability of further developing this hit optimisation programme. Hit compound **24** and the analogues synthesised were therefore deemed unsuitable for further structural optimisation, so we instead chose to take a more chemical biology approach and explore in more detail the biological interactions of hit compound **24** in order to better understand its mode of action.

Chapter 3

Tool Compounds for Mode of Action Studies

3.1 Introduction

The unclear SAR of hit **24** presented in the previous chapter forced us to reconsider the next steps in this project. We therefore opted to explore the way our family of hit compounds interacts with AspRS, our target enzyme, and other mycobacterial enzymes. In particular we decided to pursue two different paths:

- creating a photoaffinity probe that could covalently bind the target enzyme. This would allow us to obtain a protein–hit conjugate that after proteolysis and sequence analysis will be compared with the crystal structure of the enzyme in order to identify the binding pocket.

- creating a biotin–tagged tool compound that could probe the whole–cell behaviour our hit **24** (Figure 3.1). This would help asses the promiscuity of our hit molecule, a particularly important feature to consider given that rhodanine has been classified as a PAINS scaffold.[42]

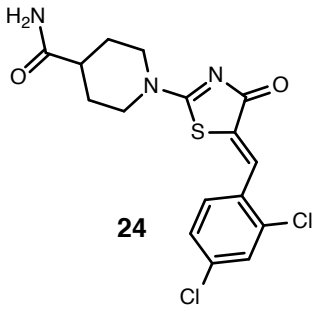

24

Figure 3.1: **Structure of hit 24.**

3.2 Biotin–based Probe

The glutathione–trapping experiment discussed in Chapter 2 had left open the possibility that our family of inhibitors are acting as Michael acceptors at a cellular level, and could therefore react in this way with other proteins than our target. This observation falls within the larger, and currently ongoing, debate as to whether the rhodanine scaffold present in hit **24** should be considered a PAINS structure and therefore eliminated from screening libraries.[45,42] We therefore decided to test this hypothesis by designing an experiment that could provide an insight into which other proteins, if any, might interact with our hit once it crosses the bacterial cell–wall. After discussing plausible strategies with our microbiology colleagues and exploring literature methods, we decided the best option would be a pull–down experiment where the hit would first be incubated with bacterial cell lysate and then recovered from the lysate together with any bound proteins. In order to recover the hit–bound proteins from the cell lysate, it would be necessary to modify the chemical structure of hit **24**, for instance through the addition of a tag. In this sense, given previous literature examples employing *M. tuberculosis*[60] and other bacteria,[61,62] we decided to biotinylate our hit and exploit the high affinity of biotin for streptavidin in a pull–down experiment

using streptavidin–coated beads.[63]

Biotin (Figure 3.2) is an ideal tag because, providing it is incorporated into a region of the molecule that is remote from the pharmacophore, its small size (244 Da) makes it unlikely to interfere with the functions of the original molecule. We can then exploit the interaction between biotin and streptavidin[a] (Figure 3.3), which is one of the strongest non–covalent interactions known ($K_d = 10^{-14}$ M).[65] Biotin and streptavidin have a high affinity and specificity for one another, their binding is fast, and their union is resistant to heat and the pH conditions within a cellular environment. This has led to the use of the biotin–streptavidin interaction in a wide range of applications from labelling, immobilization and purification of biological molecules to the study of protein–protein interactions in living cells.[64]

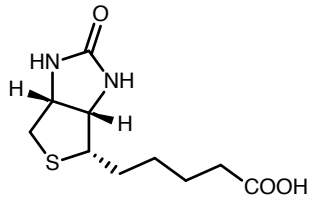

Figure 3.2: **Structure of biotin.**

This methodology has proven to be robust enough to be considered a standard protocol in chemical proteomics[63], used for the analysis of protein modifications across most species used in normal research settings. For instance a specific example can be found in the work of Liu *et al.*,[61] which showed that fluorophosphates, known inhibitors of serine hydrolases, when biotinylated, can be employed to study the behavior of mammalian serine hydrolases directly from crude cell and tissue samples, in the presence of related enzymes such as cysteine or aspartyl hydrolases. They achieved this by tagging fluorophosphates (Figure 3.4) with biotin, followed by incubation

[a]Streptavidin is a 52.8 kDa protein that forms a tetramer, with each monomer capable of binding one biotin molecule or biotinylated compound.[64]

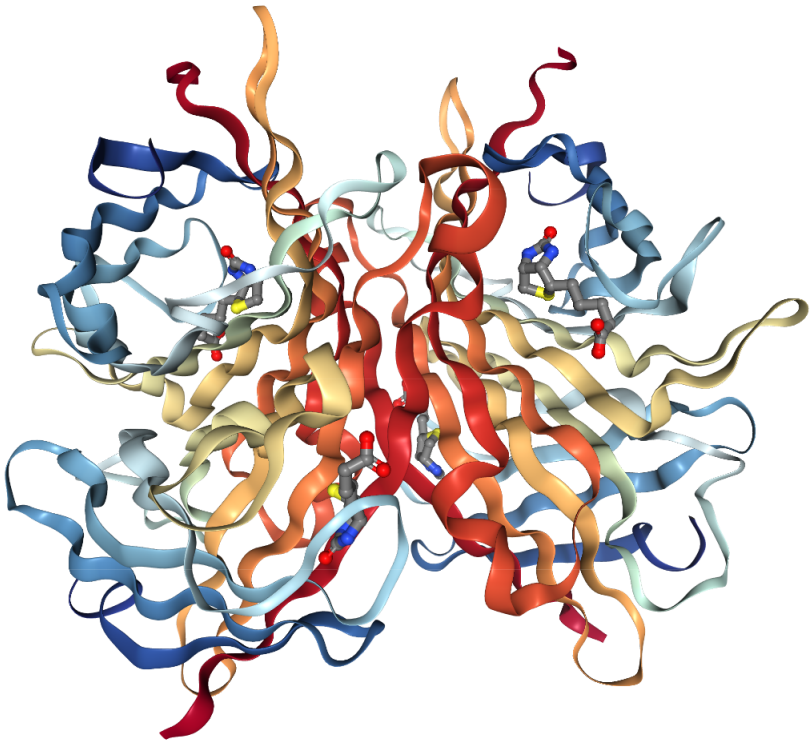

Figure 3.3: **Crystal structure of streptavidin isolated form *Streptomyces avidinii* attached to four molecules of biotin.** Adapted from RSCB Protein Databank entry 1MK5.[66]

in cellular media and by separation of the target proteins through biotin–streptavidin affinity and analysis on SDS–PAGE gels.

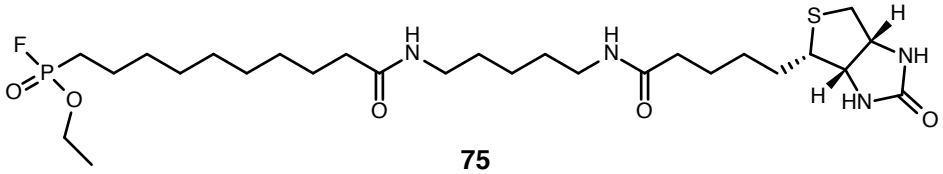

75

Figure 3.4: **A biotin–tagged fluorophosphate used in the work of Liu *et al.*** [61]

Another example of the utility of biotin tagging can be found in the work of Thompson *et al.*,[62] who used biotin in probes that bind to specific amino acids, in particular arginine, in both folded and unfolded proteins (Figure 3.5). In this case, taking advantage of the specificity of the probes, the biotin tag allows the probes to be used in monitoring protein expression, which in certain cases can be associated with disease progression.[67] Alternatively, tagging the probes with biotin is an initial step in increasing molecular complexity which can lead to the preparation of useful protein–drug conjugates.[62]

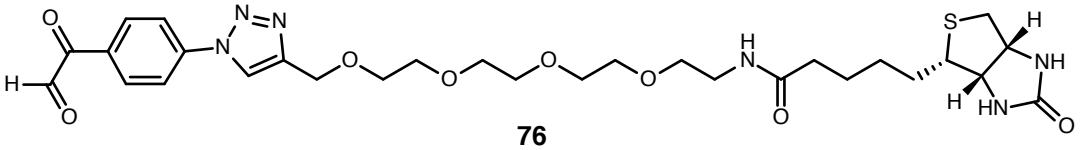

76

Figure 3.5: **A biotinylated probe employed by Thompson *et al.*** [62]

Of particular relevance to this project is the work of Zhao *et al.*,[60] who employed a biotin–streptavidin affinity approach in an attempt to identify the *M. tuberculosis* targets of agrimorphol[b] (Figure 3.6). Using *M. bovis BCG* as a surrogate for *M. tuberculosis*, they first incubated biotinylated agrimorphol and related biotinylated analogues in bacterial cell lysate. Then, taking advantage of the affinity between streptavidin and biotin, they extracted the tagged compounds from the cell lysate, and the proteins they had bound to. In doing so, they were able to separate the proteins that interacted with their compounds from the remaining cellular proteins and subsequently analyzed these proteins to identify the targets of agrimorphol.

[b]Agrimorphol is a phloroglucinol from *Agrimonia pilosa*, a plant whose extracts have been used in traditional Chinese medicine to treat pulmonary infections. The compound was shown to kill *M. tuberculosis in vitro* by disrupting the homeostatic control of intrabacterial pH.[60]

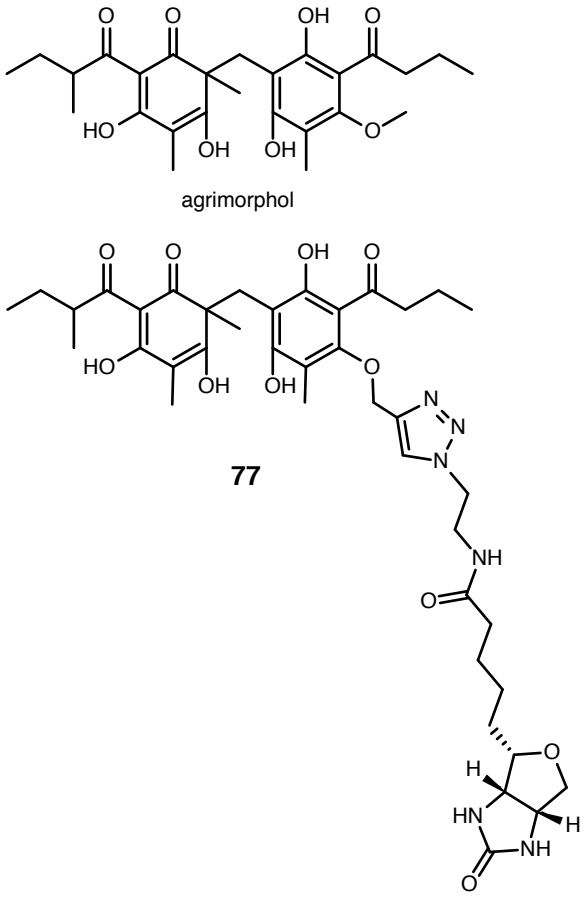

Figure 3.6: **Structure of agrimorphol and biotinylated agrimorphol.** Rendered with the stereochemistry shown in the work of Zhao *et al.*[60]

The work of Zhao *et al.* shares a similar purpose to ours, since our starting hypothesis is that by incubating a biotinylated analogue of hit **24** in mycobacterial cell lysate, we would be able to separate the proteins that interact with our hit from the remaining bacterial proteins. To this end we explored two options for attaching the biotin tag, namely the aromatic region of our hit and the primary amide. Since our SAR had been unclear, we decided to explore both options and make a decision on which path to follow after evaluating the activity of the intermediates we would be synthesising. Given the potency of analogue **38** with a 4–chloro substitution pattern in the aromatic ring, we initially explored attaching the biotin tag in that position.

Following the synthetic route depicted in Scheme 3.1, we synthesised analogue **83** containing an azide as a *para* substituent in the aromatic ring.

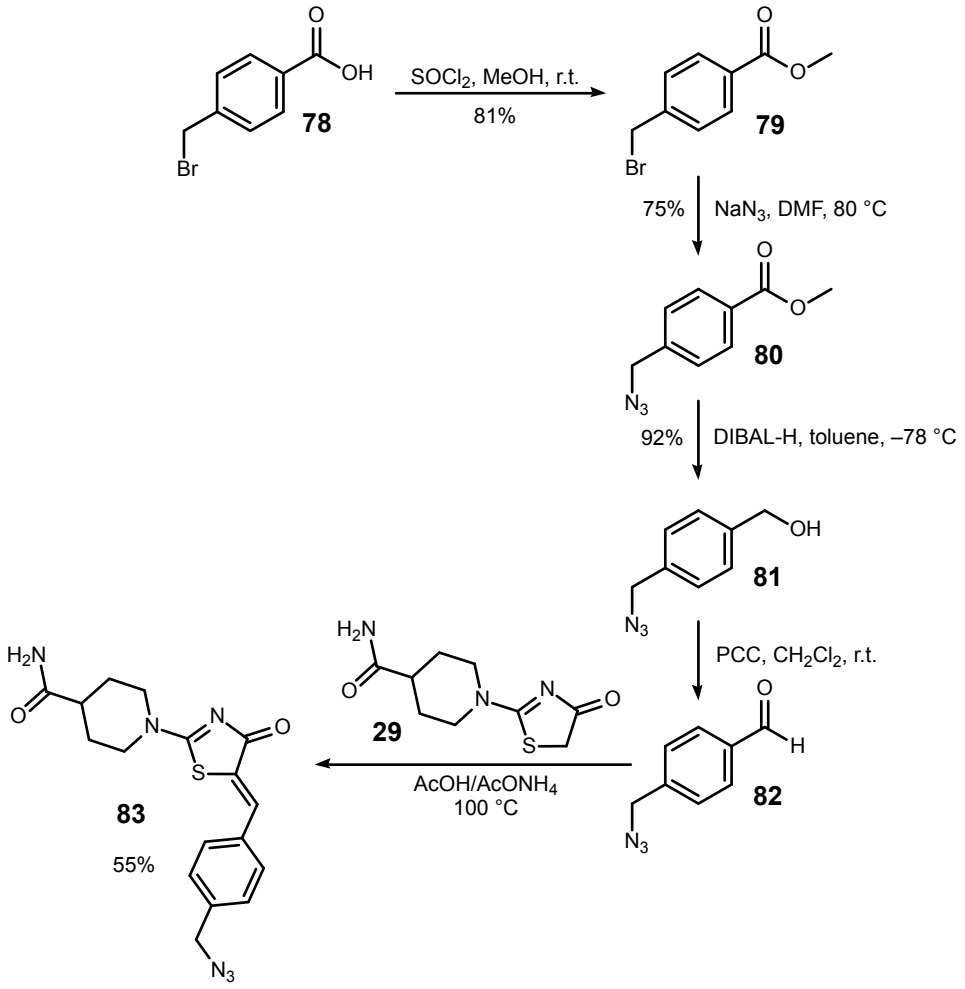

Scheme 3.1: **Synthetic pathway for analogue 83.**

The synthesis of azide analogue **83** (30% yield over 5 steps) was relatively straightforward from synthetic point of view. The first step consisted in the esterification of acid **78** to provide ester **79**. The bromide substituent of this product was then displaced using NaN_3 with DMF as solvent under relatively mild conditions to provide azide **81**. The ester functional group of this azide was then reduced to the corresponding alcohol to provide azide **81**. The alcohol contained in azide **81** was then oxidized to an aldehyde, providing azide **82**. Finally, when submitted to the Knoevenagel condensation

conditions previously optimised in our group, azide **82** reacted with amide **29** to provide azide analogue **83**. Despite this, experimentally, the handling of azides made the work challenging, with special safety measures used in particular for compound **82**. Because of its relatively low molecular weight, azide **82** was deemed to possess a significant risk of explosion and was never isolated from solution, rather it was used without purification or isolation.

Our alternative placement for the biotin tag on hit **24** led us to the synthesis of azide analogue **89** according to the sequence depicted in Scheme 3.2.

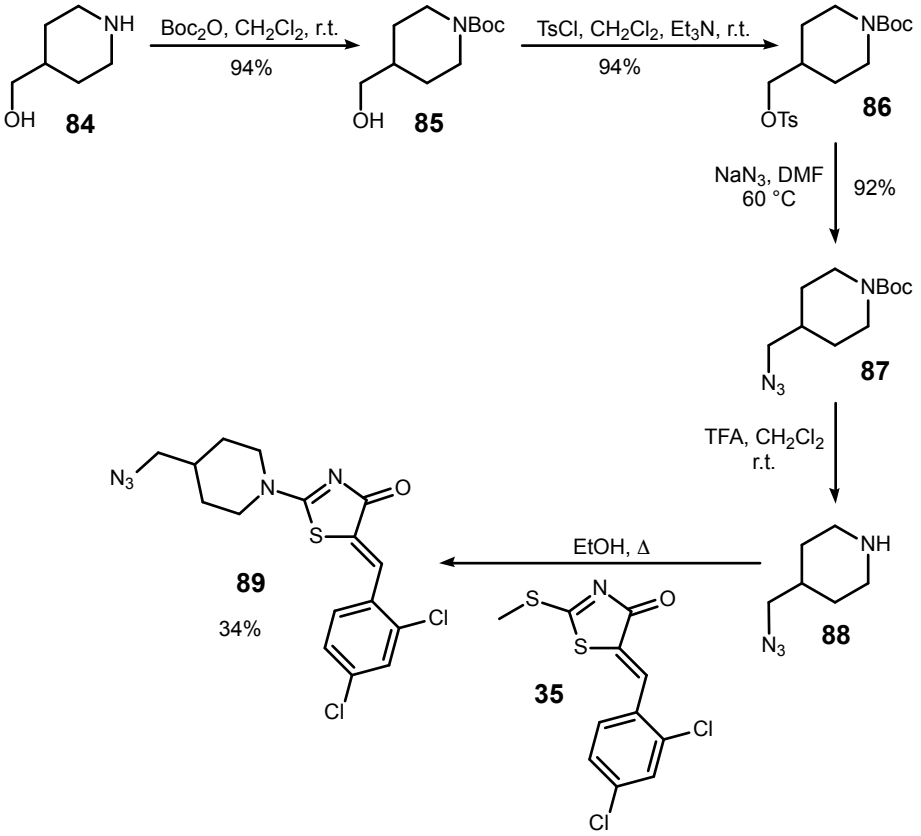

Scheme 3.2: **Synthetic pathway for analogue 89.**

Azide **89** was obtained with slightly lower overall yield (27% over 4 steps) than analogue **83**. The synthesis started with the protection of piperidine **84** as a carbamate to obtain alcohol **85**. This alcohol was in turn reacted with TsCl to provide tosylated alcohol **86**. The tosyl group of compound **86**

was displaced using NaN_3 to obtain azide **87**. Finally, the Boc protecting group in **87** was removed under acidic conditions to obtain azide **88** which was reacted without being isolated in order to obtain azide analogue **89** through sulfur displacement. Similarly to the synthesis of azide **83**, the only remarkable difficulty was the careful handling of azide intermediates, especially intermediate **88** which as mentioned was used without isolation as a solution in CH_2Cl_2.

Both analogues **83** and **89** were tested in our enzymatic assay against AspRS, with compound **83** showing and IC_{50} = 104 μM and compound **89** an IC_{50} = 714 μM. Compared with hit **24** (IC_{50} = 85 μM), analogue **83** therefore presented a similar potency, whereas compound **89** has a much weaker affinity for the target enzyme. Based on these enzymatic activity results we therefore decided to focus our efforts on developing analogue **83** into the biotinylated analogue that would we would then use in the pull–down experiments.

As shown in the literature examples presented above (Figure 3.4 and Figure 3.5), the biotin tag and the molecule are usually separated by a linker that reduces the potential interference of the biotin moiety in the interaction of the hit molecule with its target. In our case, using a linker that allows sufficient flexibility in the movement of the tagged molecule was especially important. Since we had no crystal structure of hit **24** interacting with AspRS, we do not know whether the interaction takes places at the surface of the enzyme or in a binding pocket within it. We therefore had to make sure the hit analogue had enough conformational flexibility so that its interaction with the enzyme would not be constrained by the presence of the biotin tag. Analysing literature examples[61,62] and commercial availability of biotin and building blocks, we opted for a biotin–PEG4 structure as a

linker. From a biological point of view, polyethylene glycol (PEG) linkers are non–toxic and non–immunogenic, thus perfectly suited for our purpose, and from a structural point of view they are aqueous–soluble and conformationally highly flexible. Additionally, the terminal alkyne would allow us to attach the biotin tag to our molecule through the known copper azide alkyne cycloaddition click reaction previously utilised in our research group.[68]

Biotinylated analogue **90** was synthesised in one step from azide **83** with a yield of 82%. As described in Scheme 3.3, an aqueous solution of $CuSO_4$ was used as the source of copper for the azide–alkyne cycloaddition reaction. When submitted for testing in our enzymatic assay, this compound provided an inconclusive result and its IC_{50} value could not be determined. We suspect this was caused by difficulties in handling the molecule and perhaps solubility issues, as the testing results were not reproducible. Similarly, its whole–cell activity could not be measured and was determined to be over MIC_{90}>80 μM. This should not be interpreted as the compound displaying no whole–cell activity; rather, as 80 μM is the cut–off line set for GSK for this assay, it means its MIC_{90} is higher than 80 μM. This result was not unexpected. In fact we hypothesised that such a large compound with a hydrophilic PEG chain would find it difficult to cross the highly hydrophobic mycobacterium cell wall, resulting in only small amounts of compound **90** being available within the cytosol to disrupt the bacterial cell functions.

With biotinylated analogue **90** in hand, we progressed to the microbiology. The first step was to design a protocol for incubating our biotinylated hit with *M. bovis* BCG cell lysate. This was done in collaboration with our microbiology colleagues from industry using the work of Zhao *et al.*[60] as a basis for our design. Additionally, we also had a number of existing protocols used at GSK that could be adapted to our specific purpose. Since our tar-

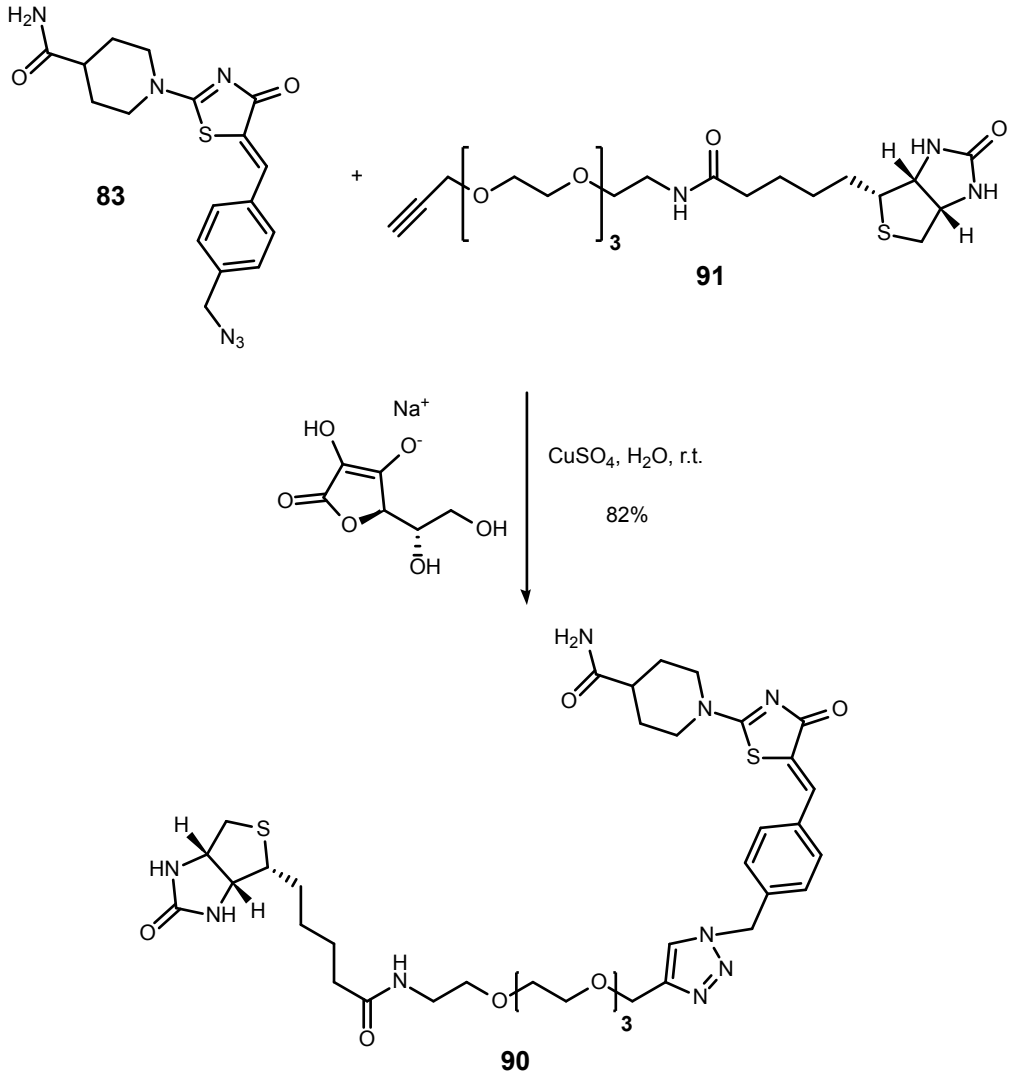

Scheme 3.3: **Synthesis of biotinylated analogue 90.**

get protein (AspRS) is found in the cytosol, we had to prepare a cell lysate containing only cytosolic proteins, therefore discarding cell–membrane proteins. Moreover, since we planned to exploit the strong interaction between biotin and streptavidin to separate the proteins that interacted with our hit, it would be necessary to remove endogenously biotinylated proteins from the cell lysate in order that these proteins would not interfere with our experiment. In both cases, new protocols, presented in the experimental section, were re–written to include the additional steps required for our purposes.

Guided by the new protocols, the next steps taken involved culture and growth of *M. bovis* and preparation of cell lysate from these bacteria. Once the fresh cell lysate was obtained, endogenously biotinylated proteins were removed by washing with streptavidin. We next proceeded with the incubation of compound **90** with the lysate. Following literature precedent[60] and the recommendations of microbiologists in our team, we adjusted the protein concentration in the lysate to 1 mg/mL. At the outset, given we had no clear indication of the strength of the interaction between analogue **90** and our target enzyme, we decided to use two different concentrations of compound in the incubation procedure: 500 μM and 1000 μM. After incubating biotinylated hit **90** with bacterial cell lysate at room temperature for 1 hour, we proceeded to the extraction of the biotinylated analogue **90** with the addition of streptavidin.

In order to facilitate the experimental work we opted to use streptavidin immobilized on magnetic beads (GE Healthcare Streptavidin Mag Sepharose, Figure 3.7) rather than the more commonly used streptavidin attached to agarose beads. These magnetic beads, designed for small–scale purification of biotinylated biomolecules, allow an easy separation of biotinylated compounds present in the lysate solution using a magnet, avoiding lengthy centrifugation steps and possible loss of material.

In this way, those proteins that were bound to analogue **90** were separated from the cell lysate. The resulting streptavidin beads were then washed with aqueous buffer to remove any proteins that could have been dragged through any unspecific binding. The streptavidin–biotin interaction was then broken by heating at 90 ℃, a procedure that also denatured the proteins that had arrived at this point. This process meant the proteins could be directly loaded on SDS–PAGE gels. We decided to use this well–known technique

Figure 3.7: **Streptavidin Mag Sepharose vials (left) and magnet containing rack for separating magnetic beads from aqueous solutions (right). ©GE Healthcare**

because of its relative rapidity and ease of use and because it would allow us to compare the molecular weight of the proteins interacting with compound **90** with that of AspRS used as a reference. This would provide us with a quick qualitative way of determining the presence of AspRS or other proteins interacting with analogue **90**. At a later stage, if the preliminary results obtained through this technique were encouraging, more specific techniques for protein identification could be used.

The SDS–PAGE gels obtained are presented in Figure 3.8, and were encouraging. In wells *A* and *D*, analogue **90** was incubated with a wild–type, or standard, strain of *M. bovis* BCG at a concentration of 500 μM and 1000 μM, respectively. It can be observed that in both of these wells a protein sample was obtained from the pull–down experiment with a similar size to AspRS when compared to the reference size ladder in well *H*. Moreover, given the intensity of the spot serves as a qualitative measure of the amount of protein present in the gel, when using a higher concentration of analogue **90**, a higher concentration of protein sample seems to be obtained. Nonetheless, at this point, it is not possible to determine definitively whether the proteins observed in wells *A* and *D* are AspRS, since other proteins of similar size could

also have been pulled–down. We therefore repeated the experiment, this time performing the incubation with a strain of *M. bovis* that over–expresses AspRS. This would allow us to see if for a determined concentration of analogue **90** (*i.e.* 500 μM and 1000 μM), having more AspRS present in the cytosol leads in turn to more protein being extracted after the incubation. As can be observed when comparing wells *C* and *A*, and wells *F* and *D*, wells *C* and *F*, corresponding to the AspRS over–expressing strain of *M. bovis* BCG do seem to contain more protein sample than wells *A* and *D*, respectively. These observations provide a preliminary indication that AspRS might indeed be the major protein obtained in these pull–down experiments, although this would need to be confirmed by alternative methods such as protein recognition using specific antibodies. Finally, wells *B* and *E* contain a strain of *M. bovis* BCG modified with the same plasmid used to over–express AspRS, but in this case the plasmid is empty, not codifying the expression of any protein. This serves as a control to verify that the presence of the plasmid does not alter the behaviour of the wild–type bacteria. The results in wells *B* and *E* should therefore be the same as in wells *A* and *D*. As can be observed in Figure 3.8, this is true except for the lower apparent concentration in well *E*, which, we attribute to an experimental error when loading this well.

The most significant observation from all these pull–down combinations explored in the gel in Figure 3.8 is that analogue **90** seems to interact with a single protein (or perhaps different proteins of the same size), but not with a wide range of proteins of different sizes. In turn, when translated to hit **24**, this would imply that it does not interact with a wide range of proteins and therefore might not behave as a promiscuous inhibitor. This is in line with the observations of Mendgen *et al.* regarding the rhodanine scaffold in the larger PAINS debate.[45] Although rhodanine–based compounds, and

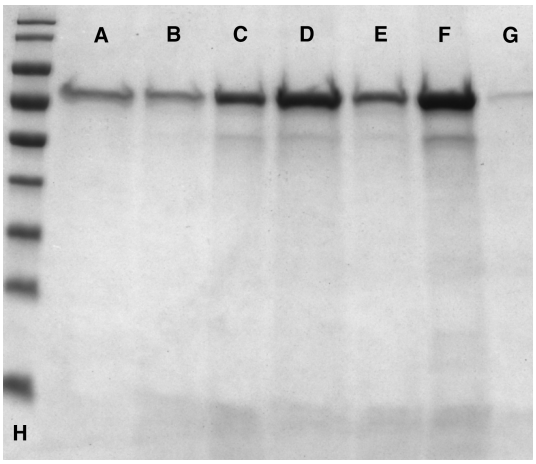

Figure 3.8: **SDS–PAGE gel obtained after incubating analogue 90 in cell lysate of different strains of *M. bovis***. A: wild–type strain, compound 500 μM; B: strain containing an empty plasmid, compound 500 μM; C: AspRS over–expressing strain, compound 500 μM; D: wild–type strain, compound 1000 μM; E: strain containing an empty plasmid, compound 1000 μM; F: AspRS over–expressing strain, compound 1000 μM; G: pure AspRS reference; H: protein size reference ladder.

especially benzylidene rhodanines such as hit **24**, tend to bind to a large number of targets, they do so with weak or moderate affinity.[45] It can be argued that, as proven by the rhodanine–based marketed drugs described in Chapter 1, this should not be interpreted as a lack of specificity or promiscuity, but as a chance to establish clear cut criteria for candidate development (*e.g.* nanomolar affinity); those rhodanine–based compounds that pass these criteria can be, and have been, developed successfully to clinical stages.

At this point, encouraged by the results obtained so far, we decided to try and confirm whether the protein pulled–down when incubating biotinylated analogue **90** with *M. bovis* cell lysate, of similar size to reference AspRS, was indeed out target enzyme. To this end, we repeated the incubation experiment in the same conditions as before, and after confirming the reproducibility of the results by SDS–PAGE gel analysis, we performed a Western blot, incubating both the pulled–down protein and the reference AspRS with an antibody capable of specifically recognising AspRS (Figure 3.9).

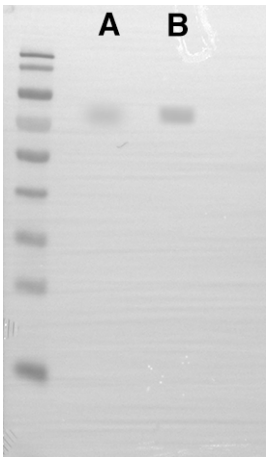

Figure 3.9: **Superposed protein size ladder and Western blot result of incubation of analogue 90 at a concentration of 1000 μM (A) and reference AspRS (B).**

Whilst limitations in the amount of antibody available meant that we could not perform the Western blot on all combinations from the gel in Figure 3.8, the result from Figure 3.9 shows that the protein obtained in the pull–down experiment when incubating with biotinylated analogue **90** at a concentration of 1000 μM is indeed AspRS. The AspRS polyclonal antibody used in the Western blot binds the pure AspRS and the protein obtained from the pull–down experiment in the same fashion, confirming the equivalence between both proteins.

The result obtained from the pull–down experiment using the biotin–streptavidin system adapted to our hit molecule validates our initial hypothesis. Although hit compound **24** could potentially act as a promiscuous compound, neither the incubation experiment described here nor the chemical reactivity testing explained in Chapter 2 seem to indicate such behaviour. It should be noted however, that these experiments indicate a lack of promiscuity within bacterial cells. We do not discard the possibility that such behaviour might be observed under different settings. For instance, when undergoing liver metabolism, where activation can promote the reactivity

of hit **24** as a Michael acceptor, the compound could react promiscuously leading to cytotoxicity issues.

3.3 Photoaffinity Labelling

One of the main hurdles we encountered throughout our hit–optimisation project (Chapter 2) was the lack of a crystal structure of AspRS and hit **24**. Such a structure could have helped to guide us in the development of new analogues. As the project shifted towards a chemical–biology path, we decided to seize this opportunity and try to determine the binding mode of hit **24** with AspRS by means of alternative techniques. It is in this context that we explored the possibility of photoaffinity labelling.

Photoaffinity labelling is a technique introduced in the 1960s that involves the use of a probe which in the presence of light produces a highly reactive species that then undergoes a reaction with a biological receptor (*e.g.* a protein or DNA) at the site of interaction.[69] This strategy requires the incorporation of a photo–labile group within an otherwise reversibly binding ligand of the biological receptor. This technique has been used for many purposes: study of protein–ligand interactions, identification of unknown targets of ligands, elucidation of protein structures, monitoring protein functions and conformational changes, and the identification of novel binding sites in proteins (Figure 3.10).[70]

This methodology has the advantage that the covalent bond formed between the ligand and protein upon photoactivation is created in a non–selective way, allowing any amino acid in the binding site to be tagged. This was a critical feature to consider in our case, since we had no knowledge of the specific molecular interactions between hit **24** and its protein

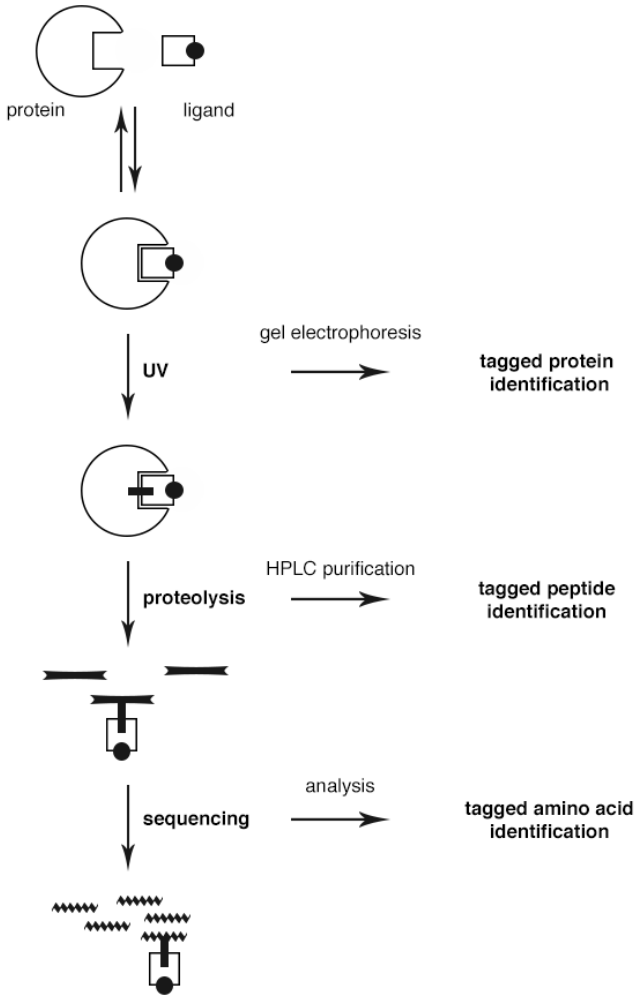

Figure 3.10: **Scheme of protein identification options available through photoaffinity labelling.**

target. Our working hypothesis was that we could use this methodology to form a covalent bond between our hit molecule **24** and its target protein (AspRS). We would subsequently enzymatically degrade this protein–hit conjugate through proteolysis and use mass spectrometry analysis to compare the fragment sequence with that obtained from the enzymatic degradation of the pure protein. This would then allow us to discover which part of the amino acid sequence the hit molecule is covalently bound to. We could then exploit the crystal structure of AspRS to identify the binding site and

through the aid of computational docking studies build a 3D model of the enzyme–hit interaction that could then be used for rational drug design.

The most commonly used functional groups for photoaffinity labelling are aryl azides, benzophenones and aryl diazirines.[71] For instance, Zhang *et al.* have synthesised a benzophenone–based probe (**92**, Figure 3.11) while attempting to use photoaffinity labelling to identify the target proteins of oleanoic acid.[72] After confirming the activity of their probe against phosphorylase RMGPa, a known target of oleanolic acid, they incubated the probe in the soluble proteasome from HepG2 cells and after photoirradiation, were able to capture two currently unidentified proteins of 40–50 kDa.[72] Kotake *et al.* have prepared aryl diazirine–based photoaffinity probes of pladienolides (**93**, Figure 3.11), natural products exhibiting *in vitro* and *in vivo* anti–tumour activity. Using a combination of techniques, they identified the main target of this class of natural products after treating fractionated HeLa cells with the photoaffinity probe. This allowed them to demonstrate that pladienolides inhibit mRNA splicing, discovering a potentially novel anti–tumour drug target.[73] Similarly, Jessen *et al.* chose an aryl azide photoaffinity probe (**94**, Figure 3.11) to identify the target of their apoptosis–inducing drug MX–126374, which they discovered was a protein implicated in IGF–IIR signalling, highlighting the promise of targeting IGF–IIR signalling in cancer treatment.[74]

Whilst a range of photosensitive groups have been proven useful for photoaffinity labelling, we opted to investigate the aryldiazirine option, specifically to use a 3–phenyl–3–(trifluoromethyl)diazirine (Figure 3.12). The aryl diazirine functionality is often a preferred choice for a number of reasons, which include its chemical stability and the wavelength required for its photoactivation (350–355 nm).[70,71] In comparison, aryl azides are typically

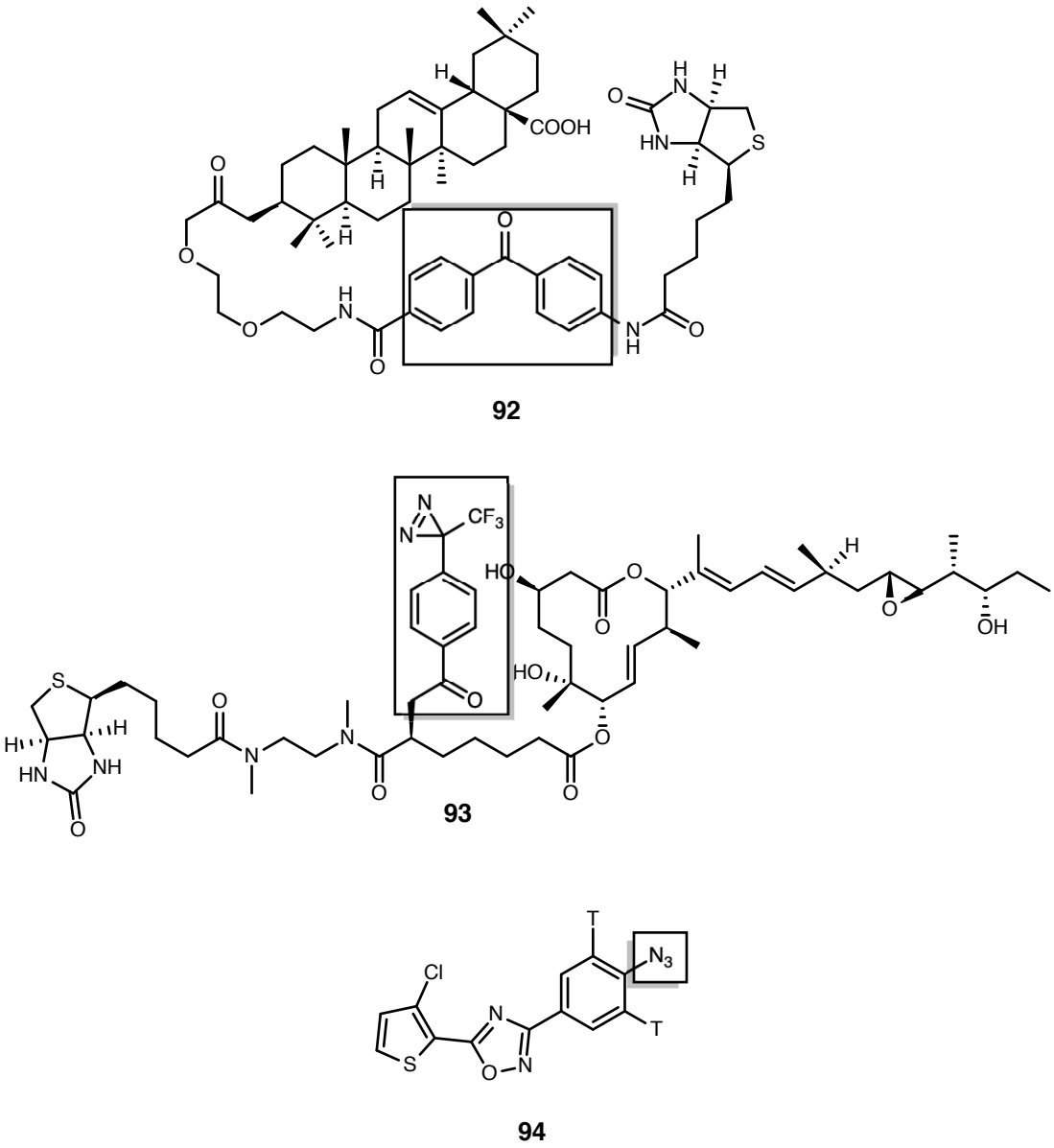

Figure 3.11: **Structure of the probes used by Zhang *et. al* 92, Kotake *et. al* 93 and Jessen *et. al* 94.** Photosensitive groups are highlighted. Compounds are rendered with the stereochemistry shown in the corresponding publication.[72,73,74]

photo–activated using wavelengths below 300 nm.[71] Given proteins absorb UV light at 280 nm (aromatic amino acids) and 200 nm (peptide bonds), irradiation at short wavelengths can damage biomolecules and should be minimised.[70] This was confirmed through irradiation studies comparing the

aforementioned three photophore types in living cells. The long irradiation times needed for incorporation into cell–membrane surface biomolecules in the case of azide and benzophenone active species caused cell death, whereas no such negative impact was observed using 3–phenyl–3–(trifluoromethyl)diazirines as reactive carbene precursors.[71]

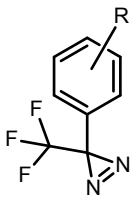

Figure 3.12: **General structure of 3–phenyl–3–(trifluoromethyl)diazirines.**

An additional advantage of using aryl–diazirines is that they produce singlet–state carbenes upon photoirradiation. Whilst their high reactivity means carbenes are normally quickly quenched by water, which can be a disadvantage in terms of photoaffinity yields, it can also be regarded as advantageous, since it minimizes non–specific binding. Finally, one practical disadvantage, particularly when compared to benzophenones, is that aryl diazirines are relatively more difficult to prepare.[70]

Once the photo–labile functional group was selected, we next had to choose its placement within the structure of our hit molecule. Based on our previous experience attaching a biotin tag, we opted for the *para* position of the aromatic ring of hit **24**, a position in which we had previously observed that different substitutions are tolerated without causing a significant reduction in potency compared with the hit compound. Therefore, following literature precedent such as the work of Delfino *et al.*,[75] we designed the synthetic route depicted in Scheme 3.4 as the path to follow in order to obtain diazirine analogue **102**.

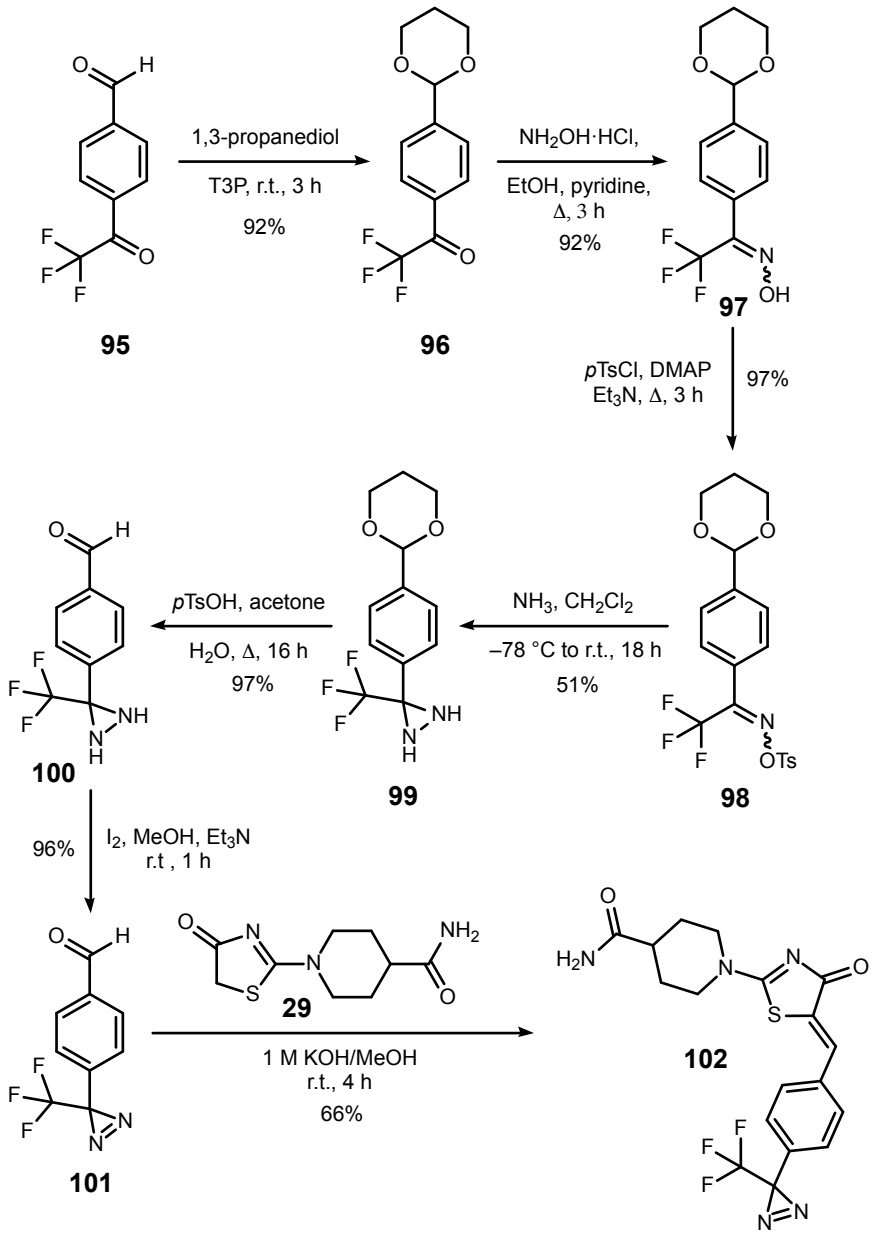

Scheme 3.4: **Synthesis of diazirine analogue 102.**

Analogue **102**, containing a 3–aryl–3–(trifluoromethyl)diazirine as the photo–labile moiety, was synthesised in seven steps with a 27% overall yield. Although most steps were performed without complications, obtaining good yields, there were two notable exceptions, namely the incorporation of the diaziridine moiety using NH_3 gas, and the Knoevenagel condensation in the final step. We attribute the moderate yield in the formation of diaziridine **99**

to the difficult experimental setting for achieving this transformation. The reaction was performed in a steel, pressure–resistant vessel that could only be cooled by submersion into a dry ice/acetone bath. This cooling method was not particularly efficient and did not allow a direct control of the reaction temperature, which combined with the difficulty in controlling the gas flow into the reactor, provided varying yields of diaziridine when the transformation was repeated. The oxidation of diaziridine **100** to diazirine **101**, was achieved in good yield; however special care was taken to protect the product from light in order to avoid its premature decomposition and to avoid loss of starting material and product through evaporation caused by their volatility. The most challenging step however, proved to be the Knoevenagel condensation to obtain the final product product **102**. To effect this transformation we explored different Knoevenagel condensation variations of our previous methodology that had been used to successfully synthesise analogues of hit **24**. However, we quickly discovered that using heat or acidic conditions did not provide the expected product. It was only after a literature review on condensation conditions and the stability of diazirines that we identified conditions for performing this condensation while maintaining the stability of the diazirine in the work of Takanori *et al.*[76] As can be seen in Scheme 3.4, final product **91** was synthesised at room temperature instead of the high temperature (*i.e.* 100 ℃) used to synthesise hit **24**, and instead of glacial AcOH as solvent, we used a dilute solution of KOH. Finally, in the synthesis of oxime **97** and tosyl oxime **98**, we observed the formation of both stereoisomers in a ratio of 1:1, and both products were used as mixtures without attempting to separate the isomers.

Having obtained diazirine analogue **102**, the next step was to perform a photoconjugation with freshly purified AspRS. However, we first needed to

make sure the experimental conditions we had chosen were appropriate for our purposes. We first recorded the UV–Vis spectrum of analogue **102** (Figure 3.13) which confirmed that its absorbance range did not shift significantly from the expected 350 nm value for diazirines reported in literature.[71] As can be seen in Figure 3.13 our analogue shows an absorbance peak with a $\lambda_{max} = 368$ nm. We next compared these absorbance data with the spectral distribution provided by the manufacturer of our UV lamp in order to make sure the UV light emitted by the lamp coincided with the same range of absorbance of our compound (Figure 3.14). Comparing Figure 3.14 and Figure 3.13, the strongest emission by the UV lamp falls around 350 nm, where our analogue **102** shows a significant UV absorbance peak.

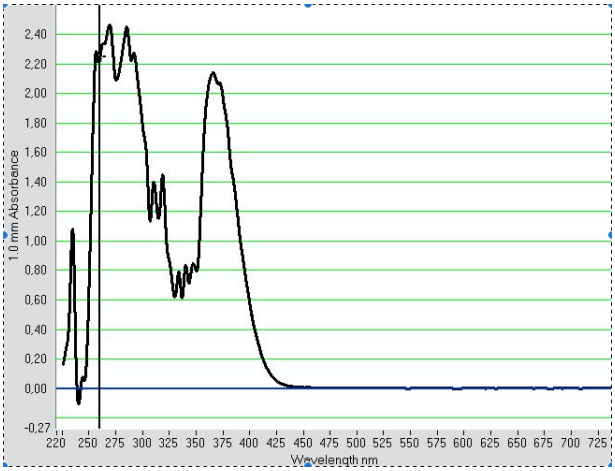

Figure 3.13: **UV-Vis spectrum of analogue 102.**

As mentioned previously, proteins also absorb UV light, which can lead to their degradation. We did not want the irradiation time of our conjugation experiment to be long enough to cause significant photodegradation of our target protein. We therefore studied the behaviour of diazirine analogue **102** when irradiated with UV light in a DMSO solution at the same concentration that we expected to perform the incubation with our target protein, *i.e.* 100 μM. The reaction was monitored by ^{19}F–NMR spectroscopy and the results

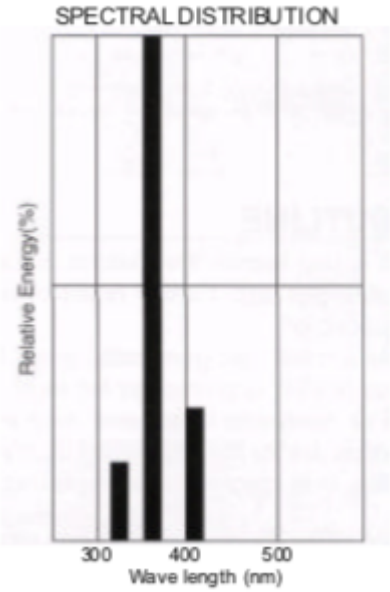

Figure 3.14: **Spectral distribution of the 4 W UV lamp used to irradiate analogue 102.**

are presented in Figure 3.15. As can be observed, after approximately 120 minutes of irradiation, analogue **102** had decomposed entirely. Using the quadratic fit function of Wolfram Mathematica® 7 we estimated the time required for its concentration in solution to be half of the initial value at approximately 66 minutes. The decomposition of the starting material was quantified in relation to an initial impurity contained in the sample corresponding to the small peak at approximately –68 ppm next to the starting material peak. The relation between the integration of the newly formed products and the integration of the impurity peak is plotted in Figure 3.16. As the starting material peak disappears over time, the integral ratio of the newly formed product with the purity used as an internal standard increases, suggesting the formation of multiple decomposition products corresponding to the peaks between –80 and -90 ppm after 2 hours of irradiation.

With this information in hand we finally proceeded to the incubation of diazirine analogue **91** with AspRS. The samples were incubated at room tem-

perature for 1 hour at a concentration of 100 μM of compound and 1 mg/mL of protein. After this time, as exemplified in Figure 3.17, the samples were irradiated with a 4 W FL4 BLB type UV lamp for 2 hours. The experiment was carried out in a specially conditioned fumehood with darkened crystals to avoid solar light contamination. The samples were situated at 5 cm from the UV light source and the experiment was performed as two replicates. An additional sample of pure AspRS was submitted to the same procedure as control for possible protein degradation. All samples were finally frozen at -80 ℃ and shipped to the University of Birmingham for proteolytic cleavage and analysis. This analysis is currently ongoing.

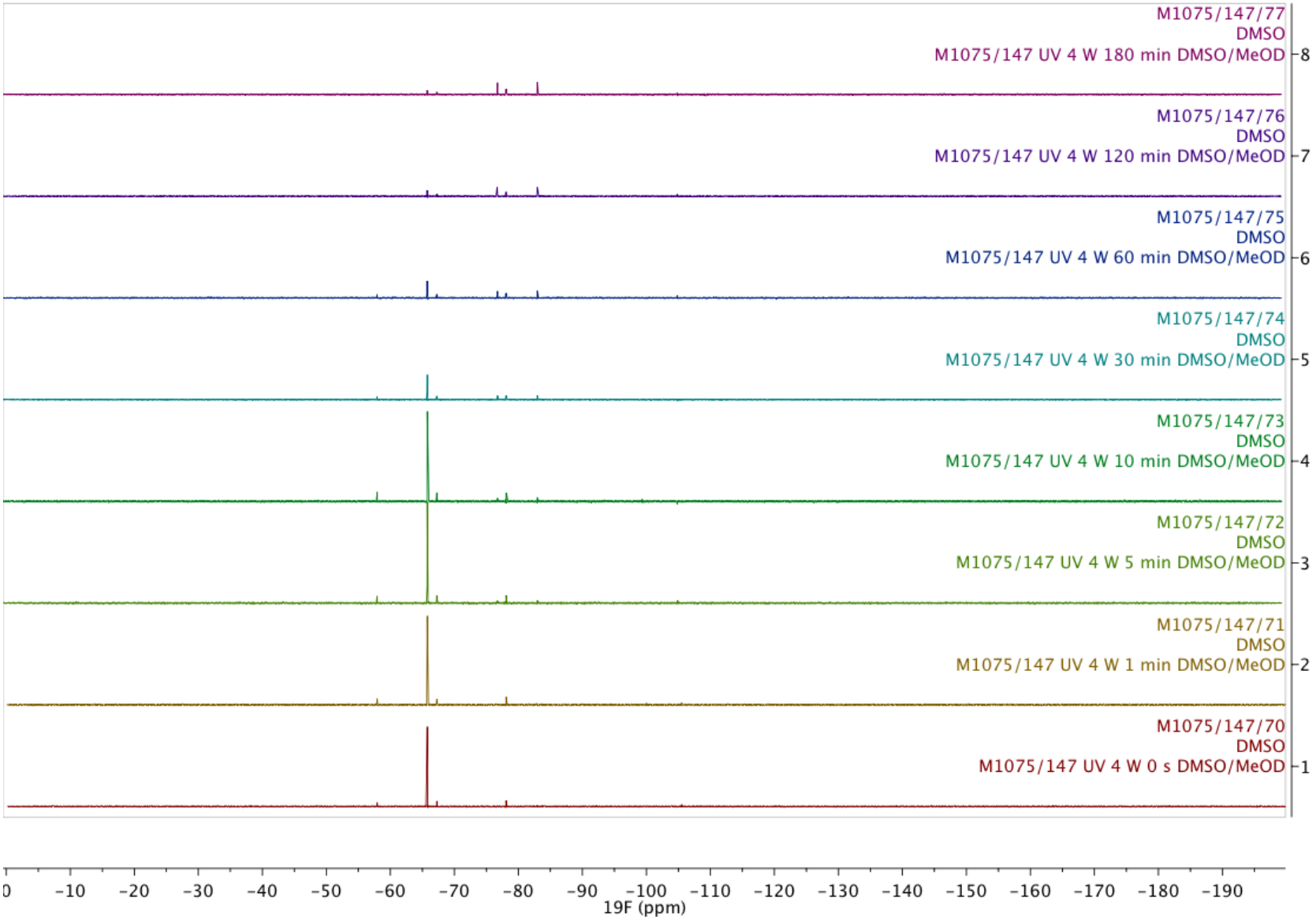

Figure 3.15: **UV light–mediated time–dependent decomposition of analogue 91 studied by ^{19}F–NMR spectroscopy.**

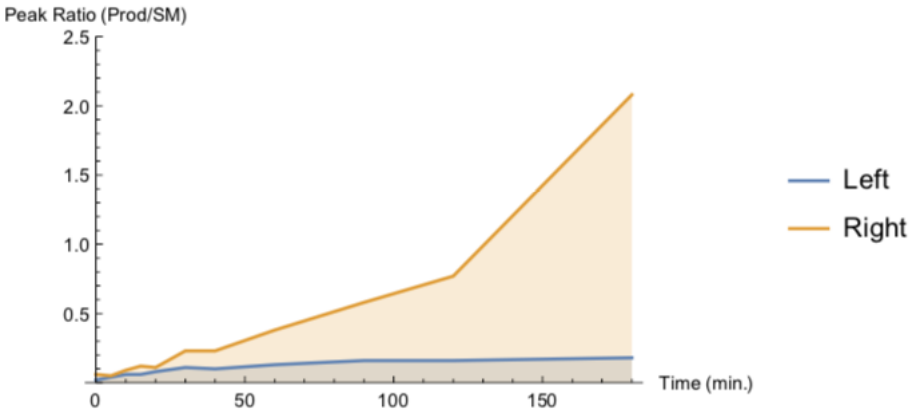

Figure 3.16: **Ratio between product formation and impurity used as an internal standard when irradiating diazirine 102 with UV light.** Legend term *left* corresponds to the internal standard and *right* to the products formed upon irradiation.

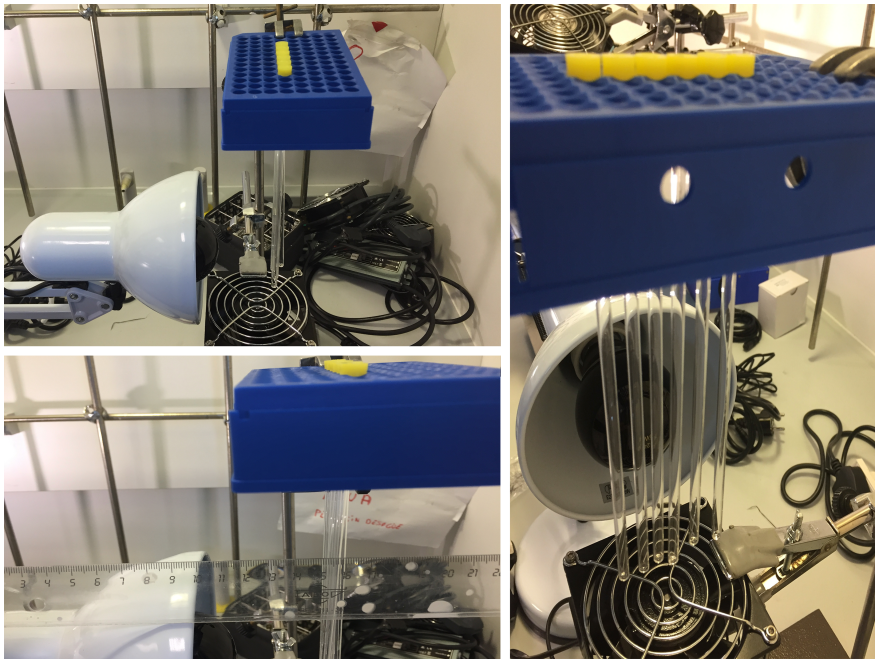

Figure 3.17: **Example of the experimental setting for the photoirradiation experiment.**

3.4 Conclusions

The purpose of the studies presented in this chapter was two–fold: to assess the whole–cell *in vitro* behaviour of our hit molecule **24** and to obtain a better understanding of its interaction with our target enzyme AspRS at a molecular level. Although for the latter case we do not have the final results, our approach has been successfully applied in literature for similar purposes.[69] We are thus confident that the proteolysis/mass spectrometry analysis of our conjugation product will help us locate the binding site of our hit with our target enzyme. As for the whole–cell behaviour of hit **24**, the pull–down experiments described in this chapter employing a biotin–tagged analogue of hit **24** has allowed us to understand two different things. First, by identifying the protein extracted from the *M. bovis* cell lysate as AspRS through the use of an AspRS–specific antibody, we have provided additional confirmation that AspRS is indeed the target protein of hit **24**. But more importantly, through its design and results, this experiment indicates that hit **24** is selective for its AspRS target, which in turn suggests its unlikely engagement in the non–discriminant interactions observed with many PAINS molecules.[42] This result also suggests that perhaps the presence of an exo–cyclic double bond might not be the cause for the unclear SAR discussed in Chapter 2.

Chapter 4

Alternative Chemical Entities Targeting AspRS

4.1 Inhibitor Repurposing

When the hit–to–lead programme for hit **24** was halted, we turned our attention to a different molecule, namely compound **103** (Figure 4.1).[a] This molecule, part of the GSK compound collection, was shown to be active against *M. tuberculosis* in a whole–cell HTS campaign carried out by GSK. Together with 176 other compounds, its structure was made available to the public in an effort to promote research on TB.[77] However, given the nature of the screening, the bacterial targets of these compounds were unknown at the time of their release into the public domain. Having developed an enzymatic assay against AspRS, our group therefore decided to screen these 177 compounds against our enzyme target. As a result of this screening three molecules were identified as potential inhibitors of AspRS (Figure 4.2) .

[a]This study was carried out at the same time as the chemical biology studies described in the preceding chapter.

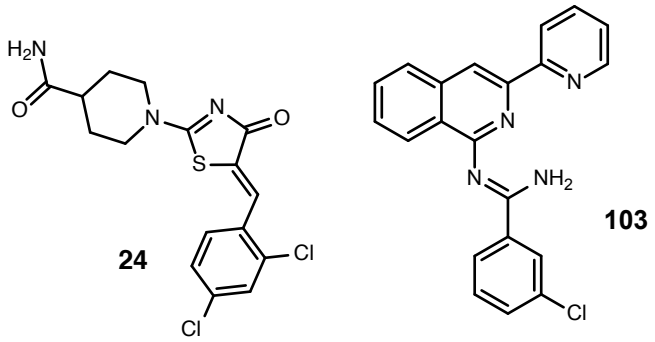

Figure 4.1: **Structure of hits 24 and 103.**

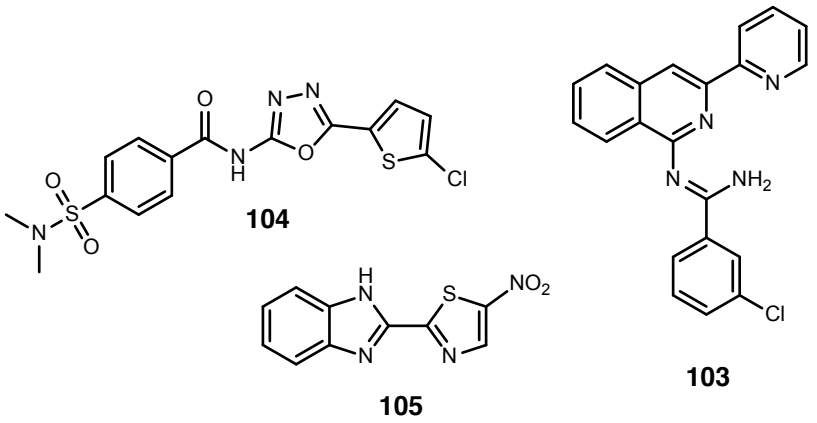

Figure 4.2: **Molecules showing inhibition against AspRS.**

Of these three new hits, compound **103** presented the strongest structural novelty compared to compounds involved in other TB drug discovery programmes at GSK. However, the limited amount of compound available in the GSK collection meant that the enzymatic assay could not be repeated and its IC_{50} could not be determined. Therefore, in order to obtain this information and combine it with other preliminary data on hit **103** (Figure 4.3), we decided to re–synthesise the compound. This would then allow us to confirm its activity against AspRS and allow us to examine its potential for further development.

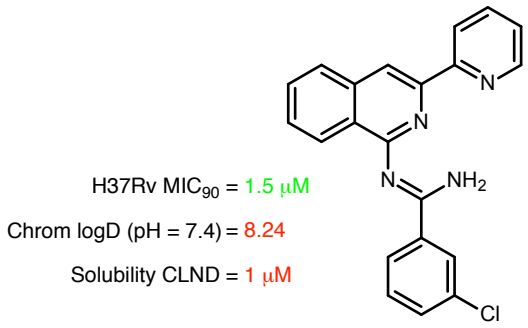

Figure 4.3: **Preliminary data available for hit 103.**

Whilst exploring synthetic strategies we discovered that hit **103** had been previously identified as showing activity against *Mycoplasma gallisepticum*[b] and it had already been part of an SAR study. We therefore attempted to re-synthesise hit compound **103** using the same synthetic route published by De Zwart *et al.*(Scheme 4.1).[79]

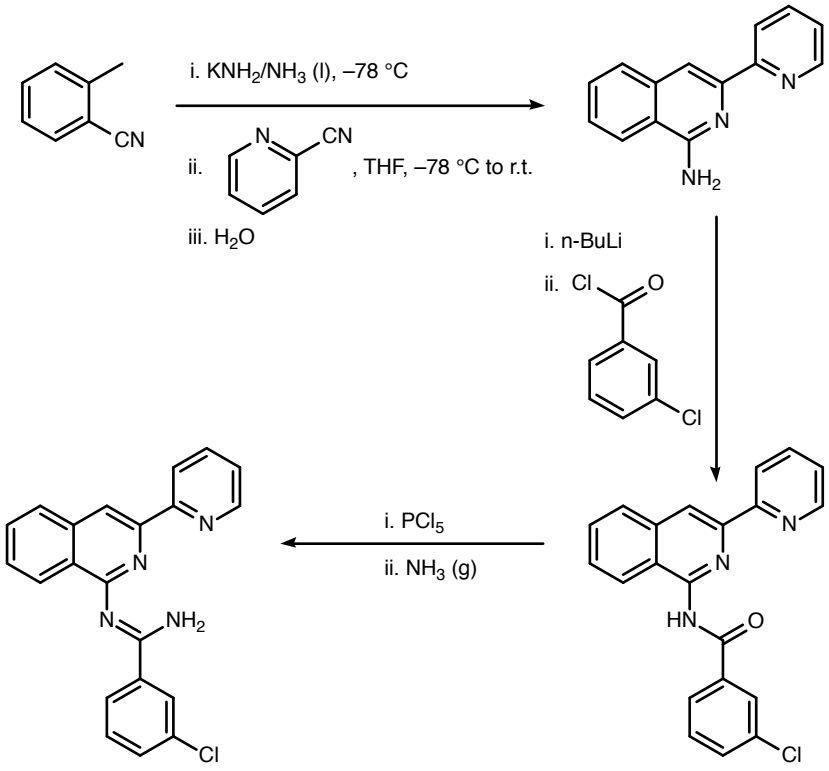

Scheme 4.1: **Literature synthetic route for hit 103.**

[b] *Mycoplasma gallisepticum* is a bacterial pathogen that causes chronic respiratory disease in chickens and sinusitis in turkeys.[78]

However, despite our best attempts we were unable to replicate the first step of the chemistry summarised in Scheme 4.1. Whilst we were confident that we were able to generate KNH_2, and observed a colour change from yellow to red upon addition 2–cyanotoluene consistent with deprotonation, no product was ever isolated after the addition of 2–cyanopyridine. After the use of different bases (*i.e.* LDA or *n*–BuLi) provided the same result, we abandoned this route and sought alternative methods (Scheme 4.2).

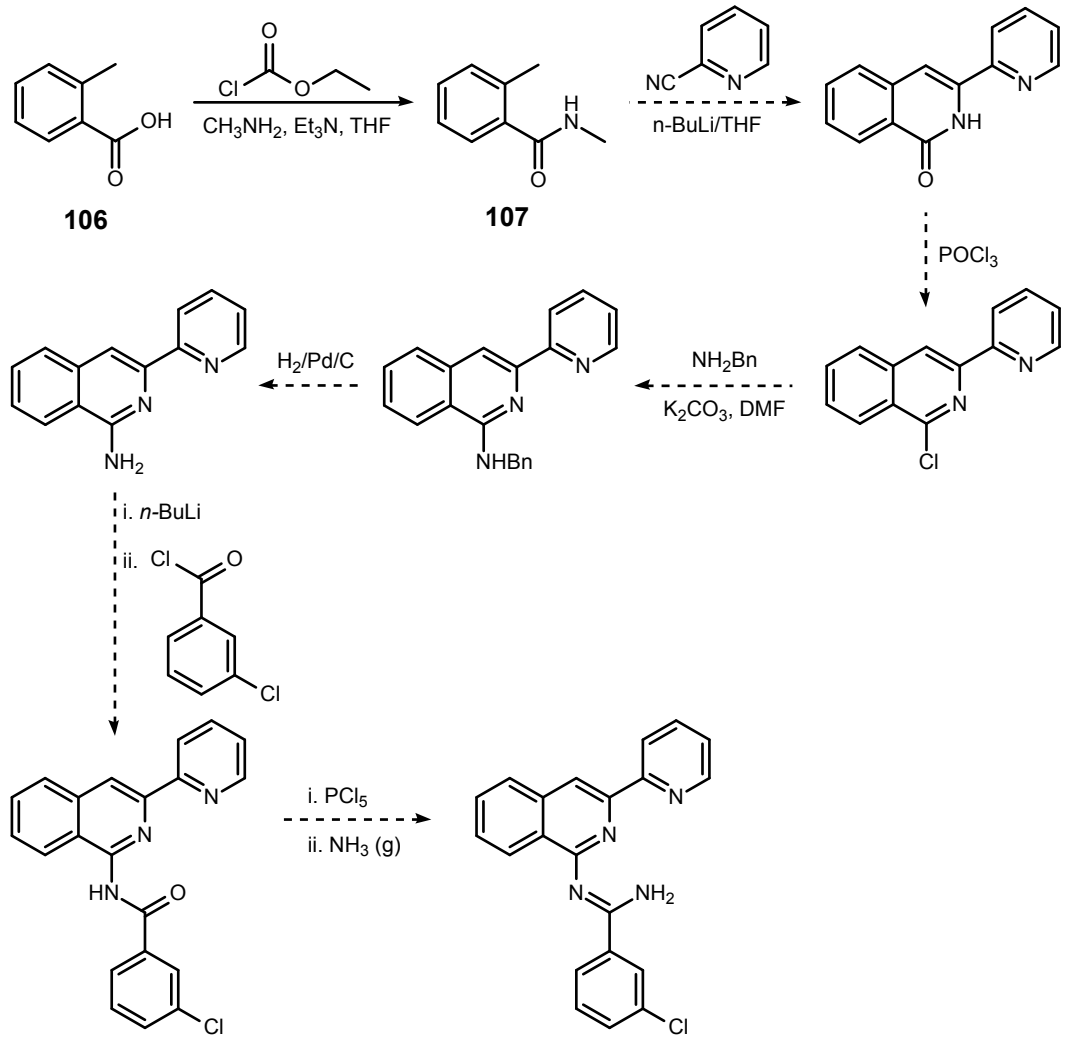

Scheme 4.2: **First alternative for the synthesis of hit 103.**

Although the alternative synthetic route we summarised in Scheme 4.2 was longer, we hoped to avoid the problems encountered when deprotonating 2–cyanotoluene by replacing the cyano functionality with an amide.[80,81] Additionally, since we only required small quantities of hit **103** for testing in the enzymatic assay, we would optimise the route at a later stage if hit compound **103** was deemed worthy of additional development. However, despite achieving the formation of secondary amide **107**, we were unable to effect the deprotonation/addition sequence in the second step.

At this point we opted for a complete overhaul of our approach to hit **103**. As outlined in Scheme 4.3, our new strategy would start from 1,3–dichloroisoquinoline **108** and selectively substitute the chloro at position 1 by displacement with benzylamine to obtain isoquinoline **109**.[82] This would be followed by a Suzuki coupling between isoquinoline **109** and 2–pyridineboronic acid[83] and subsequent hydrogenolysis to obtain amine **112**. The final two synthetic steps, acylation of amine **112** and formation of amidine **103** would be performed using the original conditions reported by De Zwart *et al.*[79]

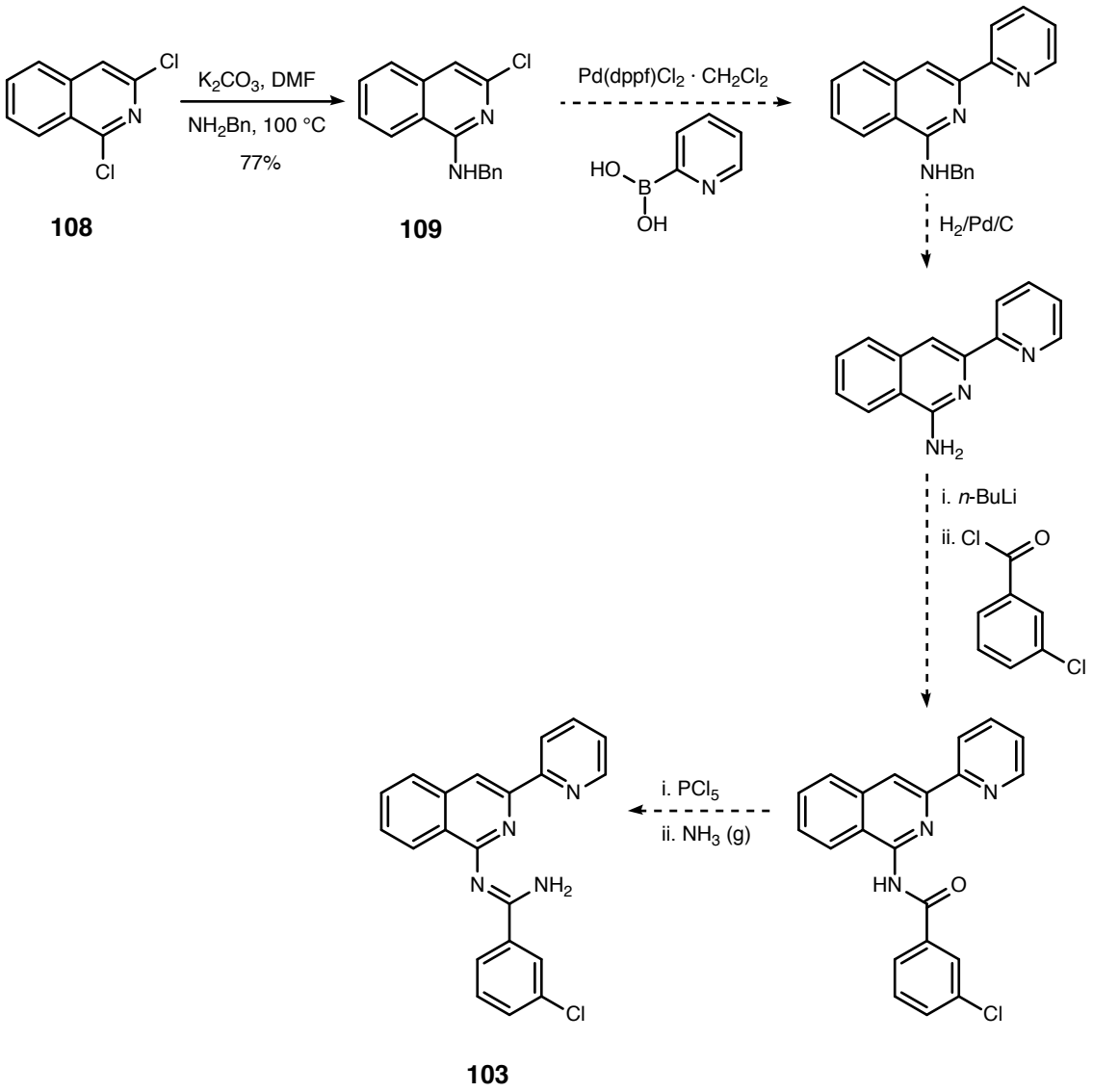

Scheme 4.3: **Second alternative for the synthesis of hit 103.**

The regioselective displacement on 1,3–dichloroisoquinoline **108** with benzylamine proceeded uneventfully, providing 3–chloroisoquinoline **109** in 77% yield. However, we encountered reactivity issues when attempting the Suzuki–Miyaura coupling using 2–pyridineboronic acid. Literature examples using this boronic acid highlighted a lack of stability of pyridineboronic acids, in particular the 2–substituted regioisomer.[83,84] We therefore explored alternative reagents and focused on the corresponding MIDA boronic acids, which

are air stable and slow–releasing alternative cross–coupling reagents developed by Knapp *et al.*[85] At this stage we opted to optimise the synthetic route by changing the benzyl protecting group for a *p*–methoxybenzyl in order to facilitate the deprotection procedure.[82] With these changes, we successfully advanced to the synthesis of hit **103** (Scheme 4.4).

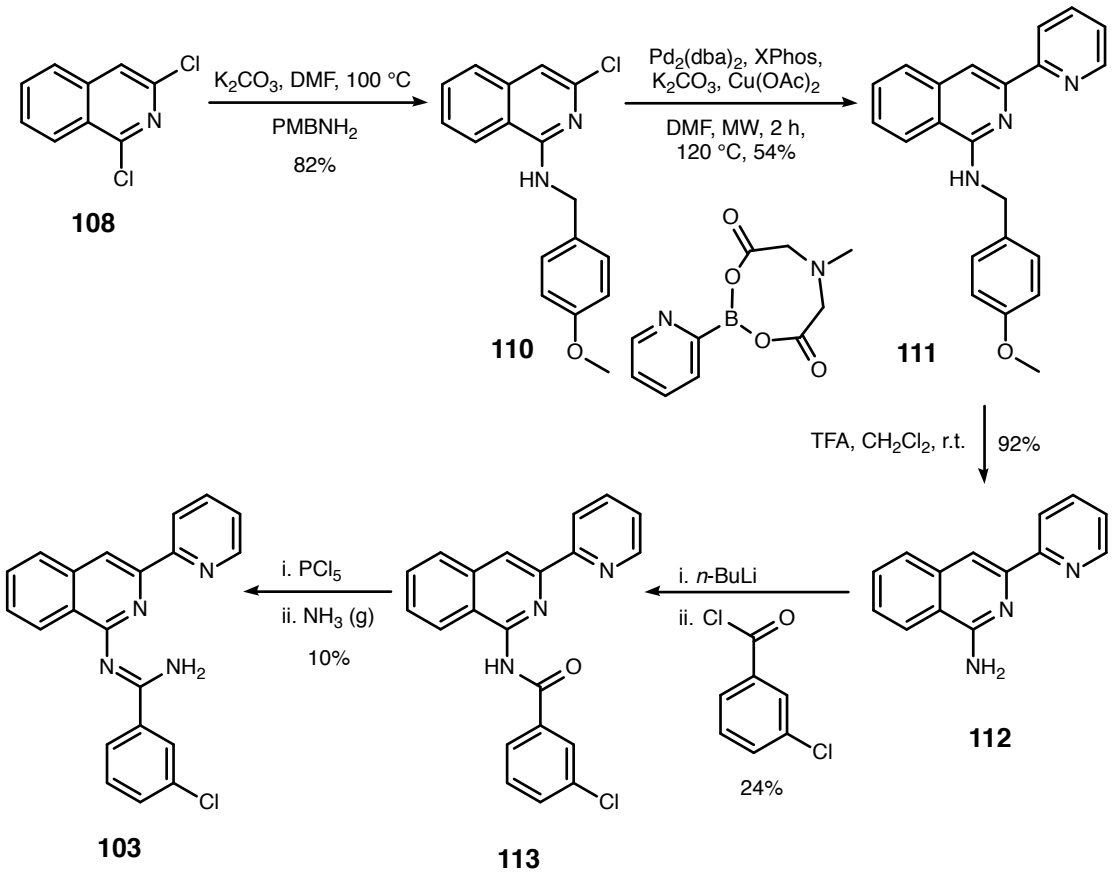

Scheme 4.4: **Final synthetic route of hit 103.**

Using this synthetic route, hit compound **103** was obtained in five steps and an overall yield of 1%. After having optimised the first steps of the synthesis, the final two steps also proved troublesome. The low yield of the acylation step of aminoisoquinoline **112** to amide **113** was a known issue of this route, having been previously reported by De Zwart *et al.*[79]. These authors have hypothesised that the high resonance stability of the anionic

species formed by deprotonation of amine **112** lowers its nucleophilicity. The low yield for the transformation of amide **113** into amidine **103** could have been caused by two factors: either the chlorination step was not completed under the reaction conditions and thus the second step could not proceed, or the efficiency of bubbling gaseous NH_3 was not as high as expected using the protocol adopted.

In spite of these problems, we were able to secure enough compound **103** to be submitted for biological testing. Compound **103** was assessed against AspRS by measuring the shift caused in the MIC_{90} value of wild–type *M. bovis BCG* and of AspRS over–expressing *M. bovis BCG* (Figure 4.4). However, no shift between the two values was observed, leading to the conclusion that AspRS, contrary to our initial hypothesis, was not the target of compound **103**.

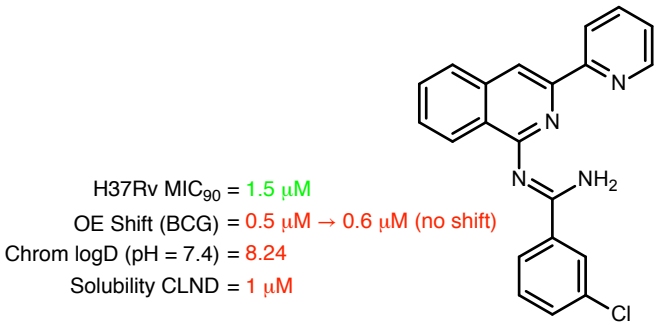

Figure 4.4: **Lack of significant shift in the value of MIC_{99} hit 113 when using an AspRS over–expressing strain of *M. bovis* BCG.**

4.2 Computational Selection

While exploring the molecular interactions of hit **24** and our target enzyme, in order to identify new hits against AspRS, our biology collaborators performed a whole–cell screening of the GSK TB collection, comprised of more

than 11000 compounds. In this HTS they assessed the activity of the compounds against *M. bovis* BCG genetically modified to over–express AspRS and compared the results with the activity against wild–type *M. bovis* BCG. They observed a shift in the MIC_{50} in 250 compounds. They then proceded to further validate these hits using our AspRS enzymatic assay by testing the activity of these molecules in a dose–response assay at a concentration range of 0.1 up to 100 μM. The results obtained in this screening campaign and the work discussed in this section have been recently published by Soto *et al.*[86]

From a chemical perspective, our input to this part of the project was the assessment and analysis of the hits obtained in this screening campaign. In total, after validation against AspRS, 14 different hits were obtained. We then proceeded to gather all the relevant physicochemical and biological activity data at GSK on each one of these molecules, and based on their structural analogy, we grouped them in seven clusters of compounds with different structural characteristics. Next, we analysed current GSK TB development programmes for structure similarity between our clusters and the molecules already being studied. The information obtained from the different drug development programes we analysed led us to discard two clusters of molecules.

Having chosen our five families of compounds, we proceeded to screening over the GSK compound library, which contains over 2 million molecules, for structurally similar compounds that could fit in each one of the 5 clusters. This work resulted in the identification of over 250 new compounds, approximately 50 analogues for each cluster. We next gathered the available biological data for these compounds and based on this information we selected over 30 compounds to be tested against the AspRS over–expressing

M. bovis BCG and in the AspRS enzymatic assay. As a result, four compounds deemed to show potential for further optimisation were identified and released to public domain. The criteria for this selection was their structural differentiation from other drug discovery programes and their activity against our target enzyme. Their structure and IC_{50} values are presented in Figure 4.5.

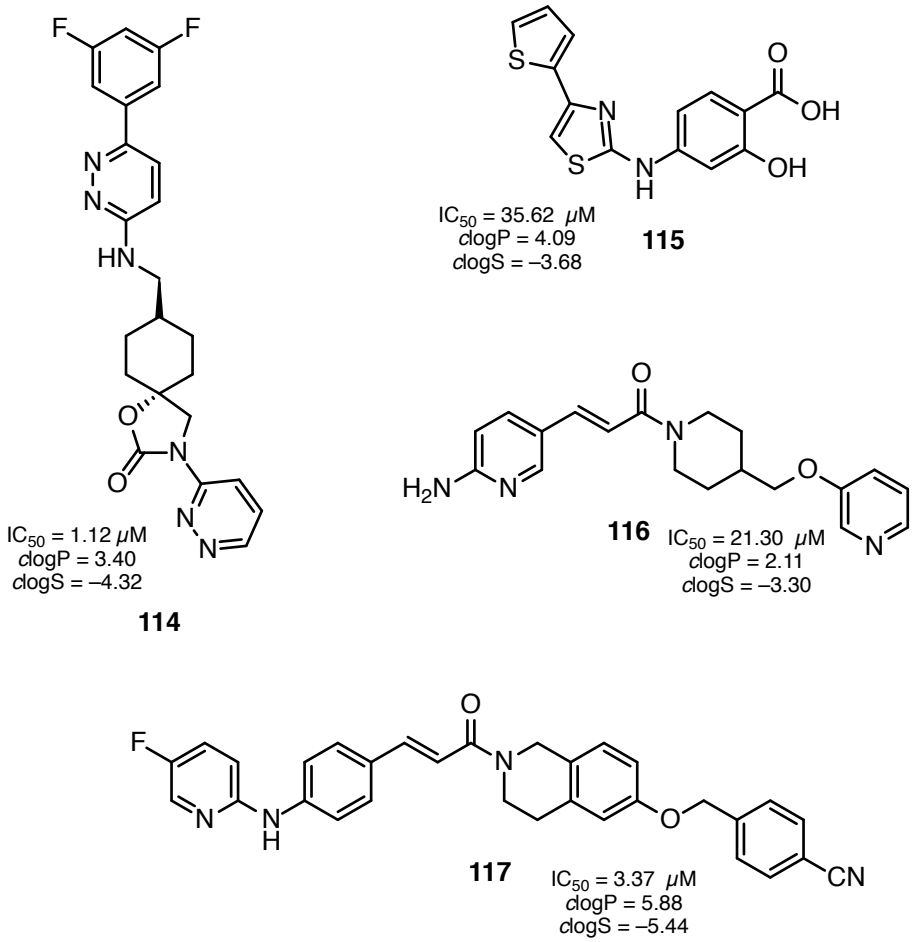

Figure 4.5: **Structure of hits published in the work of Soto *et al.*** [86] Experimental values measured in duplicates using AspRS enzymatic assay.

Chapter 5

Conclusions and Future Work

This project started as an SAR study trying to optimise the physicochemical properties of hit **24** (Figure 5.1), a compound previously shown by our research group to target AspRS.[17] We particularly focused on improving solubility and potency, measuring the latter through IC_{50} values.

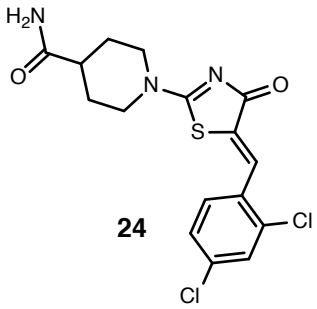

24

Figure 5.1: **Structure of hit 24.**

Working together with our collaborators at GSK, as described in Chapter 2, we managed to synthesise a number of analogues of hit **24** improving both the solubility in some cases and the potency in other. However, when putting all the data together we did not observe any clear trend that we could follow in order to obtain a biological activity in the range expected by GSK for developable hits.

On its own, this situation might not seem critical when working in medicinal chemistry programs. However, hit **24** contains a rhodanine core, a scaffold classified as a PAINS structure, a class of compounds that tend to interact with a range of enzymes and are thus generally considered as potential promiscuous inhibitors. In addition, a GSK assay probing the interaction of hit **24** with GSH, showed the formation of a hit–GSH conjugate. Given that GSH is a known substrate for conjugate addition reactions in the cytosol, the result was interpreted as an indication of the potential cytotoxicity of hit **24**. These data put together resulted in the termination of the hit optimisation programme that started the project.

However, we knew that our group had managed to grow resistant mutants to hit **24** when probing its target, which is an uncommon results for promiscuous compounds.[17] Therefore, we decided to study the whole–cell behaviour of our hit in order to probe its promiscuity. As explained in Chapter 3, we did this by attaching a biotin probe to hit **24** in order to obtain analogue **90** (Figure 5.2).

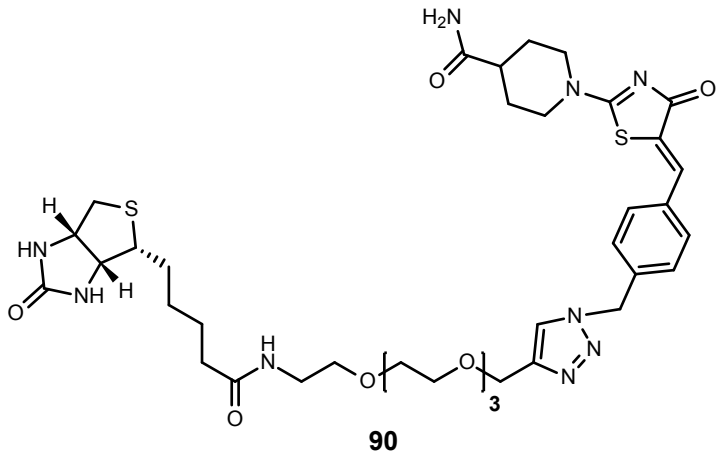

90

Figure 5.2: **Structure of biotinylated analogue 90.**

The results obtained when incubating analogue **90** with mycobacterium cell lysate not only confirmed AspRS as the enzymatic target of **24**, but

showed no other interactions with mycobacterial cytosolic proteins whatsoever. This supports the hypothesis that the promiscuity of our initial hit **24** is not likely to be the responsible factor for the unclear SAR described in Chapter 2, and therefore additional studies to root its cause are required.

As described in the second part of Chapter 3, in order to achieve a clear understanding of the molecular interaction between AspRS and our initial hit **24**, lacking an enzyme–hit co–crystal, we considered that the best way to achieve this is to force the creation of a covalent bond between the enzyme and a hit analogue. To this end we synthesised analogue **102** (Figure 5.3).

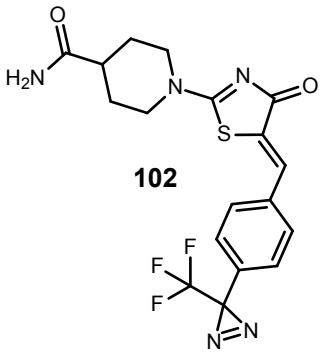

102

Figure 5.3: **Structure of diazirine analogue 102.**

Analogue **102** was designed to be attached to our target enzyme AspRS after incubating them together under UV irradiation. As the proteolysis and mass spectrometry analysis stages are still ongoing, we can only hypothesise which path will be followed in the future. However, we are confident that this experiment will help us identify the enzymatic binding site of our hit.

Separately, we worked on the discovery of additional hits that can interact with AspRS, our target enzyme. As exemplified in Chapter 4, we synthesised hit **113** (Figure 5.4), which although in an initial screening seemed to interact with AspRS, it target within *M. tuberculosis* remains yet unknown.

In addition we collaborated in further screenings by supporting our biology colleagues in selecting and discriminating a wide number of molecules of

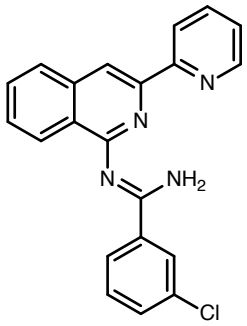

103

Figure 5.4: **Structure of amidine hit 113.**

diverse chemical structures, leading to the publication of a list of potential targets (Figure 4.5) for AspRS that can be subjected to further studies in the future.

All in all, as it stands today, the project leaves the door open for a number of additional studies to be carried in the future exploring the interactions with AspRS as a means to inhibit the growth of *M. tuberculosis*. First and foremost, a reliable computational model describing the molecular interaction between hit **24** and AspRS should be built. This should be facilitated by the results from the ongoing proteolysis study of analogue **102**. The data this study will provide should be used to create a pharmacophore hit–enzyme 3D interaction model that can be used to understand and rationalise the binding of the analogues synthesised in Chapter 2. Moreover, it should provide the basis for the design of future analogues that provide a stronger interaction with our target enzyme. Perhaps a good starting point for this are analogues **36** and **37** (Figure 5.5), the most potent and potentially versatile analogues synthesised in the SAR study described in Chapter 2.

Similarly, future work should build upon the results obtained with our biotinilated analogue **90**. Additional studies should be carried out to explore the interaction of hit **24** and AspRS, perhaps to obtain additional information

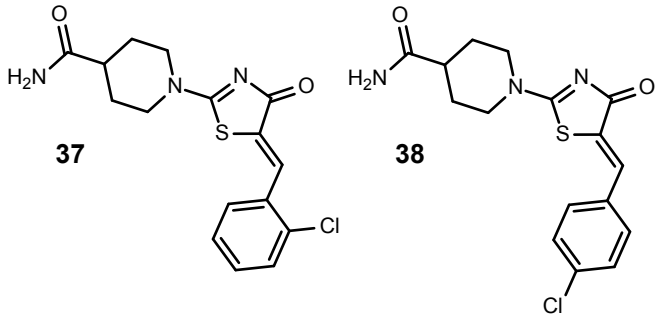

Figure 5.5: **Structure of analogues 37 and 38.**

on the strength of this interaction or to use this methodology to study the selectivity for mycobacterium AspRS against. human AspRS.

Finally, the work exemplified in Chapter 4 shows the potential of AspRS as a molecular target in order to inhibit *M. tuberculosis*. The potential hits described in this chapter should be used as justification for additional screening campaigns against a diverse set of chemical libraries. Although the compound libraries of many biopharmaceutical companies have many common elements, many of their compounds are different, with many of these compounds being potential hits against AspRS if given the opportunity. A good path forward in the fight against tuberculosis is to use this work to fine–tune the potential of AspRS as an enzymatic target and explore novel hits through additional screening campaigns.

Chapter 6

General Methods and Experimental

6.1 General Methods and Instruments

6.1.1 Instrumentation

Infra–red spectra were recorded neat as thin films. The intensity of each band is described as s (strong), m (medium) or w (weak) and with the prefix v (very) and suffix br (broad) where appropriate. ^{1}H–NMR and proton–decoupled ^{13}C–NMR spectra were recorded in a 1:1 mixture of $CDCl_3/CD_3OD$ at r.t. unless specified otherwise. ^{1}H–NMR spectra were recorded on either Bruker 300 (300 MHz) or Bruker 400 (400 MHz) spectrometers, and are reported as follows: δ_H (frequency of spectrometer, solvent) chemical shift (multiplicity, coupling constant(s) J (Hz), number of protons, assignment). Multiplicities of ^{1}H–NMR resonances are reported as follows: s–singlet, d–doublet, t–triplet, q–quartet, m–multiplet, v–very, br–broad resonance, stack and apparent (app.). The term "stack" is used to describe a region in the spectrum where resonances arising from non–equivalent nuclei are coincident

while multiplet, m, is used to describe a resonance arising from a single nucleus (or equivalent nuclei) in which coupling constants cannot be readily assigned. In analysing ABX (and similar) systems, where the resonance pattern forms two, clearly separated groups of lines (two sets of four lines for an ABX system), these are reported as "A of ABX" and "B of ABX", along with $J_{\mathrm{A-B}}$, which can be directly measured from the spectra. Whilst $J_{\mathrm{A-X}}$ cannot be measured directly from the spectrum, the value obtained from the spectrum is sufficiently close to the actual value for it still to be useful; however it is acknowledged that the value quoted for $J_{\mathrm{A-X}}$ is not the true value. Proton–decoupled ^{13}C–NMR spectra, unless stated otherwise, were recorded on a Bruker 400 (100 MHz) spectrometer and are reported as follows: chemical shift δ_C ppm [multiplicity (CH_3, CH_2, CH or C), assignment]. ^{19}F–NMR spectra, unless stated otherwise, were recorded on a Bruker 400 (375 MHz) spectrometer and are reported as follows: chemical shift δ_F ppm. Chemical shifts are reported as δ values (ppm) referenced to the following solvent resonances: $CHCl_3$, δ_H 7.26; $CHCl_3$, δ_C 77.0, CH_3OH, δ_H 3.31; CH_3OH δ_C 49.0, DMSO, δ_H 2.50; DMSO δ_C 39.52. Connectivities were deduced from COSY90, HSQC and HMBC experiments. Mass spectra are reported as m/z (%) and were recorded utilising EI (Electron Ionisation) or TOF ES+ (Time of Flight Electrospray Ionisation) on a Xevo G2-XS TOF with Waters e2695 separation module, a Synapt G2-S with Waters e2695 separation module, an LCT Premier with Waters 600 controller, and a GCT Premier with Agilent 789OA controller. HRMS were recorded utilising a QSTAR Elite Syste spectrometer. Melting points were determined using open capillaries and are uncorrected.

6.1.2 Reactions

Reactions were monitored by thin layer chromatography (TLC) using pre-coated glass-backed silica plates (60 F_{254}, Merck) and visualised by UV detection (254 nm) followed by staining with $KMnO_4$. Reactions were also monitored by LC–MS on a Agilent 6120 Quadrupole spectrometer coupled to an Agilent 1100 series HPLC system. Column chromatography was performed manually on silica gel (40–60 μm) or using a Biotage Isolera™ Prime advanced automated flash purification system with a 200–400 nm variable detector and a single collector bed.

All reactions were conducted with magnetic stirring in oven–dried (140 °C) or flame–dried glassware under a nitrogen atmosphere and at room temperature (20 to 25 °C) unless specified otherwise. Volumes of 1 mL or less were measured and dispensed using gas–tight syringes. Evaporation of volatiles and concentration of solutions under reduced pressure were performed at 20–600 mbar at 42 °C. Residual solvent was removed under high vacuum (< 1 mbar). Before use, molecular sieves were activated by heating at 100 °C under high vacuum (< 1 mbar) for 60 min.

6.1.3 Chemicals and reagents

All chemicals and reagents were obtained from commercial sources and used without further purification unless stated otherwise. All aqueous solutions are saturated unless stated otherwise.

6.1.4 General Procedures

General procedure A

Knoevenagel condensation products **36**–**47** were prepared following a literature procedure for the condensation of rhodanine **33** and aldehydes.[47] Rhodanine derivative **29** (41 mg, 0.18 mmol) and the corresponding aldehyde (0.18 mmol) were added to a solution of NH_4OAc (7.7 mg, 0.1 mmol) in glacial AcOH (2.5 mL). The solution was heated at 100 ℃ for 16 h and then cooled to r.t. and diluted with H_2O ($\approx$ 10 mL). The resulting precipitate was collected by filtration and, unless stated otherwise, purified using flash column chromatography (eluent: MeOH in CH_2Cl_2) to provide the Knoevenagel condensation product.

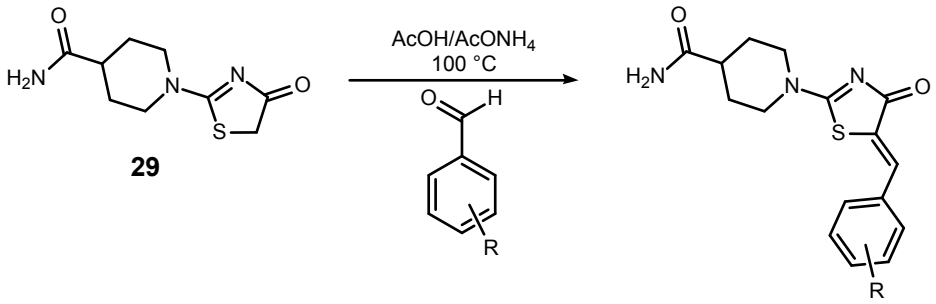

Figure 6.1: **General procedure A.**

General procedure B

Substitution products **48**–**68** were prepared following a previously reported procedure.[47] Rhodanine derivative **35** (99 mg, 0.33 mmol) and the corresponding amine (0.33 mmol) were dissolved in EtOH (20 mL). The solution was heated under reflux for 16 h and after cooling to r.t., unless stated otherwise, the resulting precipitate was recovered by filtration and recrystallised in the reaction solvent to provide the substitution product.

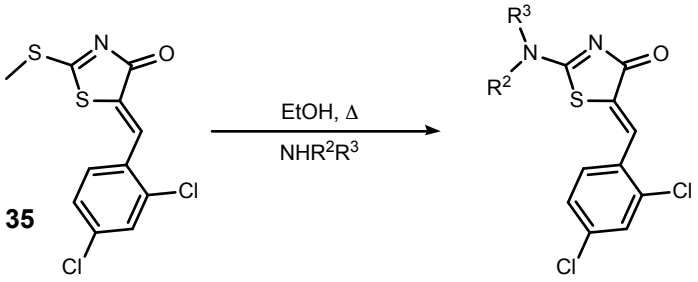

Figure 6.2: **General procedure B.**

6.2 Characterisation

2–(methylthio)–4,5–dihydrothiazol–4–one (**32**)[46]

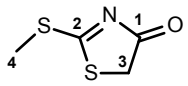

MeI (0.51 mL, 8.18 mmol) was added to a yellow suspension of rhodanine (**33**) (1.00 g, 7.43 mmol) in 2% NaOH (aq.) (20 mL). The resulting biphasic mixture was stirred for 16 h and then extracted with CH_2Cl_2 (3 × 50 mL). The combined organic fractions were washed sequentially with $NaHCO_3$ soln. (50 mL) and brine (50 mL), dried (Na_2SO_4), filtered and evaporated under reduced pressure to yield a yellow solid. Purification by flash column chromatography (eluent: 1% MeOH in CH_2Cl_2) provided the product **32** as a white powder (0.54 g, 50%): m.p. 71–74 °C; lit.[46] 72–74 °C; R_f = 0.25 (CH_2Cl_2); IR (neat) ν_{max} = 3348br, 3181br, 3005w, 2987w, 2911m, 1696s (C=O), 1491s cm^{-1}; ^1H NMR (300 MHz, $CDCl_3$): δ 3.98 (s, 2H, C(3)$\underline{H}_2$), 2.71 (s, 3H, C(4)$\underline{H}_3$); ^{13}C NMR (101 MHz, $CDCl_3$): δ 202.8 (C, C(2)), 187.5 (C, C(1)), 39.8 (CH_2, C(3)), 16.4 (CH_3, C(4)); MS (TOF–ES+) m/z 170.0 ($[M + Na]^+$, 100%).

Data are in agreement with those reported in the literature.[46]

2–(4'–carboxamidepiperidin–1'–yl)–4,5–dihydrothiazol–4–one (**29**)

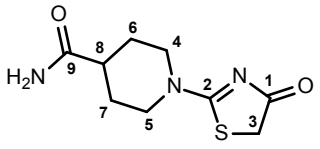

Isonipecotamide (**31**) (89 mg, 0.68 mmol) was added to a solution of **32** (100 mg, 0.68 mmol) in absolute EtOH (8 mL). The resulting mixture was heated at 60 ℃ for 16 h, after which time, evaporation of the solvent under reduced pressure provided a brown solid, which was purified by flash column chromatography (eluent: 5% MeOH in CH_2Cl_2 to 10% MeOH in CH_2Cl_2) to provide the product **29** as a white powder (98 mg, 64%): m.p. 188–190 ℃; R_f = 0.28 (1% MeOH in CH_2Cl_2); IR (neat) ν_{max} = 3363br (N–H), 3152br, 2956w, 2932w, 1667s (C=O), 1540s (C=O), 1347s cm^{-1}; ^1H NMR (300 MHz, 1:1 $CDCl_3$:CD_3OD): δ 4.63 (app. dtd, J = 13.2, 4.1, 1.4, 1H, C(4)$\underline{H}_aH_b$), 3.94 (s, 2H, C(3)$\underline{H}_2$), 3.80 (app. dtd, J = 13.6, 4.0, 1.3, 1H, C(5)$\underline{H}_aH_b$), 3.38–3.17 (stack, 2H, C(4)$H_a\underline{H}_b$ and C(5)$H_a\underline{H}_b$), 2.53 (app. tt, J = 10.9, 4.0, 1H, C(8)$\underline{H}_2$), 2.02–1.87 (stack, 2H, C(6)$\underline{H}_aH_b$ and C(7)$\underline{H}_aH_b$), 1.87–1.66 (stack, 2H, C(6)$H_a\underline{H}_b$ and C(7)$H_a\underline{H}_b$), N$\underline{H}_2$ not observed; ^{13}C NMR (101 MHz, 1:1 $CDCl_3$:CD_3OD): δ 189.4 (C, C(2)), 182.6 (C, C(1)), 178.0 (C, C(9)), 48.9 (CH_2, C(4)), 48.8 (CH_2, C(5)), 41.6 (CH, C(8)), 40.6 (CH_2, C(3)), 28.80 (CH_2, C(6)), 28.79 (CH_2, C(7)); MS (TOF–ES+) m/z 250.1 ($[M + Na]^+$, 100%); HRMS (TOF–ES+) calcd for $C_9H_{13}N_3O_2SNa$ $[M + Na]^+$ 250.0626, found 250.0630.

(*Z*)–5–(2,4–dichlorobenzylidene)–2–thioxothiazolidin–4–one (**34**)[43]

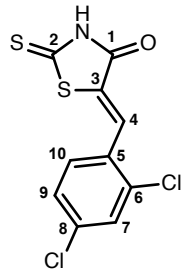

NaOAc (1.23 g, 14.86 mmol) was added to solution of rhodanine (**33**) (1.08 g, 7.43 mmol) and 2,4–dichlorobenzaldehyde (**30**) (1.27 g, 7.43 mmol) in EtOH (25 mL). The mixture was heated to reflux for 16 h. After cooling to r.t., the solvent was removed under reduced pressure to obtain a yellow solid which was dissolved in CH_2Cl_2 (400 mL) and washed sequentially with H_2O (200 mL) and brine (200 mL). The organic phase was then dried (Na_2SO_4) and the organic solvent was removed under reduced pressure. The yellow solid obtained was dissolved in acetone (100 mL) and upon adding H_2O (150 mL) a yellow precipitate was formed. After filtration and drying the product was purified by flash column chromatography (eluent: 1% MeOH in CH_2Cl_2) to obtain the title compound **34** as yellow flakes (1.29 g, 60%): m.p. 233–235 ℃; R_f = 0.53 (1% MeOH in CH_2Cl_2); IR (neat) ν_{max} = 3099br, 3019w, 2826w, 1728s, 1577s (C=O), 1192s cm^{-1}; ^{1}H NMR (300 MHz, DMSO–d_6): δ 7.87 (d, J = 2.1, 1H, C(7)H), 7.68 (s, 1H, C(4)H), 7.62 (dd, J = 8.5, 2.1, 1H, C(9)H), 7.55 (d, J = 8.5, 1H, C(10)H), NH not observed; ^{13}C NMR (101 MHz, 1:1 $CDCl_3$:CD_3OD): δ 195.7 (C, C(2)), 169.1 (C, C(1)), 135.5 (C, C(8)), 134.6 (CH, C(9)), 132.3 (C, C(6)), 131.8 (C, C(3)), 129.3 (CH, C(7) and C(10), resonance overlap), 129.1 (C, C(5)), 127.4 (CH, C(4)); MS (TOF–ES+) m/z 291.2 ($[M + H]^+$, 100%).

Data are in agreement with those reported in literature.[43]

(*Z*)-5-(2,4-dichlorobenzylidene)-2-(methylthio)thiazol-4(5*H*)-one (**35**)[43]

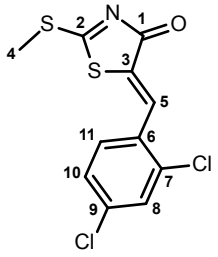

MeI (100 μL, 1.56 mmol) was added to a solution of **34** (300 mg, 1.03 mmol) in EtOH (10 mL). The mixture was heated at reflux for 2 h. Upon cooling, a pale yellow precipitate was formed. After filtration and purification by flash column chromatography (eluent: 1% MeOH in CH_2Cl_2 to 2% MeOH in CH_2Cl_2) the title compound **35** was obtained as pale yellow flakes (263 mg, 84%): m.p. 187–189 ℃; R_f = 0.9 (5% MeOH in CH_2Cl_2); IR (neat) ν_{max} = 3065w, 3019w, 1706m, 1579m (C=O), 1464m, 1136s cm^{-1}; ^{1}H NMR (300 MHz, 1:1 $CDCl_3$:CD_3OD): δ 8.11 (s, 1H, C(5)H), 7.54 (d, J = 2.0, 1H, C(8)H), 7.52 (d, J = 8.5, 1H, C(11)H), 7.41 (dd, J = 8.5, 2.0, 1H, C(10)H), 2.83 (s, 3H, C(4)H_3); ^{13}C NMR (101 MHz, DMSO–d_6): δ 195.5 (C, C(2)), 180.2 (C, C(1)), 137.7 (C, C(9)), 137.4 (C, C(7)), 131.4 (C, C(3)), 131.1 (CH, C(10)), 130.9 (CH, C(8)), 130.7 (CH, C(11)), 130.5 (C, C(6)), 128.5 (CH, C(5)), 16.2 (CH_3, C(4)); MS (TOF–ES+) m/z 325.8 ([M + Na]$^+$, 100%). Data are in agreement with those reported in literature.[43]

(*Z*)–5–benzylidene–2–(4'–carboxamidepiperidin–1'–yl)thiazol–4(*5H*)–one (**36**)

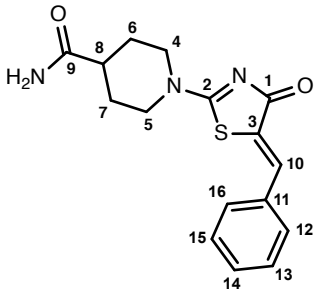

Knoevenagel product **36** was prepared from rhodanine derivative **29** (110 mg, 0.49 mmol) and benzaldehyde (50 μL, 0.49 mmol) according to general procedure A. Purification by flash column chromatography (eluent: 2% MeOH in CH_2Cl_2 to 10% MeOH in CH_2Cl_2) provided the title compound **36** as a white powder (92 mg, 60%): m.p. 221–224 ℃; R_f = 0.5 (10% MeOH in CH_2Cl_2); IR (neat) ν_{max} = 3347br (N–H), 3184br, 2923w, 1666m (C=O), 1550s (C=O), 1281m, 1218m cm^{-1}; ^{1}H NMR (300 MHz, 1:1 $CDCl_3$:CD_3OD): δ 7.72 (s, 1H, C(10)H), 7.57–7.51 (m, 2H, C(12)H and C(16)H), 7.49–7.38 (stack, 3H, C(13)H and C(14)H and C(15)H), 4.81–4.69 (d with unresolved fine coupling, 1H, J = 13.1, C(4)H_aH_b), 3.99–3.88 (d with unresolved fine coupling, J = 12.8, 1H, C(5)H_aH_b), 3.54–3.37 (stack, 2H, C(4)H_aH_b and C(5)H_aH_b), 2.72–2.60 (m, 1H, C(8)H), 2.10–1.94 (stack, 2H, C(6)H_aH_b and C(7)H_aH_b), 1.94–1.72 (stack, 2H, C(6)H_aH_b and C(7)H_aH_b), NH_2 not observed; ^{13}C NMR (101 MHz, 1:1 $CDCl_3$:CD_3OD): δ 182.9 (C, C(2)), 178.9 (C, C(1)), 176.6 (C, C(9)), 135.2 (C, C(3)), 132.9 (C, C(11)), 131.1 (CH, C(14)), 130.8 (CH, C(12) and C(16)), 130.1 (CH, C(13) and C(15)), 129.1 (CH, C(10)), 49.9 (CH_2, C(5)), 49.1 (CH_2, C(4)), 42.4 (CH, C(8)), 29.7 (CH_2, C(6)), 29.4 (CH_2, C(7)); MS (TOF–ES+) m/z 337.9 ($[M + Na]^+$, 100%); HRMS (TOF–ES+) calcd for $C_{16}H_{17}N_3O_2SNa$ $[M + Na]^+$ 338.0939, found 338.0938.

(*Z*)–5–(2"–chlorobenzylidene)–2–(4'–carboxamidepiperidin–1'–yl)thiazol–4(*5H*)–one (**37**)

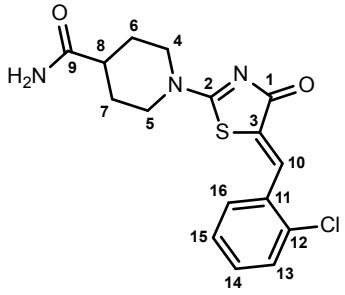

Knoevenagel product **37** was prepared from rhodanine derivative **29** (97 mg, 0.43 mmol) and 2–chlorobenzaldehyde (61 mg, 0.43 mmol) according to general procedure A. Purification by flash column chromatography (eluent: 5% MeOH in CH_2Cl_2 to 10% MeOH in CH_2Cl_2) provided the title compound **37** as white crystals (126 mg, 84%): m.p. 210–212 ℃; R_f = 0.49 (10% MeOH in CH_2Cl_2); IR (neat) ν_{max} = 3400br (N–H), 3174br, 2991w, 2955w, 2920w, 2870w, 1663s (C=O), 1571s (C=O), 1385m, 1277m cm^{-1}; ^{1}H NMR (300 MHz, 1:1 CD_2Cl_2:CD_3OD): δ 8.07 (s, 1H, C(10)H), 7.64–7.61 (m, 1H, C(13)H), 7.51–7.47 (m, 1H, C(16)H), 7.42–7.33 (stack, 2H, C(14)H and C(15)H), 3.92 (d with unresolved fine coupling, J = 12.5, 1H, C(4)H_aH_b), 3.54–3.35 (stack, 2H, C(4)H_aH_b and C(5)H_aH_b), 3.26–3.22 (m, 1H, C(5)H_aH_b), 2.63 (app. tt, J = 10.9, 4.0, 1H, C(8)H), 2.07–1.95 (stack, 2H, C(6)H_aH_b and C(7)H_aH_b), 1.93–1.73 (stack, 2H, C(6)H_aH_b and C(7)H_aH_b), NH_2 not observed; ^{13}C NMR (101 MHz, 1:1 CD_2Cl_2:CD_3OD): δ 180.6 (C, C(2)), 177.3 (C, C(1)), 175.1 (C, C(9)), 135.5 (C, C(12)), 132.5 (C, C(11)), 130.9 (CH, C(13) and C(16), resonance overlap), 130.2 (C, C(3)), 128.6 (CH, C(14)), 127.9 (CH, C(15)), 127.2 (CH, C(10)), 45.6 (CH_2, C(4)), 45.4 (CH_2, C(5)), 40.9 (CH, C(8)), 28.4 (CH_2, C(6)), 28.2 (CH_2, C(7)); MS (TOF–ES+) *m/z* 372.06 ($[M + Na]^+$, 100%); HRMS (TOF–ES+) calcd for $C_{16}H_{16}{}^{35}ClN_3O_2SNa$ $[M + Na]^+$ 372.0549, found 372.0538.

(*Z*)–5–(4"–chlorobenzylidene)–2–(4'–carboxamidepiperidin–1'–yl)thiazol–4(*5H*)–one (**38**)

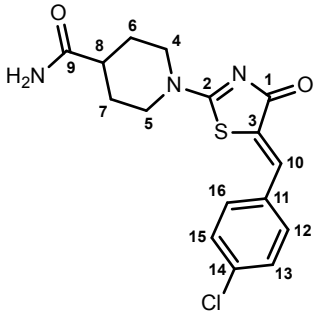

Knoevenagel product **38** was prepared from rhodanine derivative **29** (61 mg, 0.43 mmol) and 4–chlorobenzaldehyde (62 mg, 0.43 mmol) according to general procedure A. Purification by flash column chromatography (eluent: 2.5% MeOH in CH_2Cl_2 to 10% MeOH in CH_2Cl_2) provided the title compound **38** as white needle–like crystals (90 mg, 60%): m.p. 247–249 ℃ dec.; R_f = 0.53 (10% MeOH in CH_2Cl_2); IR (neat) ν_{max} = 3392br (N–H), 3197br, 2943w, 2920w, 2856w, 1612m (C=O), 1548s (C=O), 1388m cm^{-1}; ^{1}H NMR (300 MHz, 1:1 $CDCl_3$:CD_3OD): δ 7.67 (s, 1H, C(10)$\underline{H}$), 7.52–7.39 (stack, 4H, C(Ar)$\underline{H}$), 4.74 (d with unresolved fine coupling, J = 13.7, 1H, C(4)$\underline{H}_aH_b$), 3.92 (d with unresolved fine coupling, J = 13.7, 1H, C(5)$\underline{H}_aH_b$), 3.55–3.21 (stack, 2H, C(4)$H_a\underline{H}_b$ and C(5)$H_a\underline{H}_b$), 2.69–2.52 (m, 1H, C(8)$\underline{H}$), 2.09–1.93 (stack, 2H, C(6)$\underline{H}_aH_b$ and C(7)$\underline{H}_aH_b$), 1.93–1.73 (stack, 2H, C(6)$H_a\underline{H}_b$ and C(7)$H_a\underline{H}_b$), N$\underline{H}_2$ not observed; ^{13}C NMR (101 MHz, 1:1 $CDCl_3$:CD_3OD): δ 181.5 (C, C(2)), 177.2 (C, C(1)), 175.0 (C, C(9)), 135.9 (C, C(14)), 132.5 (C, C(11)), 130.9 (CH, C(16) and C(12)), 130.6 (C, C(3)), 129.2 (CH, C(13) and C(15)), 128.4 (CH, C(10)), 48.7 (CH_2, C(5)), 47.9 (CH_2, C(4)), 40.9 (CH, C(8)), 28.3 (CH_2, C(6)), 28.2 (CH_2, C(7)); MS (TOF–ES+) m/z 372.25 ([M + Na]$^+$, 100%); HRMS (TOF–ES+) calcd for $C_{16}H_{16}{}^{35}ClN_3O_2SNa$ [M + Na]$^+$ 372.0549, found 372.0556.

(*Z*)–2–(4'–carboxamidepiperidin–1'–yl)–5–(2",4"–dichlorobenzylidene)thiazol–4(*5H*)–one (**24**)

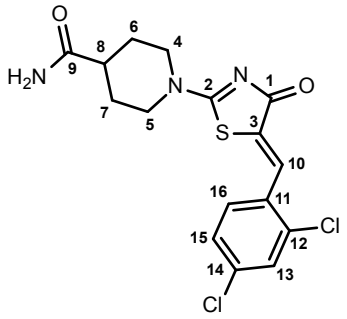

Knoevenagel product **24** was prepared from rhodanine derivative **29** (41 mg, 0.18 mmol) and 2,4–dichlorobenzaldehyde (32 mg, 0.18 mmol) according to general procedure A. Purification by flash column chromatography (eluent: 5% MeOH in CH_2Cl_2 to 10% MeOH in CH_2Cl_2) provided the title compound **24** as white flakes (140 mg, 84%): m.p. 254–255 ℃ dec.; R_f = 0.55 (10% MeOH in CH_2Cl_2); IR (neat) ν_{max} = 3368br (N–H), 3180br, 2941w, 1641m (C=O), 1549s (C=O), 1276s, 1215m cm^{-1}; ^1H NMR (300 MHz, 1:1 $CDCl_3$:CD_3OD): δ 7.97 (s, 1H, C(10)H), 7.55 (d, J = 8.4, 1H, C(16)H), 7.50 (d, J = 2.1, 1H, C(13)H), 7.36 (dd, J = 8.4, 2.1, 1H, C(15)H), 4.73 (d with unresolved fine coupling, J = 14.2, 1H, C(4)H_aH_b), 3.89 (d with unresolved fine coupling, J = 13.6, 1H, C(5)H_aH_b), 3.52–3.33 (stack, 2H, C(4)H_aH_b and C(5)H_aH_b), 2.61 (app. tt, J = 10.9, 3.9, 1H, C(8)H), 2.08–1.94 (stack, 2H, C(6)H_aH_b and C(7)H_aH_b), 1.91–1.75 (stack, 2H, C(6)H_aH_b and C(7)H_aH_b), NH_2 not observed; ^{13}C NMR (101 MHz, 1:1 $CDCl_3$:CD_3OD): δ 181.4 (C, C(2)), 177.8 (C, C(1)), 175.5 (C, C(9)), 136.8 (C, C(12)), 136.0 (C, C(14)), 132.3 (C, C(11)), 131.9 (C, C(3)), 130.7 (CH, C(16)), 130.0 (CH, C(13)), 128.2 (CH, C(15)), 127.21 (CH, C(10)), 49.4 (CH_2, C(5)), 48.7 (CH_2, C(4)), 41.6 (CH, C(8)), 29.0 (CH_2, C(6)), 28.8 (CH_2, C(7)); MS (TOF–ES+) m/z 384.03 ($[M + H]^+$, 100%); HRMS (TOF–ES+) calcd for $C_{16}H_{16}{}^{35}Cl^{37}ClN_3O_2S$ $[M + H]^+$ 386.0311, found 386.0305.

(*Z*)–2–(4'–carboxamidepiperidin–1'–yl)–5–(2",6"–dichlorobenzylidene)thiazol–4(*5H*)–one (**39**)

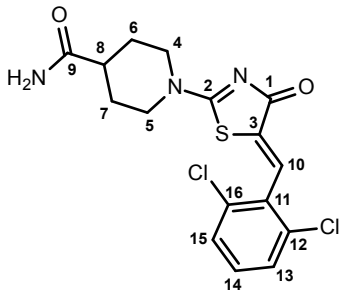

Knoevenagel product **39** was prepared from rhodanine derivative **29** (100 mg, 0.44 mmol) and 2,6–dichlorobenzaldehyde (78 mg, 0.44 mmol) according to general procedure A. Purification by recrystallisation from $CHCl_3$ provided the title compound **39** as white crystals (135 mg, 80%): m.p. 227–230 ℃ (from $CHCl_3$); R_f = 0.37 (10% MeOH in CH_2Cl_2); IR (neat) ν_{max} = 3344br (N–H), 3175br, 2971w, 2952w, 2925w, 2875w, 1671m (C=O), 1557s (C=O), 1429m, 1288s cm^{-1}; ^1H NMR (300 MHz, 1:1 $CDCl_3$:CD_3OD): δ 7.62 (s, 1H, C(10)H), 7.42–7.36 (stack, 2H, C(13)H and C(15)H), 7.33–7.26 (m, 1H, C(14)H), 4.72 (d with unresolved fine coupling, J = 14.0, 1H, C(4)H_aH_b), 3.77 (d with unresolved fine coupling, J = 13.3, 1H, C(5)H_aH_b), 3.45–3.34 (stack, 2H, C(4)H_aH_b and C(5)H_aH_b), 2.59 (app. tt, J = 10.9, 4.0, 1H, C(8)H), 2.03–1.92 (stack, 2H, C(6)H_aH_b and C(7)H_aH_b), 1.87–1.72 (stack, 2H, C(6)H_aH_b and C(7)H_aH_b), NH_2 not observed; ^{13}C NMR (101 MHz, 1:1 $CDCl_3$:CD_3OD): δ 180.6 (C, C(2)), 178.1 (C, C(1)), 175.7 (C, C(9)), 137.8 (C, C(11)), 134.7 (C, C(12) and C(16)), 133.7 (C, C(3)), 131.3 (CH, C(14)), 129.1 (CH, C(13) and C(15)), 127.4 (CH, C(10)), 49.6 (CH_2, C(5)), 48.7 (CH_2, C(4)), 41.7 (CH, C(8)), 29.1 (CH_2, C(6)), 28.9 (CH_2, C(7)); MS (TOF–ES+) *m/z* 406.02 ($[M + Na]^+$, 100%); HRMS (TOF–ES+) calcd for $C_{16}H_{15}{}^{35}Cl_2N_3O_2SNa$ $[M + Na]^+$ 406.0160, found 406.0156.

(*Z*)–2–(4–carboxamidepiperidin–1–yl)–5–(1-phenylethylidene)thiazol–4(*5H*)–one (**40**)

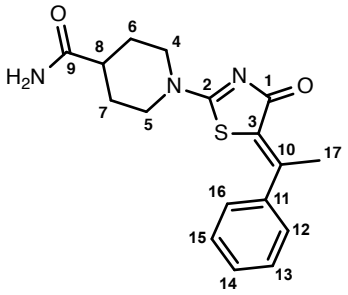

Knoevenagel product **40** was prepared from rhodanine derivative **29** (98 mg, 0.43 mmol) and acetophenone (50 μL, 0.43 mmol) according to general procedure A. Purification by flash column chromatography (eluent: 2% MeOH in CH_2Cl_2 to 8% MeOH in CH_2Cl_2) provided the title **40** compound as an orange powder (5 mg, 4%): m.p. 215–218 ℃; R_f = 0.53 (10% MeOH in CH_2Cl_2); IR (neat) ν_{max} = 3285w, 3140w, 2956w, 1658m (C=O), 1548s (C=O), 1368m, 1288m cm^{-1}; ^{1}H NMR (300 MHz, $CDCl_3$): δ 7.45–7.29 (stack, 5H, C(Ar)H), 5.85 (s, 1H, NH$_a$H$_b$), 5.68 (s, 1H, NH$_a$H$_b$), 4.72 (d with unresolved fine coupling, J = 12.4, 1H, C(4)H$_a$H$_b$), 3.64 (d with unresolved fine coupling, J = 12.9, 1H, C(5)H$_a$H$_b$), 3.32–3.12 (stack, 2H, C(4)H$_a$H$_b$ and C(5)H$_a$H$_b$), 2.72 (s, 3H, C(17)H), 2.58–2.42 (m, 1H, C(8)H), 2.02–1.90 (stack, 2H, C(6)H$_a$H$_b$ and C(7)H$_a$H$_b$), 1.88–1.69 (stack, 2H, C(6)H$_a$H$_b$ and C(7)H$_a$H$_b$); ^{13}C NMR (101 MHz, $CDCl_3$): δ 179.5 (C, C(2)), 175.6 (C, C(1)), 174.2 (C, C(9)), 147.6 (C, C(11)), 144.6 (C, C(3)), 128.9 (CH, C(12) and C(16)), 128.8 (CH, C(14)), 127.8 (C, C(10)), 126.7 (CH, C(13) and C(15)), 47.8 (CH_2, C(5)), 46.8 (CH_2, C(4)), 41.5 (CH, C(8)), 28.4 (CH_2, C(6) and C(7)), 21.1 (CH_3, C(17)); MS (TOF–ES+) m/z 352.1 ([M + Na]$^+$, 100%); HRMS (TOF–ES+) calcd for $C_{17}H_{20}N_3O_2S$ [M + H]$^+$ 330.1276, found 330.1277.

(*Z*)–2–(4–carboxamidepiperidin–1–yl)–5–cyclohexylmethylenethiazol–4(*5H*)–one (**41**)

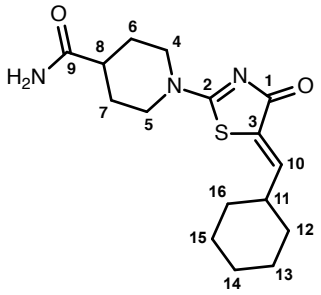

Et_3N (0.23 mL, 1.61 mmol) was added to a solution of rhodanine derivative **29** (102 mg, 0.45 mmol) and cyclohexanecarboxaldehyde (56 μL, 0.46 mmol) in EtOH (2.5 mL). The mixture was heated under reflux and the reaction was monitored by TLC. After cooling to r.t., the solvent was evaporated under reduced pressure and the product was purified by flash column chromatography (eluent: 2% MeOH in CH_2Cl_2 to 10% MeOH in CH_2Cl_2) to obtain the title compound **41** as a thick yellow oil (17 mg, 12%): R_f = 0.51 (10% MeOH in CH_2Cl_2); IR (neat) ν_{max} = 3333br (N–H), 2926w, 2853w, 1665m (C=O), 1546s (C=O), 1354m, 1290m cm^{-1}; ^1H NMR (300 MHz, $CDCl_3$): δ 6.74 (d, J = 9.3, 1H, C(10)$\underline{H}$), 6.44 (s, 1H, N$\underline{H}_a$H$_b$), 5.97 (s, 1H, NH$_a\underline{H}_b$), 4.68 (d with unresolved fine coupling, J = 13.4, 1H, C(4)$\underline{H}_a$H$_b$), 3.78 (d with unresolved fine coupling, J = 13.4, 1H, C(5)$\underline{H}_a$H$_b$), 3.32 (stack, 2H, C(4)H$_a\underline{H}_b$ and C(5)H$_a\underline{H}_b$), 2.66–2.53 (m, 1H, C(8)$\underline{H}$), 2.20–1.58 (stack, 9H, C(6)$\underline{H}_2$ and C(7)$\underline{H}_2$ and C(11)$\underline{H}$ and C(12)$\underline{H}_2$ and C(16)$\underline{H}_2$), 1.34–1.12 (stack, 6H, C(13)$\underline{H}_2$ and C(14)$\underline{H}_2$ and C(15)$\underline{H}_2$); ^{13}C NMR (101 MHz, $CDCl_3$: δ 180.2 (C, C(2)), 176.1 (C, C(1)), 174.8 (C, C(9)), 140.5 (CH, C(10)), 130.1 (C, C(3)), 48.5 (CH_2, C(5)), 47.5 (CH_2, C(4)), 42.8 (CH, C(8)), 41.2 (CH, C(11)), 31.6 (CH_2, C(12) and C(16)), 28.4 (CH_2, C(6) and C(7)), 25.7 (CH_2, C(14)), 25.4 (CH_2, C(13) and C(15)); MS (TOF–ES+) m/z 322.5 ([M + H]$^+$, 100%); HRMS (TOF–ES+) calcd for $C_{16}H_{24}N_3O_2S$ [M + H]$^+$ 322.1584, found 322.1591.

(*Z*)–5–(4–fluorobenzylidene)–2–(4–carboxamidepiperidin–1–yl)thiazol–4(*5H*)–one (**42**)

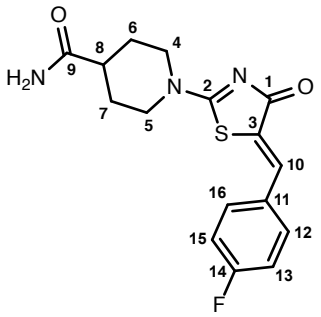

Knoevenagel product **42** was prepared from rhodanine derivative **29** (54 mg, 0.24 mmol) and 4–fluorobenzaldehyde (29 mg, 0.24 mmol) according to general procedure A. Purification by flash column chromatography (eluent: 1% MeOH in CH_2Cl_2 to 10% MeOH in CH_2Cl_2) provided the title compound **42** as a white powder (62 mg, 78%): m.p. 224–226 ℃; R_f = 0.7 (10% MeOH in CH_2Cl_2); IR (neat) ν_{max} = 3367br (N–H), 2962w, 2922w, 2484br, 2066m, 1612m (C=O), 1548s (C=O), 1119m cm^{-1}; ^{1}H NMR (400 MHz, 1:1 $CDCl_3$:CD_3OD): δ 7.68 (s, 1H, C(10)H), 7.56–7.50 (m, 2H, C(12)H and C(16)H), 7.17–7.10 (m, 2H, C(13)H and C(15)H), 4.73 (d with unresolved fine coupling, J = 13.4, 1H, C(4)H_aH_b), 3.91 (d with unresolved fine coupling, J = 13.6, 1H, C(5)H_aH_b), 3.52–3.33 (stack, 2H, C(4)H_aH_b and C(5)H_aH_b), 2.66–2.56 (m, 1H, C(8)H), 2.08–1.95 (stack, 2H, C(6)H_aH_b and C(7)H_aH_b), 1.93–1.74 (stack, 2H, C(6)H_aH_b and C(7)H_aH_b), NH_2 not observed; ^{13}C NMR (101 MHz, 1:1 $CDCl_3$:CD_3OD): δ 182.1 (C, C(2)), 177.8 (C, C(1)), 175.7 (C, C(9)), 164.0 (d, $^1J_{C-F}$ = 252.4, C(14)), 132.3 (d, $^3J_{C-F}$ = 8.6, C(12) and C(16)), 131.4 (CH, C(10)), 130.8 (d, $^4J_{C-F}$ = 3.5, C(11)), 128.1 (C, C(3)), 116.7 (d, $^2J_{C-F}$ = 22.1, C(13) and C(15)), 49.3 (CH_2, C(5)), 48.5 (CH_2, C(4)), 41.6 (CH, C(8)), 28.9 (CH_2, C(6)), 28.7 (CH_2, C(7)); ^{19}F NMR (376 MHz, 1:1 $CDCl_3$:CD_3OD): δ –32.8; MS (TOF–ES+) m/z 356.1 ($[M + Na]^+$, 100%); HRMS (TOF–ES+) calcd for $C_{16}H_{16}FN_3O_2S$ $[M + Na]^+$ 356.0845, found 356.0847.

(*Z*)–5–(4–hydroxybenzylidene)–2–(4–carboxamidepiperidin–1–yl)thiazol–4(*5H*)–one (**43**)

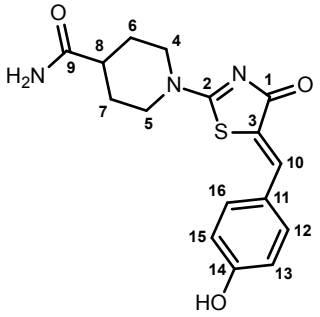

Knoevenagel product **43** was prepared from rhodanine derivative **29** (86 mg, 0.38 mmol) and 4–hydroxybenzaldehyde (46 mg, 0.38 mmol) according to general procedure A. Purification by flash column chromatography (eluent: 1% MeOH in CH_2Cl_2 to 10% MeOH in CH_2Cl_2) provided the title compound **43** as a pale white powder (106 mg, 84%): m.p. 235–238 ℃; R_f = 0.5 (10% MeOH in CH_2Cl_2); IR (neat) ν_{max} = 3358br (N–H), 2973w, 2934w, 2066m, 1618m (C=O), 1552s (C=O), 1137m cm^{-1}; ^1H NMR (400 MHz, 1:1 $CDCl_3$:CD_3OD): δ 9.65 (br s, 1H, O$\underline{H}$), 7.64 (s, 1H, C(10)$\underline{H}$), 7.51–7.38 (m, 2H, C(12)$\underline{H}$ and C(16)$\underline{H}$), 7.12–7.03 (m, 2H, C(13)$\underline{H}$ and C(15)$\underline{H}$), 4.75 (d with unresolved fine coupling, J = 13.4, 1H, C(4)$\underline{H}_aH_b$), 3.93 (d with unresolved fine coupling, J = 13.6, 1H, C(5)$\underline{H}_aH_b$), 3.54–3.39 (stack, 2H, C(4)$H_a\underline{H}_b$ and C(5)$H_a\underline{H}_b$), 2.68–2.57 (m, 1H, C(8)$\underline{H}$), 2.09–1.94 (stack, 2H, C(6)$\underline{H}_aH_b$ and C(7)$\underline{H}_aH_b$), 1.93–1.72 (stack, 2H, C(6)$H_a\underline{H}_b$ and C(7)$H_a\underline{H}_b$), N$\underline{H}_2$ not observed; ^{13}C NMR (101 MHz, 1:1 $CDCl_3$:CD_3OD): δ 181.8 (C, C(2)), 177.6 (C, C(1)), 175.4 (C, C(9)), 162.2 (C, C(14)), 136.1 (C, C(11)), 131.7 (CH, C(12) and C(16)), 130.6 (C, C(3)), 129.8 (CH, C(13) and C(15)), 128.8 (CH, C(10)), 48.9 (CH_2, C(5)), 47.7 (CH_2, C(4)), 41.2 (CH, C(8)), 28.6 (CH_2, C(6)), 28.3 (CH_2, C(7)); MS (TOF–ES+) *m/z* 354.4 ($[M + Na]^+$, 100%); HRMS (TOF–ES+) calcd for $C_{16}H_{17}N_3NaO_3S$ $[M + Na]^+$ 354.0887, found 354.0879.

(*Z*)–2–(4–carboxamidepiperidin–1–yl)–5–(furan–2–ylmethylene)thiazol–4(*5H*)–one (**45**)

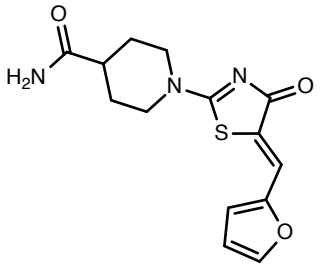

Knoevenagel product **45** was prepared from rhodanine derivative **29** (105 mg, 0.46 mmol) and furfural (38 μL, 0.46 mmol) according to general procedure A. Purification by flash column chromatography (eluent: 2% MeOH in CH_2Cl_2 to 10% MeOH in CH_2Cl_2) provided the title compound **45** as a brown powder (55 mg, 40%): m.p. 199–202 °C; $R_f = 0.53$ (10% MeOH in CH_2Cl_2); IR (neat) ν_{max} = 3346br (N–H), 2931w, 2480br, 1660m (C=O), 1545s (C=O), 1290m cm^{-1}; ^{1}H NMR (400 MHz, 1:1 $CDCl_3$:CD_3OD): δ 7.67 (d, J = 1.7, 1H, C(14)H), 7.47 (s, 1H, C(10)H), 6.79 (d, J = 3.5, 1H, C(12)H), 6.58 (dd, J = 3.5, 1.7, 1H, C(13)H), 4.72 (d with unresolved fine coupling, J = 13.9, 1H, C(4)H_aH_b), 3.93 (d with unresolved fine coupling, J = 13.9, 1H, C(5)H_aH_b), 3.49–3.41 (m, 1H, C(4)H_aH_b), 3.30 (app. d, J = 4.4, 1H, C(5)H_aH_b), 2.65–2.55 (m, 1H, C(8)H), 2.09–1.93 (stack, 2H, C(6)H_aH_b and C(7)H_aH_b), 1.92–1.73 (stack, 2H, C(6)H_aH_b and C(7)H_aH_b), NH_2 not observed; ^{13}C NMR (101 MHz, CD_3OD): δ 182.3 (C, C(2)), 178.0 (C, C(1)), 176.7 (C, C(9)), 150.6 (C, C(11)), 146.4 (CH, C(14)), 126.2 (C, C(3)), 118.9 (CH, C(10)), 117.3 (CH, C(12)), 113.7 (CH, C(13)), 49.3 (CH_2, C(5)), 48.3 (CH_2, C(4)), 41.7 (CH, C(8)), 29.0 (CH_2, C(6)), 28.9 (CH_2, C(7)); MS (TOF–ES+) m/z 328.4 ($[M + Na]^+$, 100%); HRMS (TOF–ES+) calcd for $C_{14}H_{16}N_3O_3S$ $[M + H]^+$ 306.0907, found 306.0912.

(*Z*)–2–(4–carboxamidepiperidin–1–yl)–5–(thiophen–2–ylmethylene)thiazol–4(*5H*)–one (**46**)

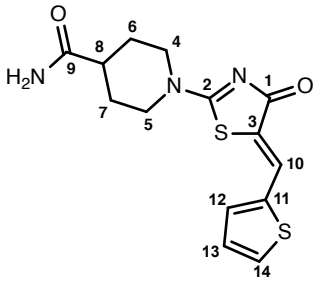

Knoevenagel product **46** was prepared from rhodanine derivative **29** (99 mg, 0.44 mmol) and 2–thiophenecarboxaldehyde (41 μL, 0.44 mmol) according to general procedure A. Purification by flash column chromatography (eluent: 2% MeOH in CH_2Cl_2 to 10% MeOH in CH_2Cl_2) provided the title compound **46** as a dark orange powder (71 mg, 50%): m.p. 222–226 ℃; R_f = 0.5 (10% MeOH in CH_2Cl_2); IR (neat) ν_{max} = 3362br (N–H), 3150br, 3025w, 2959w, 2925w, 1671m (C=O), 1558s (C=O), 1383m, 1268m cm^{-1}; ^{1}H NMR (300 MHz, 1:1 $CDCl_3$:CD_3OD): δ 7.63 (d, J = 5.0, 1H, C(14)$\underline{H}$), 7.53 (s, 1H, C(10)$\underline{H}$), 7.39 (d, J = 3.5, 1H, C(12)$\underline{H}$), 7.16 (dd, J = 5.0, 3.5, 1H, C(13)$\underline{H}$), 4.75 (d with unresolved fine coupling, J = 13.7, 1H, C(4)$\underline{H}_aH_b$), 3.93 (d with unresolved fine coupling, J = 13.6, 1H, C(5)$\underline{H}_aH_b$), 3.55–3.34 (stack, 2H, C(4)$H_a\underline{H}_b$ and C(5)$H_a\underline{H}_b$), 2.66–2.53 (m, 1H, C(8)$\underline{H}$), 2.10–1.94 (stack, 2H, C(6)$\underline{H}_aH_b$ and C(7)$\underline{H}_aH_b$), 1.94–1.73 (stack, 2H, C(6)$H_a\underline{H}_b$ and C(7)$H_a\underline{H}_b$), N$\underline{H}_2$ not observed; ^{13}C NMR (101 MHz, 1:1 $CDCl_3$:CD_3OD): δ 182.1 (C, C(2)), 177.8 (C, C(1)), 175.1 (C, C(9)), 139.2 (C, C(11)), 133.2 (CH, C(12)), 131.2 (CH, C(13)), 129.1 (CH, C(14)), 126.6 (C, C(3)), 125.3 (CH, C(10)), 49.4 (CH_2, C(5)), 48.4 (CH_2, C(4)), 41.6 (CH, C(8)), 28.9 (CH_2, C(6)), 28.7 (CH_2, C(7)); MS (TOF–ES+) m/z 344.5 ($[M + Na]^+$, 100%); HRMS (TOF–ES+) calcd for $C_{14}H_{16}N_3O_2S_2$ $[M + H]^+$ 322.0678, found 322.0671.

(*Z*)–2–(4–carboxamidepiperidin–1–yl)–5–((*1H*–indol–3–yl)methylene)thiazol–4(*5H*)–one (**47**)

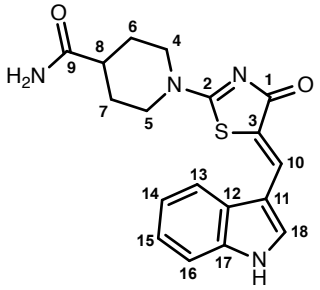

Knoevenagel product **47** was prepared from rhodanine derivative **29** (69 mg, 0.31 mmol) and indole–3–carboxaldehyde (44 mg, 0.31 mmol) according to general procedure A. Purification by flash column chromatography (eluent: 2% MeOH in CH_2Cl_2 to 10% MeOH in CH_2Cl_2) provided the title compound **47** as a yellow powder (22 mg, 20%): m.p. 294–295 ℃ dec.; R_f = 0.4 (10% MeOH in CH_2Cl_2); IR (neat) ν_{max} = 3366br (N–H), 3188br, 2921w, 1654m (C=O), 1546s (C=O), 1279m, 1213s cm^{-1}; ^{1}H NMR (300 MHz, d_6–DMSO): δ 12.04 (s, 1H, indole N$\underline{H}$), 7.87 (s, 1H, C(10)$\underline{H}$), 7.85 (d, J = 7.8, 1H, C(18)$\underline{H}$), 7.74 (d, J = 2.4, 1H, C(13)$\underline{H}$), 7.49 (d, J = 8.0, 1H, C(16)$\underline{H}$), 7.38 (s, 1H, N$\underline{H}_a$H$_b$), 7.28–7.12 (stack, 2H, C(14)$\underline{H}$ and C(15)$\underline{H}$), 6.90 (s, 1H, NH$_a\underline{H}_b$), 4.55 (d with unresolved fine coupling, J = 13.7, 1H, C(4)$\underline{H}_a$H$_b$), 3.86 (d with unresolved fine coupling, J = 13.4, 1H, C(5)$\underline{H}_a$H$_b$), 3.54–3.25 (stack, 2H, C(4)H$_a\underline{H}_b$ and C(5)H$_a\underline{H}_b$), 2.52–2.48 (m, 1H, C(8)$\underline{H}$), 1.97–1.83 (stack, 2H, C(6)$\underline{H}_a$H$_b$ and C(7)$\underline{H}_a$H$_b$), 1.74–1.49 (stack, 2H, C(6)H$_a\underline{H}_b$ and C(7)H$_a\underline{H}_b$); ^{13}C NMR (101 MHz, d_6–DMSO): δ 179.6 (C, C(2)), 175.2 (C, C(1)), 172.6 (C, C(9)), 136.3 (C, C(17)), 127.2 (C, C(3)), 126.7 (CH, C(18)), 122.7 (C, C(12)), 122.5 (C, C(11)), 121.7 (CH, C(15)), 120.6 (CH, C(14)), 118.2 (CH, C(10)), 112.2 (CH, C(13)), 110.9 (CH, C(16)), 48.1 (CH_2, C(5)), 47.1 (CH_2, C(4)), 40.7 (CH, C(8)), 28.4 (CH_2, C(6)), 27.9 (CH_2, C(7)); MS (TOF–ES+) m/z 377.1 ([M + Na]$^+$, 100%); HRMS (TOF–ES+) calcd for $C_{18}H_{18}N_4O_2NaS$ [M + Na]$^+$ 377.1048, found 377.1047.

(*Z*)–5–(2,4–dichlorobenzylidene)–2–(piperidin–1–yl)thiazol–4(*5H*)–one (**48**)

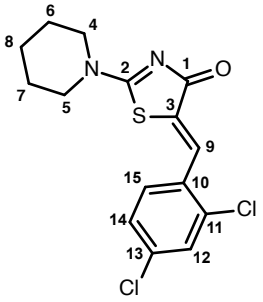

Substitution product **48** was prepared from compound **35** (99 mg, 0.33 mmol) and piperidine (33 μL, 0.33 mmol) according to general procedure B. The reaction product was crystallised from ethanol to obtain the title compound **48** as yellow crystals (42 mg, 37%): m.p. 202–204 ℃ (from EtOH); R_f = 0.5 (10% MeOH in CH_2Cl_2); IR (neat) ν_{max} = 3061w, 2944w, 2860w, 1680s, 1547s (C=O), 1445m, 1257s cm^{-1}; ^{1}H NMR (300 MHz, $CDCl_3$): δ 8.03 (s, 1H, C(10)H), 7.52 (d, J = 8.4, 1H, C(12)H), 7.47 (d, J = 2.1, C(15)H), 7.30 (dd, J = 8.4, 2.1, 1H, C(14)H), 4.02 (t, J = 5.2, 2H, C(4)H_2), 3.55 (t, J = 5.9, 2H, C(5)H_2), 1.81–1.65 (stack, 5H, C(6)H_2 and C(7)H_2 and C(8)H_aH_b), 1.62 (s, 1H, C(8)H_aH_b; ^{13}C NMR (101 MHz, $CDCl_3$): δ 180.2 (C, C(2)), 174.1 (C, C(1)), 136.4 (C, C(11)), 135.6 (C, C(13)), 132.3 (C, C(10)), 131.9 (C, C(3)), 130.2 (CH, C(12)), 129.4 (CH, C(15)), 127.5 (CH, C(14)), 126.0 (CH, C(9)), 50.5 (CH_2, C(4)), 50.0 (CH_2, C(5)), 26.3 (CH_2, C(6)), 25.6 (CH_2, C(7)), 24.1 (CH_2, C(8)); MS (TOF–ES+) m/z 364.3 ($[M + Na]^+$, 100%); HRMS (TOF–ES+) calcd for $C_{15}H_{15}{}^{35}Cl_2N_2OS$ $[M + H]^+$ 341.0277, found 341.0269.

(*Z*)–5–(2,4-dichlorobenzylidene)-2-(4-(*tert*–butyloxycarbonyl)piperazin-1-yl)thiazol-4(*5H*)-one (**49**)

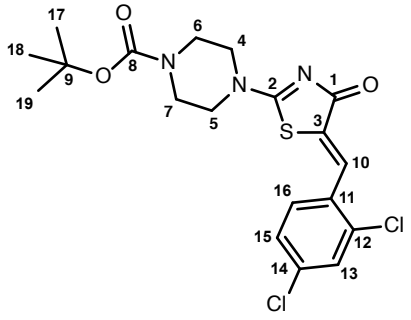

Boc–protected amine **49** was prepared from methylated rhodanine derivative **35** (58 mg, 0.19 mmol) and *N*–Boc–piperazine (36 mg, 0.19 mmol) according to general procedure B. The product was purified by flash column chromatography (eluent: 1% MeOH in CH_2Cl_2 to 10% MeOH in CH_2Cl_2) to obtain the title compound **49** as light brown crystals (71 mg, 84%): m.p. 238–241 °C dec.; R_f = 0.6 (5% MeOH in CH_2Cl_2); IR (neat) ν_{max} = 3368w, 3180w, 2958w, 1651m (C=O), 1549s (C=O), 1352m, 1223m cm^{-1}; ^1H NMR (300 MHz, 1:1 $CDCl_3$:CD_3OD): δ 7.98 (s, 1H, C(10)H), 7.61 (d, J = 8.4, 1H, C(16)H), 7.56 (d, J = 2.1, 1H, C(13)H), 7.42 (dd, J = 8.4, 2.1, 1H, C(15)H), 4.07–3.97 (m, 4H, C(4)H and C(5)H), 3.72–3.54 (m, 4H, C(6)H and C(7)H), 1.48 (s, 9H, C(17)H and C(18)H and C(19)H); ^{13}C NMR (101 MHz, 1:1 $CDCl_3$:CD_3OD): δ 180.7 (C, C(2)), 177.1 (C, C(8)), 174.8 (C, C(1)), 136.1 (C, C(12)), 134.9 (C, C(14)), 131.6 (CH, C(13)), 131.2 (CH, C(16)), 129.4 (C, C(3)), 128.5 (C, C(11)), 127.2 (CH, C(15)), 124.8 (CH, C(10)), 80.3 (C, C(9)) 46.4 (CH_2, C(5)), 46.1 (CH_2, C(4)), 40.9 (CH_2, C(6)), 40.8 (CH_2, C(7)), 28.3 (CH_3, C(17) and C(18) and C(19)); MS (TOF–ES+) *m/z* 465.4 ($[M + Na]^+$, 100%); HMRS (TOF–ES+) calcd for $C_{19}H_{22}{}^{35}Cl_2N_3O_3S$ $[M + H]^+$ 442.0753, found 442.0760.

(*Z*)–5–(2,4–dichlorobenzylidene)–2–(piperazin–1–yl)thiazol–4(*5H*)–one (**50**)

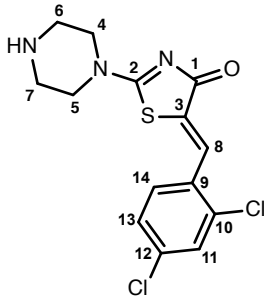

TFA (0.1 mL, 1.3 mmol) was added to a solution of **49** (115 mg, 0.26 mmol) in CH_2Cl_2 (2 mL). The mixture was stirred at r.t. and the reaction was monitored by TLC. After 6 h the solvent was removed under reduced pressure to give a red–brownish solid. Purification of the product by flash column chromatography (eluent: 2% MeOH in CH_2Cl_2 to 10% MeOH in CH_2Cl_2) provided the title compound **50** as a brown powder (87 mg, 98%): m.p. 203–206 ℃; R_f = 0.4 (10% MeOH in CH_2Cl_2); IR (neat) ν_{max} = 3346w (N–H), 2970w, 1662m, 1557s (C=O), 1443m, 1275s cm^{-1}; ^1H NMR (300 MHz, CD_3OD): δ 7.97 (s, 1H, C(8)H), 7.69 (d, J = 8.5, 1H, C(14)H), 7.64 (d, J = 2.1, 1H, C(11)H), 7.48 (dd, J = 8.5, 2.1, 1H, C(13)H), 4.05–3.95 (m, 2H, C(4)H_2), 3.71–3.61 (m, 2H, C(5)H_2), 3.03–2.90 (stack, 4H, C(6)H_2 and C(7)H_2), NH not observed; ^{13}C NMR (101 MHz, 1:1 CD_2Cl_2:CD_3OD): δ 180.5 (C, C(2)), 175.5 (C, C(1)), 136.2 (C, C(10)), 136.1 (C, C(12)), 131.2 (C, C(9)), 131.1 (C, C(3)), 130.08 (CH, C(14)), 129.4 (CH, C(11)), 127.6 (CH, C(13)), 127.2 (CH, C(8)), 44.4 (CH_2, C(6) and C(7)), 44.1 (CH_2, C(4) and C(5)); MS (TOF–ES+) m/z 343.2 ($[M + H]^+$, 100%); HRMS (TOF–ES+) calcd for $C_{14}H_{14}{}^{35}Cl_2N_3OS$ $[M + H]^+$ 342.0229, found 342.0221.

(*Z*)-2-(4-acetylpiperazin-1-yl)-5-(2,4-dichlorobenzylidene)thiazol-4(*5H*)-one (**51**)

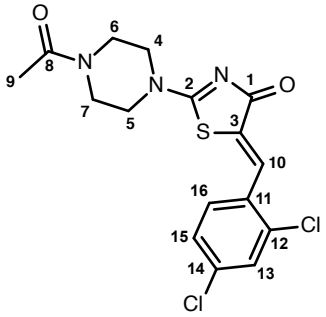

Ac_2O (15 μL, 0.17 mmol) was added to a solution of **50** (50 mg, 0.15 mmol) in CH_2Cl_2 (10 mL). The mixture was stirred at r.t and the reaction was monitored by TLC. Upon completion the reaction mixture was quenched with H_2O (5 mL). The organic phase was separated, washed with H_2O (2×5 mL), dried (Na_2SO_4) and evaporated under reduced pressure. The product was purified by flash column chromatography (eluent: 1% MeOH in CH_2Cl_2 to 10% MeOH in CH_2Cl_2) to provide the title compound **51** as a yellow powder (20 mg, 34%): m.p. 243–246 ℃ dec.; R_f = 0.7 (10% MeOH in CH_2Cl_2); IR (neat) ν_{max} = 3012w, 2922w, 2941w, 1642m (C=O), 1546s (C=O), 1429m, 1236m cm^{-1}; ^1H NMR (300 MHz, 1:1 $CDCl_3$:CD_3OD): δ 8.00 (s, 1H, C(10)H), 7.55 (d, J = 8.4, 1H, C(16)H), 7.51 (d, J = 2.1, 1H, C(13)H), 7.37 (dd, J = 8.4, 2.1, 1H, C(15)H), 4.13–3.98 (m, 4H, C(4)H_2 and C(5)H_2), 3.84–3.66 (m, 2H, C(6)H_2), 3.72–3.61 (m, 2H, C(7)H_2), 2.16 (s, 3H, C(9)H_3); ^{13}C NMR (101 MHz, 1:1 $CDCl_3$:CD_3OD): δ 180.9 (C, C(2)), 176.5 (C, C(8)), 171.1 (C, C(1)), 136.9 (C, C(12)), 131.7 (C, C(14)), 130.7 (CH, C(13)), 130.0 (CH, C(16)), 128.22 (CH, C(15)), 128.20 (C, C(3)), 127.9 (CH, C(10)), 127.8 (C, C(11)), 46.1 (CH_2, C(5)), 45.9 (CH_2, C(4)), 41.4 (CH_2, C(6)), 41.3 (CH_2, C(7)), 21.3 (CH_3, C(9)); MS (TOF–ES+) *m/z* 384.3 ([M + H]$^+$, 100%); HRMS (TOF–ES+) calcd for $C_{16}H_{16}{}^{35}Cl^{37}ClN_3O_2S$ [M + H]$^+$ 384.0335, found 384.0341.

(*Z*)-5-(2,4-dichlorobenzylidene)-2-(4-(methylsulfonyl)piperazin-1-yl)thiazol-4(*5H*)-one (**52**)

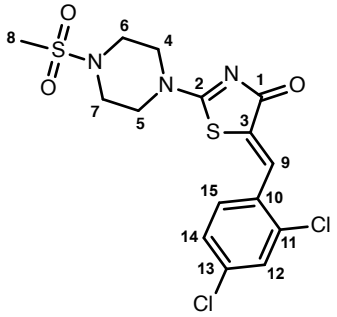

Et_3N (40 μL, 0.3 mmol) was added to a solution **50** (50 mg, 0.15 mmol) in CH_2Cl_2 (5 mL). After cooling to 0 ℃, MsCl (13 μL, 0.18 mmol) was added dropwise over 1 min. After 30 min. the ice bath was removed and the reaction was left stirring for another 30 min. After completion, Et_3N (20 μL) was addded to the reaction mixture and left stirring for 5 min. The mixture was then diluted with CH_2Cl_2 (10 mL), washed with H_2O (2×10 mL) and brine (10 mL), dried (Na_2SO_4) and and evaporated under reduced pressure. The orange residue obtained was purified by flash column chromatography (eluent: 1% MeOH in CH_2Cl_2 to 10% MeOH in CH_2Cl_2) to provide the title compound **52** as an orange powder (34.6 mg, 55%): m.p. 281–282 ℃ dec.; R_f = 0.92 (10% MeOH in CH_2Cl_2); IR (neat) ν_{max} = 3362w, 2924w, 1681m, 1549s (C=O), 1253m, 1319m, 1151m cm^{-1}; ^1H NMR (300 MHz, $CDCl_3$): δ 8.10 (s, 1H, C(9)H), 7.51 (d, J = 1.2, 1H, C(12)H), 7.49 (d, J = 5.1, 1H, C(15)H), 7.33 (dd, J = 5.1, 1.2, 1H, C(14)H), 4.21 (t, J = 5.1, 2H, C(6)H_2), 3.70 (t, J = 5.9, 2H, C(7)H_2), 3.46–3.37 (m, 4H, C(4)H_2 and C(5)H_2), 2.85 (s, 3H, C(8)H_3); ^{13}C NMR (101 MHz, 1:1 $CDCl_3$:CD_3OD): δ 181.1 (C, C(2)), 171.7 (C, C(1)), 135.1 (C, C(11)), 131.3 (C, C(13)), 130.2 (CH, C(12)), 129.7 (CH, C(15)), 128.3 (CH, C(14)), 127.8 (C, C(3)), 127.1 (C, C(10)), 126.2 (CH, C(9)), 48.3 (CH_2, C(6)), 47.6 (CH_2, C(7)), 42.6 (CH_2, C(4)), 42.2 (CH_2, C(5)), 26.4 (CH_3, C(8)). MS (TOF–ES+) *m/z* 421.4 ([M + H]$^+$, 100%); HRMS (TOF–ES+) calcd for $C_{15}H_{15}{}^{35}Cl^{37}ClN_3O_3S_2$ [M + H]$^+$ 421.0005, found 421.0011.

(*Z*)–5–(2,4–dichlorobenzylidene)–2–morpholinothiazol–4(5H)–one (**53**)

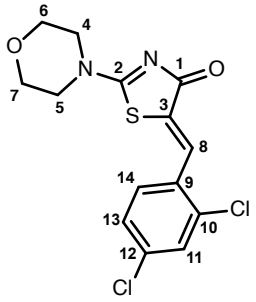

Substitution product **53** was prepared from compound **35** (110 mg, 0.36 mmol) and morpholine (31 μL, 0.36 mmol) according to general procedure B. The crude reaction product was recrystallised from EtOH to obtain the title compound **53** as a white powder (92 mg, 74%): m.p. 256–257 ℃ (from EtOH); R_f = 0.8 (1% MeOH in CH_2Cl_2); IR (neat) ν_{max} = 2984w, 2932w, 2872w, 1698m, 1551s (C=O), 1383m, 1276s cm^{-1}; ^{1}H NMR (300 MHz, 1:1 $CDCl_3$:CD_3OD): δ 8.00 (s, 1H, C(8)H), 7.58 (d, J = 8.5, 1H, C(14)H), 7.53 (d, J = 2.1, 1H, C(11)H), 7.39 (dd, J = 8.5, 2.1, 1H, C(13)H), 4.06–4.01 (stack, 2H, C(4)H_aH_b and C(5)H_aH_b), 3.86–3.79 (stack, 4H, C(4)H_aH_b and C(5)H_aH_b and C(6)H_aH_b and C(7)H_aH_b), 3.70–3.64 (stack, 2H, C(6)H_aH_b and C(7)H_aH_b); ^{13}C NMR (101 MHz, CD_3OD): δ 184.4 (C, C(2)), 178.3 (C, C(1)), 135.1 (C, C(12)), 134.8 (C, C(10)), 132.6 (C, C(3)), 131.1 (C, C(9)), 129.8 (CH, C(11)), 128.2 (CH, C(14)), 123.9 (CH, C(13)), 113.8 (CH, C(8)), 65.6 (CH_2, C(6)), 65.5 (CH_2, C(7)), 48.8 (CH_2, C(4)), 48.7 (CH_2, C(5)); MS (TOF–ES+) m/z 344.3 ([M + H]$^+$, 100%); HRMS (TOF–ES+) calcd for $C_{14}H_{13}{}^{35}Cl_2N_2O_2S$ [M + H]$^+$ 343.0069, found 343.0075.

4–phenylpyridin–2–amine (**75**)[87]

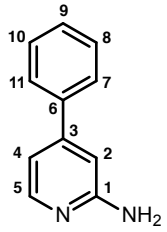

Phenylboronic acid (0.5 g, 4.1 mmol), 4–chloro–2–aminopyridine (**71**) (0.6 g, 4.8 mmol) and Na_2CO_3 (1.8 g, 17 mmol) were dissolved in a mixture of 1,4–dioxane (12 ml) and H_2O (4 mL). N_2 gas was bubbled through the suspension for 15 min. $Pd(PPh_3)_4$ (0.5 g, 0.5 mmol) was then added to the mixture, which was heated at 90 ℃ for 16 h. After cooling to r.t., the reaction mixture was extracted with EtOAc (3 × 25 mL). The combined organic phases were washed with H_2O (3 × 10 mL), dried (Na_2SO_4), filtered and evaporated under reduced pressure to obtain a brown residue. Purification by flash column chromatography (eluent: 1% MeOH in CH_2Cl_2 to 5% MeOH in CH_2Cl_2) provided the title compound **75** as a brown solid (0.12 g, 15%): m.p. 162–164 ℃ dec.; lit.[?] 162–163 ℃; R_f = 0.2 (5% MeOH in CH_2Cl_2); IR (neat) ν_{max} = 3718br (N–H), 3035m, 2969m, 2928w, 1590s, 1445s, 1329s cm^{-1}; ^{1}H NMR (400 MHz, $CDCl_3$): δ 8.13 (dd, J = 5.4, 0.8, 1H, C(5)H), 7.63–7.54 (m, 2H, C(7)H and C(11)H), 7.50–7.35 (stack, 3H, C(8)H and C(9)H and C(10)H), 6.89 (dd, J = 5.4, 1.6, 1H, C(4)H), 6.71 (dd, J = 1.6, 0.8, 1H, C(2)H), 4.51 (br s, 2H, NH_2); ^{13}C NMR (101 MHz, $CDCl_3$): δ 159.0 (C, C(1)), 150.5 (C, C(3)), 148.8 (CH, C(5)), 138.9 (C, C(6)), 129.0 (CH, C(8) and C(10)), 128.9 (CH, C(9)), 127.0 (CH, C(7) and C(11)), 113.0 (CH, C(4)), 106.4 (CH, C(2)); MS (TOF–ES+) m/z 170.9 ($[M + H]^+$, 100%). Data are in agreement with those reported in the literature.[87]

N–(4–phenylpyridin–2–yl)pivalamide (**76**)

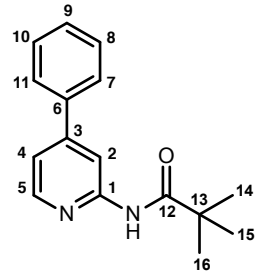

A brown solution of 4–phenylpyridin–2–amine (**75**) (107 mg, 0.63 mmol) in CH_2Cl_2 (3 mL) was cooled to 0 ℃. Et_3N (111 μL, 0.79 mmol) and pivaloyl chloride (86 μL, 0.69 mmol) were then sequentially added. After 2 h, the solution was warmed to r.t. After 1 h at r.t., the reaction mixture was washed sequentially with H_2O (2 mL) and $NaHCO_3$ soln. (2 × 2 mL). The organic phase was dried (anh. Na_2SO_4), filtered and evaporated under reduced pressure. The residue was purified by flash column chromatography (eluent: CH_2Cl_2 to 1% MeOH in CH_2Cl_2) to provide amide **76** as a white solid (152 mg, 95%): m.p. 247–249 ℃ dec.; R_f = 0.65 (CH_2Cl_2); IR (neat) ν_{max} = 3303br (N–H), 3061w, 2933w, 1636s, 1516s (C=O), 1116m cm^{-1}; ^1H NMR (400 MHz, $CDCl_3$): δ 8.58 (dd, J = 1.7, 0.8, 1H, C(2)H), 8.30 (dd, J = 5.2, 0.8, 1H, C(5)H), 8.10 (br s, 1H, NH), 7.72–7.66 (m, 2H, C(7)H and C(11)H), 7.49–7.38 (stack, 3H, C(8)H and C(9)H and C(10)H), 7.28 (dd, J = 5.2, 1.7, 1H, C(4)H), 1.35 (s, 9H, C(14)H and C(15)H and C(16)H); ^{13}C NMR (101 MHz, $CDCl_3$): δ 177.4 (C, C(12)), 152.3 (C, C(1)), 151.0 (CH, C(5)), 148.2 (C, C(3)), 138.3 (C, C(6)), 129.3 (CH, C(9)), 129.2 (CH, C(8) and C(10)), 127.3 (CH, C(7) and C(11)), 118.0 (CH, C(4)), 111.9 (CH, C(2)), 40.0 (C, C(13)), 27.7 (CH_3, C(14) and C(15) and C(16)); MS (TOF–ES+) m/z 254.3 ($[M + H]^+$, 100%); HRMS (TOF–ES+) calcd for $C_{16}H_{19}N_2O$ $[M + H]^+$ 255.1492, found 255.1495.

4–Phenyl–2–pivalamidopyridin–3–yl diethylcarbamodithioate (**72**)

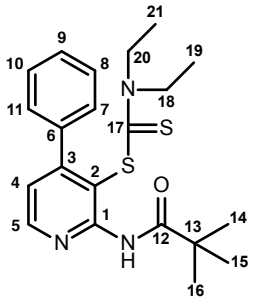

N–(4–Phenylpyridin–2–yl)pivalamide (**76**) (190 mg, 0.75 mmol) was dissolved in THF (3 mL). The colourless solution was cooled to –50 ℃ and *n*–BuLi (0.6 mL of a 2.5 M in hexanes, 1.5 mmol) was added over 2 min. The colour of the solution changed to dark yellow during the addition. After 30 min, the solution, which presented a dark red colour, was warmed to 0 ℃. After 4 h, the mixture was cooled to –50 ℃ and a solution of TETD (268 mg, 0.91 mmol) in THF (1 mL) was added. After 30 min, the solution was warmed to r.t and stirred for 16 h. Et_2O (20 mL) was then added and the organic phase was washed with H_2O (2 × 20 mL), dried (anh. Na_2SO_4) and concentrated under reduced pressure. The residue was purified by flash column chromatography (eluent: 5% EtOAc in hexane to 40% EtOAc in hexane) to obtain the title compound **72** as a yellow viscous liquid (235 mg, 78%): R_f = 0.6 (2% MeOH in CH_2Cl_2); IR (neat) ν_{max} = 3384br (N–H), 3048w, 2956w, 2872w, 1622m, 1542s (C=O), 1357m cm^{-1}; ^1H NMR (300 MHz, $CDCl_3$): δ 8.54 (d, J = 5.0, 1H, C(5)H), 7.39–7.21 (stack, 5H, C(7)H and C(8)H and C(9)H and C(10)H and C(11)H), 7.10 (d, J = 5.0, 1H, C(4)H), 3.94–3.79 (m, 2H, C(18)H), 3.69–3.46 (m, 2H, C(20)H), 1.23 (s, 9H, C(14)H and C(15)H and C(16)H), 1.19 (t, J = 7.0, 3H, C(19)H), 1.07 (t, J = 7.2, 3H, C(21)H), NH not observed;

^{13}C NMR (101 MHz, $CDCl_3$): δ 192.4 (C, C(17)), 176.6 (C, C(12)), 156.8 (C, C(1)), 154.8 (C, C(3)), 150.1 (CH, C(5)), 138.9 (C, C(6)), 128.6 (CH, C(9)), 128.5 (CH, C(8) and C(10)), 128.1 (CH, C(7) and C(11)), 122.2 (CH, C(4)), 119.1 (C, C(2)), 49.9 (CH_2, C(18)), 47.7 (CH_2, C(20)), 39.9 (C, C(13)), 27.4 (CH_3, C(14) and C(15) and C(16)), 12.7 (CH_3, C(19)), 11.5 (CH_3, C(21)); MS (TOF–ES+) m/z 402.7 ($[M + H]^+$, 100%); HRMS (TOF–ES+) calcd for $C_{21}H_{28}N_3OS_2$ $[M + H]^+$ 402.1668, found 402.1671.

7–Phenylthiazolo[4,5–*b*]pyridine–2–thiol (**73**)

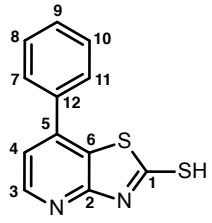

NaOH (372 mg, 9.3 mmol) was added to a solution of 4–phenyl–2–pivalamidopyridin–3–yl diethylcarbamodithioate (**72**) (124 mg, 0.31 mmol) in EtOH (2 mL). The mixture was heated at 90 ℃ for 2 h. After cooling to r.t., hydrochloric acid (10 mL, 2 M in H_2O) was added and a yellow precipitate was formed. The solid was filtered, washed with H_2O (5 mL), dried under reduced pressure and used without further purification (31 mg, 41%): m.p. 204–210 ℃; R_f = 0.5 (1% MeOH in CH_2Cl_2); IR (neat) ν_{max} = 3102m, 3028m, 2974m, 2574w (S–H), 1518m, 1354m cm^{-1}; ^1H NMR (300 MHz, CD_3OD): δ 8.34 (d, J = 5.2, 1H, C(3)H), 7.63–7.40 (stack, 5H, C(7)H and C(8)H and C(9)H and C(10)H and C(11)H), 7.27 (d, J = 5.2, 1H, C(4)H), SH not observed; ^{13}C NMR (101 MHz, CD_3OD): δ 170.5 (C, C(1)), 167.2 (C, C(2)), 151.1 (CH, C(3)), 142.8 (C, C(5)), 137.4 (C, C(12)), 128.3 (CH, C(9)), 128.1 (CH, C(8) and C(10)), 127.8 (CH, C(7) and C(11)), 120.9 (C, C(6)), 119.4 (CH, C(4)); MS (TOF–ES+) m/z 245.4 ($[M + H]^+$, 100%); HRMS (TOF–ES+) calcd for $C_{12}H_8N_2S_2$ $[M + H]^+$ 245.0202, found 245.0208.

2–(Methylthio)–7–phenylthiazolo[4,5–*b*]pyridine (**74**)

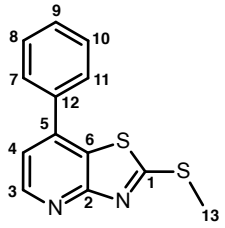

7–Phenylthiazolo[4,5–*b*]pyridine–2–thiol (**73**) (22 mg, 0.09 mmol) was dissolved in DMF (2 mL). K_2CO_3 (13 mg, 0.09 mmol) was added to the solution and the mixture was stirred at r.t. After 15 min, MeI (7 μL, 0.11 mmol) was added and the mixture was stirred for 1 h. H_2O (10 mL) was then added and the aqueous solution was washed with EtOAc (3×10 mL). The combined organic phases were washed with brine (10 mL), dried (anh. Na_2SO_4) and concentrated under reduced pressure to obtain a yellow solid that was used without further purification (21 mg, 88%): m.p. 224–228 ℃; R_f = 0.8 (1% MeOH in CH_2Cl_2); IR (neat) ν_{max} = 3098m, 3041m, 2983m, 1832w, 1578m, 1412m cm^{-1}; ^{1}H NMR (300 MHz, $CDCl_3$): δ 8.67 (d, J = 5.0, 1H, C(3)H), 7.72–7.62 (m, 2H, C(7)H and C(11)H), 7.58–7.47 (stack, 3H, C(8)H and C(9)H and C(10)H), 7.30 (d, J = 5.0, 1H, C(4)H), 2.86 (s, 3H, C(13)H); ^{13}C NMR (101 MHz, $CDCl_3$): δ 173.4 (C, C(1)), 165.0 (C, C(2)), 148.2 (CH, C(3)), 144.2 (C, C(5)), 138.2 (C, C(12)), 129.7 (CH, C(9)), 129.4 (CH, C(8) and C(10)), 127.7 (CH, C(7) and C(11)), 123.4 (C, C(6)), 118.1 (CH, C(4)), 16.0 (CH_3, C(13)); MS (TOF–ES+) m/z 260.1 ([M + H]$^+$, 100%); HRMS (TOF–ES+) calcd for $C_{13}H_{11}N_2S_2$ [M + H]$^+$ 259.0358, found 259.0361.

1–(7–Phenylthiazolo[4,5–*b*]pyridin–2–yl)piperidine–4–carboxamide (**70**)

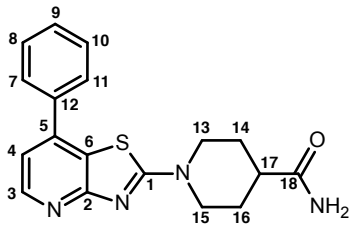

A colourless solution of 2–(methylthio)–7–phenylthiazolo[4,5–*b*]pyridine (**74**) (20 mg, 0.08 mmol) and isonipecotamide (**31**) (51 mg, 0.40 mmol) in 1–butanol (10 mL) was heated at 160 ℃ under microwave radiation for 4 h, after which time a black solution was obtained. The solvent was removed under reduced pressure and the residue dissolved in EtOAc (10 mL). The solution was washed sequentially with H_2O (10 mL) and brine (10 mL), dried (anh. Na_2SO_4) and concentrated under reduced pressure. The residue was purified by flash column chromatography (eluent: 1% MeOH in CH_2Cl_2 to 10% MeOH in CH_2Cl_2) to obtain the title compound as a white solid (21 mg, 77%): m.p. 238–241 ℃ dec.; R_f = 0.8 (10% MeOH in CH_2Cl_2); IR (neat) ν_{max} = 3452br (N–H), 3045w, 2935w, 1635m (C=O), 1368m cm^{-1}; ^1H NMR (300 MHz, 1:1 $CDCl_3$:CD_3OD): δ 8.69 (d, J = 5.1, 1H, C(3)$\underline{H}$), 7.75–7.64 (m, 2H, C(7)$\underline{H}$ and C(11)$\underline{H}$), 7.63–7.39 (stack, 3H, C(8)$\underline{H}$ and C(9)$\underline{H}$ and C(10)$\underline{H}$), 7.31 (d, J = 5.1, 1H, C(4)$\underline{H}$), 4.74 (d with unresolved fine coupling, J = 13.7, 1H, C(13)$\underline{H}_aH_b$), 3.92 (d with unresolved fine coupling, J = 13.7, 1H, C(15)$\underline{H}_aH_b$), 3.55–3.21 (stack, 2H, C(13)$H_a\underline{H}_b$ and C(15)$H_a\underline{H}_b$), 2.69–2.52 (m, 1H, C(17)$\underline{H}$), 2.09–1.93 (stack, 2H, C(14)$\underline{H}_aH_b$ and C(16)$\underline{H}_aH_b$), 1.93–1.73 (m, 2H, C(14)$H_a\underline{H}_b$ and C(16)$H_a\underline{H}_b$), N$\underline{H}_2$ not observed;

^{13}C NMR (101 MHz, 1:1 $CDCl_3$:CD_3OD): δ 181.5 (C, C(18)), 168.2 (C, C(1)), 156.8 (C, C(2)), 151.4 (CH, C(3)), 142.9 (C, C(5)), 137.7 (C, C(12)), 129.4 (CH, C(9)), 129.1 (CH, C(8) and C(10)), 127.8 (CH, C(7) and C(11)), 123.6 (C, C(6)), 119.4 (CH, C(4)), 48.7 (CH_2, C(13)), 47.9 (CH_2, C(15)), 40.9 (CH, C(17)), 28.3 (CH_2, C(14)), 28.17 (CH_2, C(16)); MS (TOF–ES+) *m/z* 362.1 ($[M + Na]^+$, 100%); HRMS (TOF–ES+) calcd for $C_{18}H_{19}N_4OS$ $[M + H]^+$ 339.1274, found 339.1280.

Methyl 4–(bromomethyl)benzoate (**79**)[88]

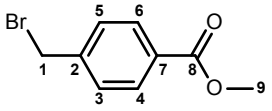

A solution of 4–(bromomethyl)benzoic acid **78** (2.1 g, 9.7 mmol) in anhydrous MeOH (20 mL) was stirred over activated 4 Å molecular sieves for 30 min. The solution was cooled to 0 ℃ and $SOCl_2$ (2.7 mL, 37 mmol) was added dropwise over 5 min. The mixture was stirred for 16 h at r.t. and then concentrated under reduced pressure. The yellow residue was purified by flash column chromatography (eluent: 10% EtOAc in hexane to 40% EtOAc in hexane) to provide ester **79** as white crystals (1.8 g, 81%): m.p. 54–56 ℃, lit.[88] 54.1–54.4 ℃; R_f = 0.5 (20% EtOAc in hexane); IR (neat) ν_{max} = 3031w, 2959w, 1718s (C=O), 1433m, 1279s cm^{-1}; ^1H NMR (400 MHz, $CDCl_3$): δ 8.01 (AA' of AA'BB', J = 8.4, 2H, C(4)H and C(6)H), 7.46 (BB' of AA'BB', J = 8.4, 2H, C(3)H and C(5)H), 4.50 (s, 2H, C(1)H_2), 3.92 (s, 3H, C(9)H_3); ^{13}C NMR (101 MHz, $CDCl_3$): δ 166.7 (C, C(8)), 142.7 (C, C(7)), 130.2 ((C, C(2)) and (CH, C(4) and C(6)), resonance overlap), 129.2 (CH, C(3) and C(5)), 52.4 (CH_3, C(9)), 32.4 (CH_2, C(1)); MS (ES+) m/z 229.0 ($[M]^+$, 100%).

Data are in agreement with those reported in the literature.[88]

Methyl 4–(azidomethyl)benzoate (**80**)[89]

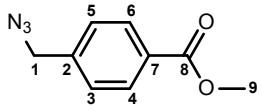

Bromide **79** (250 mg, 1.1 mmol) was dissolved in anhydrous DMF (5 mL) to provide a yellow solution. NaN_3 (140 mg, 2.2 mmol) was added portionwise over 5 min during which time the colour of the solution changed to red. The mixture was stirred at r.t. for 24 h after which time, EtOAc (25 mL) was added. The resulting solution was washed sequentially with H_2O (25 mL) and brine (25 mL), dried (Na_2SO_4), filtered and evaporated under reduced pressure to provide a colourless liquid. The product was purified by flash column chromatography (eluent: 10% EtOAc in hexane to 40% EtOAc in hexane) to provide azide **80** as a colourless liquid (157 mg, 75%): R_f = 0.75 (CH_2Cl_2); IR (neat) ν_{max} = 3002w, 2952w, 2092s (N_3), 1714s (C=O), 1272s cm^{-1}; ^1H NMR (400 MHz, $CDCl_3$): δ 7.97 (AA' of AA'BB', J = 8.3, 2H, C(3)H and C(5)H), 7.30 (BB' of AA'BB', J = 8.3, 2H, C(4)H and C(6)H), 4.32 (s, 2H, C(1)H_2), 3.84 (s, 3H, C(9)H_3); ^{13}C NMR (101 MHz, $CDCl_3$): δ 166.4 (C, C(8)), 140.3 (C, C(2)), 129.9 (CH, C(4) and C(6)), 129.8 (C, C(7)), 127.7 (CH, C(3) and C(5)), 54.0 (CH_3, C(9)), 51.9 (CH_2, C(1)); MS (TOF–ES+) m/z 214.2 ($[M + Na]^+$, 100%).

All work involving azides was performed in an empty lab in a fumehood containing an explosion shield. Working was signalled with appropriate caution signs in order to ensure the safety of workers not involved in the synthesis. Data are in agreement with those reported in the literature.[89]

4–(azidomethyl)benzenemethanol (**81**)[90]

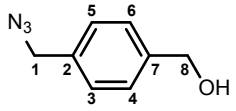

DIBAL–H (1.18 mL, 1.18 mmol, 1 M in hexanes) was added dropwise over 10 min to a colourless solution of ester **80** (151 mg, 0.79 mmol) in toluene (5 mL) at –78 ℃. The resulting yellow solution was stirred for 2 h, after which time, MeOH (10 mL) was added dropwise over 5 min. The mixture was warmed to r.t. The resulting grey precipitate was filtered through a pad of Celite and the filtrate evaporated under reduced pressure. The residue was dissolved in EtOAc (10 mL), washed with H_2O (10 mL), dried (Na_2SO_4), filtered and evaporated under reduced pressure to provide alcohol **81** as a colourless liquid (119 mg, 92%): R_f = 0.2 (40% EtOAc in cyclohexane); IR (neat) ν_{max} = 3340br (O–H), 3022w, 2929w, 2875w, 2092s (N_3), 1249m cm^{-1}; ^{1}H NMR (400 MHz, $CDCl_3$): δ 7.34 (AA' of AA'BB', J = 8.2, 2H, C(4)H and C(6)H), 7.28 (BB' of AA'BB', J = 8.2, 2H, C(3)H and C(5)H), 4.62 (s, 2H, C(8)H_2), 4.31 (s, 2H, C(1)H_2), 2.66 (s, 1H, OH); ^{13}C NMR (101 MHz, $CDCl_3$): δ 141.1 (C, C(7)), 134.6 (C, C(2)), 128.5 (CH, C(4) and C(6)), 127.4 (CH, C(3) and C(5)), 64.7 (CH_2, C(8)), 54.5 (CH_2, C(1)); MS (TOF–ES+) m/z 164.2 ([M + H]$^+$, 100%).

All work involving azides was performed in an empty lab in a fumehood containing an explosion shield. Working was signalled with appropriate caution signs in order to ensure the safety of workers not involved in the synthesis. Data are in agreement with those reported in the literature.[90]

4-(azidomethyl)benzaldehyde (**82**)[91]

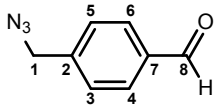

PCC (264 mg, 1.22 mmol) was added to a colourless solution of alcohol **81** (100 mg, 0.61 mmol) in CH_2Cl_2 (5 mL). After 2 h, the brown reaction mixture was diluted with CH_2Cl_2 (25 mL) and filtered through a pad of Celite. The filtrate was washed sequentially with $NaHCO_3$ soln. (20 mL) and brine (20 mL), dried (Na_2SO_4), filtered and concentrated under reduced pressure to a volume of approx. 2 mL. For safety reasons, the combined organic phase was not evaporated to dryness and the resulting yellow solution of aldehyde **82** in CH_2Cl_2 was used without purification: R_f = 0.7 (CH_2Cl_2); IR (CH_2Cl_2) ν_{max} = 2828w, 2735w, 2096s (N_3), 1694s (C=O), 1607m, 1206m cm^{-1}; ^1H NMR (300 MHz, $CDCl_3$): δ 9.82 (s, 1H, C(8)H), 7.81 (AA' of AA'BB', J = 8.0, 2H, C(4)H and C(6)H), 7.39 (BB' of AA'BB', J = 8.0, 2H, C(3)H and C(5)H), 4.39 (s, 2H, C(1)H_2); MS (TOF–ES+) m/z 162.1 ($[M + H]^+$, 100%). All work involving azides was performed in an empty lab in a fumehood containing an explosion shield. Working was signalled with appropriate caution signs in order to ensure the safety of workers not involved in the synthesis. Data are in agreement with those reported in the literature.[91]

(*Z*)–1–(5–(4"–(azidomethyl)benzylidene)–2–(4'–carboxamidepiperidin–1'–yl)thiazol–4(*5H*)–one (**83**)

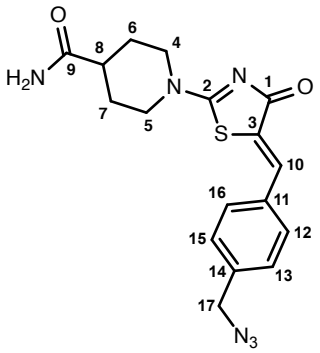

Knoevenagel product **83** was prepared from rhodanine derivative **29** (50 mg, 0.22 mmol) and aldehyde **82** (35 mg, 0.22 mmol) according to general procedure A. Purification by flash column chromatography (eluent: 1% MeOH in CH_2Cl_2 to 10% MeOH in CH_2Cl_2) provided the title compound **83** as white crystals (45 mg, 55%): m.p. 216–218 °C; R_f = 0.6 (10% MeOH in CH_2Cl_2); IR (neat) ν_{max} = 3351br (N–H), 3062w, 2988w, 2918w, 2856w, 2111m (N_3), 1671m (C=O), 1546s (C=O), 1342m cm^{-1}; ^1H NMR (300 MHz, 1:1 $CDCl_3$:CD_3OD): δ 7.43 (s, 1H, C(10)H), 7.33–7.26 (m, 2H, C(13)H and C(15)H), 7.16–7.11 (m, 2H, C(12)H and C(16)H), 4.71 (d with unresolved fine coupling, J = 13.1, 1H, C(4)H_aH_b), 3.89 (d with unresolved fine coupling, J = 13.4, 1H, C(5)H_aH_b), 3.52–3.24 (stack, 2H, C(4)H_aH_b and C(5)H_aH_b), 2.65 (s, 2H, C(17)H_2), 2.61–2.53 (m, 1H, C(8)H), 2.12–1.96 (stack, 2H, C(6)H_aH_b and C(7)H_aH_b), 1.96–1.82 (stack, 2H, C(6)H_aH_b and C(7)H_aH_b), NH_2 not observed; ^{13}C NMR (101 MHz, 1:1 $CDCl_3$:CD_3OD): δ 183.4 (C, C(2)), 178.1 (C, C(1)), 172.3 (C, C(9)), 137.2 (C, C(14)), 132.3 (C, C(11)), 128.9 (CH, C(15) and C(13)), 127.8 (CH, C(12) and C(16)), 127.1 (C, C(3)), 126.2 (CH, C(10)), 49.9 (CH_2, C(17)), 48.4 (CH_2, C(5)), 47.8 (CH_2, C(4)), 40.6 (CH, C(8)), 28.4 (CH_2, C(6)), 28.2 (CH_2, C(7)); MS (TOF–ES+) m/z 371.5 ([M + H]$^+$, 100%); HRMS (TOF–ES+) calcd for $C_{17}H_{19}N_6O_2S$ [M + H]$^+$ 371.1285, found 371.1288.

tert–butyl 4–(hydroxymethyl)piperidine–1–carboxylate (**85**)[92]

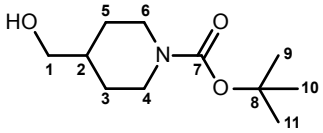

Boc_2O (2.0 mL, 8.7 mmol) was added to a cooled (0 ℃) solution of 4–piperidine-methanol **84** (1.0 g, 8.7 mmol) in CH_2Cl_2 (10 mL). The reaction mixture was stirred at r.t. for 16 h and then diluted with CH_2Cl_2 (10 mL). The resulting solution was washed sequentially with H_2O (20 mL), NH_4Cl soln. (20 mL) and brine (20 mL), dried (Na_2SO_4), filtered and evaporated under reduced pressure to provide Boc amide **85** as white crystals (1.76 g, 94%): m.p. 78–81 ℃; lit.[92] 78–82 ℃; R_f = 0.1 (20% EtOAc in cyclohexane); IR (neat) ν_{max} = 3437br (O–H), 2922w, 2849w, 1664s (C=O), 1416m, 1159s cm^{-1}; ^1H NMR (400 MHz, DMSO–d_6): δ 4.45 (t, J = 5.3, 1H, O$\underline{H}$), 3.93 (app. d, J = 12.5, 2H, C(4)$\underline{H}_aH_b$ and C(6)$\underline{H}_aH_b$), 3.23 (dd, J = 6.3, 5.3, 2H, C(1)$\underline{H}_2$), 2.66 (app br s, 2H, C(4)$H_a\underline{H}_b$ and C(6)$H_a\underline{H}_b$), 1.67–1.55 (dd, J = 12.5, 4.0, 2H, C(3)$\underline{H}_aH_b$ and C(5)$\underline{H}_aH_b$), 1.57–1.42 (m, 1H, C(2)$\underline{H}$), 1.38 (s, 9H, C(9)$\underline{H}$ and C(10)$\underline{H}$ and C(11)$\underline{H}$), 1.05–0.88 (m, 2H, C(3)$H_a\underline{H}_b$ and C(5)$H_a\underline{H}_b$); ^{13}C NMR (101 MHz, $CDCl_3$): δ 154.9 (C, C(7)), 78.3 (C, C(8)), 65.6 (CH_2, C(1)), 43.3 (br, CH_2, C(4) and C(6)), 38.3 (CH, C(2)), 28.5 (CH_2, C(3) and C(5)), 28.1 (CH_3, C(9) and C(10) and C(11)); MS (TOF–ES+) m/z 160.1 ([M - ^{t}Bu + H]$^+$, 90%), 142.10 (100)).

Data are in agreement with those reported in the literature.[92]

tert–butyl 4–(tosyloxymethyl)piperidine–1–carboxylate (**86**)[93]

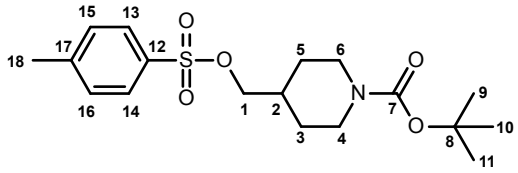

Et_3N (1.5 mL, 11 mmol) was added to a cooled (0 ℃) solution of alcohol **85** (1.5 g, 7.0 mmol) in CH_2Cl_2 (10 mL). After 5 min, TsCl (0.6 mL, 7.7 mmol) was added portionwise over 2 min, resulting in the formation of a white suspension that quickly disappeared to give a yellow solution. The reaction mixture was stirred at r.t. for 5 h and then quenched by the addition of H_2O (20 mL). The organic phase was separated, washed with brine (20 mL), dried (Na_2SO_4), filtered and evaporated under reduced pressure to give tosylate **86** as a white solid (2.4 g, 94%): m.p. 74–77 ℃; lit.[93] 76–78 ℃; R_f = 0.2 (20% EtOAc in cyclohexane); IR (neat) ν_{max} = 2926w, 2855w, 1684s (C=O), 1356m, 1169s cm^{-1}; ^1H NMR (400 MHz, DMSO–d_6): 7.78 (AA' of AA'BB', J = 8.0, 2H, C(15)H and C(16)H), 7.48 (BB' of AA'BB', J = 8.0, 2H, C(13)H and C(14)H), 3.90 (br s, 2H, C(4)H_aH_b and C(6)H_aH_b), 3.88 (d, J = 6.3, 2H, C(1)H_2), 2.64 (br s, 2H, C(4)H_aH_b and C(6)H_aH_b), 2.42 (s, 3H, C(18)H), 1.82–1.71 (m, 1H, C(2)H), 1.54 (d with unresolved fine coupling, J = 12.1, 2H, C(3)H_aH_b and C(5)H_aH_b), 1.37 (s, 9H, C(9)H and C(10)H and C(11)H), 0.96 (app dq, J = 12.7, 4.4, 2H, C(3)H_aH_b and C(5)H_aH_b); ^{13}C NMR (101 MHz, $CDCl_3$): δ 153.7 (C, C(7)), 144.9 (C, C(17)), 132.4 (C, C(12)), 130.2 (CH, C(13) and C(14)), 127.6 (CH, C(15) and C(16)), 78.5 (C, C(8)), 74.2 (CH_2, C(1)), 42.7 (CH_2, C(4) and C(6)), 34.9 (CH, C(2)), 28.0 (CH_3, C(9) and C(10) and C(11)), 27.4 (CH_2, C(3) and C(5)), 21.1 (CH_3, C(18)); MS (TOF–ES+) m/z 370.52 ($[M + H]^+$, 100%).

Data are in agreement with those reported in the literature.[93]

tert–butyl 4–(azidomethyl)piperidine–1–carboxylate (**87**)[94]

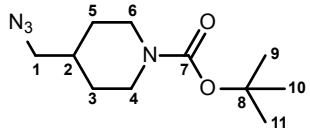

NaN_3 (97 mg, 1.5 mmol) was added to a solution of tosylate **86** (150 mg, 0.5 mmol) in DMF (5 mL). The reaction mixture was heated at 60 ℃ for 6 h and then diluted with H_2O (10 mL). The resulting solution was extracted with EtOAc (3 × 10 mL). The combined organic phases were washed with brine (10 mL), dried (Na_2SO_4), filtered and evaporated under reduced pressure to provide azide **87** as a colourless liquid that was used without further purification (113 mg, 94%): R_f = 0.8 (50% EtOAc in cyclohexane); IR (neat) ν_{max} = 2925w, 2852w, 2092s (N_3), 1684s (C=O), 1162s cm^{-1}; ^1H NMR (400 MHz, $CDCl_3$): δ 4.00 (d with unresolved fine coupling, J = 13.7, 2H, C(4)$\underline{H}_aH_b$ and C(6)$\underline{H}_aH_b$), 3.06 (d, J = 6.3, 2H, C(1)$\underline{H}_2$), 2.58 (d with unresolved fine coupling, J = 12.9, 2H, C(4)$H_a\underline{H}_b$ and C(6)$H_a\underline{H}_b$), 1.65–1.51 (stack, 3H, C(2)$\underline{H}$ and C(3)$\underline{H}_aH_b$ and C(5)$\underline{H}_aH_b$), 1.32 (s, 9H, C(9)$\underline{H}$ and C(10)$\underline{H}$ and C(11)$\underline{H}$), 1.11–0.97 (m, 2H, C(3)$H_a\underline{H}_b$ and C(5)$H_a\underline{H}_b$); ^{13}C NMR (101 MHz, $CDCl_3$): δ 154.5 (C, C(7)), 79.1 (C, C(8)), 56.8 (CH_2, C(1)), 43.3 (br, CH_2, C(4) and C(6)), 36.3 (CH, C(2)), 29.4 (CH_2, C(3) and C(5)), 28.3 (CH_3, C(9) and C(10) and C(11)); MS (TOF–ES+) m/z 263.1 ($[M + Na]^+$, 100%). All work involving azides was performed in an empty lab in a fumehood containing an explosion shield. Working was signalled with appropriate caution signs in order to ensure the safety of workers not involved in the synthesis. Data are in agreement with those reported in the literature.[94]

4–(azidomethyl)piperidine (**88**)[95]

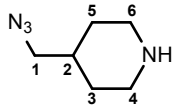

TFA (0.13 mL, 1.6 mmol) was added to a solution of Boc amide **87** (100 mg, 0.4 mmol) in EtOAc (5 mL). After 5 h, the reaction mixture was diluted with EtOAc (5 mL) and washed with $NaHCO_3$ soln. (3 × 10 mL), dried (Na_2SO_4), filtered and partially evaporated under reduced pressure to a volume of approx. 1 mL to provide piperidine **88** as a solution in EtOAc. For safety reasons, the combined organic phase was not evaporated to dryness and was used without further purification: selected data: R_f = 0.4 (50% EtOAc in hexane); IR (EtOAc) ν_{max} = 3384br (N–H), 2942w, 2894w, 2110m (N_3), 1186m cm^{-1}; MS (TOF–ES+) m/z 163.1 ($[M + Na]^+$, 100%).

All work involving azides was performed in an empty lab in a fumehood containing an explosion shield. Working was signalled with appropriate caution signs in order to ensure the safety of workers not involved in the synthesis. Data are in agreement with those reported in literature.[95]

(*Z*)–2–(4'–(azidomethyl)piperidin–1'–yl)–5–(2",4"–dichlorobenzylidene)thiazol–4(*5H*)–one (**89**)

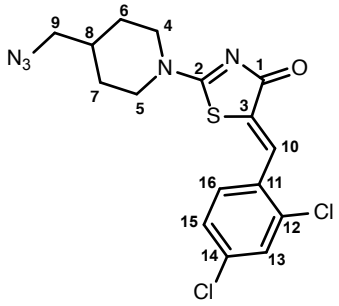

Substitution product **89** was prepared from thioether **35** (52 mg, 0.17 mmol) and piperidine **88** (24 mg, 0.17 mmol) according to general procedure B. Purification by flash column chromatography (eluent: 1% MeOH in CH_2Cl_2 to 10% MeOH in CH_2Cl_2) provided the title compound **89** as a white solid (23 mg, 34%): m.p. 194–197 °C; $R_f = 0.8$ (10% MeOH in CH_2Cl_2); IR (neat) ν_{max} = 3084w, 2961w, 2894w, 2148m (N_3), 1674m, 1561s (C=O), 1274m cm^{-1}; ^1H NMR (300 MHz, 1:1 $CDCl_3$:CD_3OD): δ 7.95 (s, 1H, C(10)H), 7.57 (d, J = 8.2, 1H, C(16)H), 7.48 (d, J = 2.2, 1H, C(13)H), 7.36 (dd, J = 8.2, 2.2, 1H, C(15)H), 4.22 (d with unresolved fine coupling, J = 13.2, 1H, C(4)H_aH_b), 3.41 (d with unresolved fine coupling, J = 13.6, 1H, C(5)H_aH_b), 3.27 (d, J = 8.1, 2H, C(9)H_2), 2.84–2.71 (stack, 2H, C(4)H_aH_b and C(5)H_aH_b), 1.98–1.89 (m, 1H, C(8)H), 1.84–1.71 (stack, 2H, C(6)H_aH_b and C(7)H_aH_b), 1.33–1.21 (stack, 2H, C(6)H_aH_b and C(7)H_aH_b); ^{13}C NMR (101 MHz, 1:1 $CDCl_3$:CD_3OD): δ 180.7 (C, C(2)), 173.1 (C, C(1)), 137.1 (C, C(12)), 135.9 (C, C(14)), 131.8 (C, C(11)), 130.6 (C, C(3)), 130.1 (CH, C(16)), 129.4 (CH, C(13)), 128.2 (CH, C(15)), 127.4 (CH, C(10)), 58.1 (CH_2, C(9)), 46.5 (CH_2, C(5)), 46.2 (CH_2, C(4)), 37.2 (CH, C(8)), 29.4 (CH_2, C(6) and C(7)); MS (TOF–ES+) m/z 419.3 ($[M + Na]^+$, 100%); HRMS (TOF–ES+) calcd for $C_{16}H_{16}{}^{35}Cl_2N_5OS$ $[M + H]^+$ 396.0447, found 396.0451.

1–(4–(1,3–dioxan–2–yl)phenyl)–2,2,2–trifluoroethan–1–one (**96**)[75]

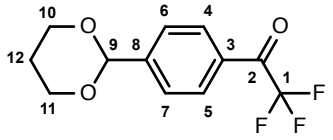

Propylphosphonic anhydride (300 mg, 1 mmol, 50% solution in EtOAc) was added to a solution of 4–(trifluoroacetyl)benzaldehyde **95** (1.00 g, 4.95 mmol) and 1,3–propanediol (0.85 g, 10.88 mmol) in EtOAc (5 mL). The mixture was stirred at r.t. for 5 h after which it time was diluted with EtOAc (15 mL) and washed sequentially with sat. $NaHCO_3$ solution (10 mL) and brine (10 mL). The organic phase was dried (anh. Na_2SO_4) and the solvent was evaporated under reduced pressure. The crude product was purified by flash column chromatography (2% EtOAc in cyclohexane to 10% EtOAc in cyclohexane) to provide acetal **96** as a yellow oil (1.16 g, 92%): R_f = 0.4 (20% EtOAc in cyclohexane); IR (neat) ν_{max} = 3350br, 2962w, 2871w, 1714s (C=O), 1378m, 1191s cm^{-1}; ^{1}H NMR (400 MHz, $CDCl_3$): δ 8.11–8.02 (AA' of AA'BB', 2H, C(4)H and C(5)H), 7.73–7.62 (BB' of AA'BB', 2H, C(6)H and C(7)H), 5.55 (s, 1H, C(9)H), 4.33–4.26 (m, 2H, C(10)H_aH_b and C(11)H_aH_b), 4.07–3.93 (m, 2H, C(10)H_aH_b and C(11)H_aH_b), 2.31–2.16 (m, 2H, C(12)H_2); ^{19}F NMR (376 MHz, $CDCl_3$) δ −71.6 (C(1)F_3); ^{13}C NMR (101 MHz, $CDCl_3$:): δ 180.2 (q, $^2J_{\text{C–F}}$ = 35, C, C(2)), 145.8 (C, C(3)), 130.1 (CH, C(4) and C(5)), 129.9 (C, C(8)), 126.7 (CH, C(6) and C(7)), 116.4 (q, $^1J_{\text{C–F}}$ = 292, C, C(1)), 100.1 (CH, C(9)), 67.4 (CH_2, C(10) and C(11)), 25.6 (CH_2, C(12)); MS (TOF–ES+) m/z 261.2 ($[M + H]^+$, 100%).

Data are in agreement with those reported in the literature.[75]

(*E*/*Z*) 1–(4–(1,3–dioxan–2–yl)phenyl)–2,2,2–trifluoroethan–1–one oxime (**97**)[75]

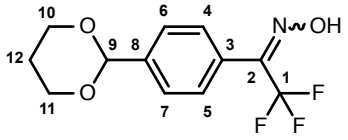

$H_2NOH \cdot HCl$ (0.20 g, 2.9 mmol) was added to a solution of acetal **96** (0.75 g, 2.9 mmol) in absolute EtOH (2 mL) and pyridine (4 mL). The mixture was heated at 60 ℃ for 3 h, after which time the solvent was evaporated under reduced pressure. The residue was partitioned between H_2O (20 mL) and Et_2O (20 mL). The organic layer was washed sequentially with H_2O (10 mL) and brine (10 mL), dried (anh. Na_2SO_4) and concentrated under reduced pressure. The yellow residue was purified by flash column chromatography (2% EtOAc in cyclohexane to 10% EtOAc in cyclohexane) to provide oxime **97** as a pale white solid (0.73 g, 92%, 1:1 mixture of isomers). The mixture was used invariably but a very careful chromatography allowed the purification of one of the isomers of unknown stereochemistry: m.p. 88–94 ℃; R_f = 0.3 (20% EtOAc in cyclohexane); IR (neat) ν_{max} = 3300br (O–H), 2864m, 1446s, 1376m, 1244m, 1159m cm^{-1}; ^1H NMR (400 MHz, $CDCl_3$): δ 7.62–7.56 (AA' of AA'BB', 2H, C(4)$\underline{H}$ and C(5)$\underline{H}$), 7.55–7.44 (BB' of AA'BB', 2H, C(6)$\underline{H}$ and C(7)$\underline{H}$), 5.54 (s, 1H, C(9)$\underline{H}$), 4.34–4.25 (m, 2H, C(10)$\underline{H}_aH_b$ and C(11)$\underline{H}_aH_b$), 4.06–3.96 (m, 2H, C(10)$H_a\underline{H}_b$ and C(11)$H_a\underline{H}_b$), 2.31–2.17 (m, 2H, C(12)$\underline{H}_2$), OH not observed; ^{19}F NMR (376 MHz, $CDCl_3$) δ −70.4 (C(1)F_3); ^{13}C NMR (101 MHz, $CDCl_3$:): δ 178.1 (q, $^2J_{C-F}$ = 34, C, C(2)), 144.3 (C, C(3)), 131.2 (CH, C(4) and C(5)), 129.4 (C, C(8)), 127.3 (CH, C(6) and C(7)), 115.7 (q, $^1J_{C-F}$ = 288, C, C(1)), 100.4 (CH, C(9)), 68.1 (CH_2, C(10) and C(11)), 25.2 (CH_2, C(12)); MS (TOF–ES+) *m/z* 276.2 ([M + H]$^+$, 100%).

Data are in agreement with those reported in the literature.[75]

(*E*/*Z*) 1–(4–(1,3–dioxan–2–yl)phenyl)–2,2,2–trifluoroethan–1–one *O*–tosyl oxime (**98**)[75]

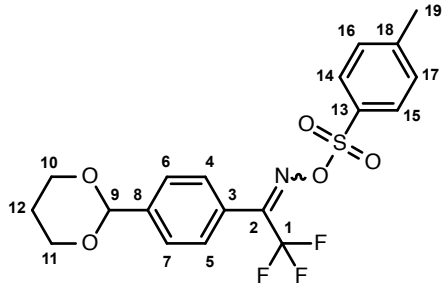

TsCl (815 mg, 4.28 mmol) was added in portions over 2 min to a cooled (0 ℃) solution of oxime **97** (1.02 g, 3.72 mmol), Et_3N (0.62 mL, 4.46 mmol) and DMAP (45 mg, 0.37 mmol) in CH_2Cl_2 (5 mL). The reaction mixture was stirred at r.t. After 3 h, the solvent was evaporated under reduced pressure and the residue was dissolved in Et_2O (50 mL). The solution was sequentially washed with H_2O (50 mL) and brine (20 mL), dried (anh. Na_2SO_4) and concentrated under reduced pressure. The crude product (yellow crystals) was used without further purification (1.55 g, 97%, 1:1 mixture of isomers), but a very careful chromatography allowed the purification of one of the isomers of unknown stereochemistry: m.p. 111–104 ℃; $R_f = 0.4$ (20% EtOAc in cyclohexane); IR (neat) $\nu_{max} = 2960w, 2911w, 2862w, 1587s, 1384s, 1235m$ cm^{-1}; ^1H NMR (400 MHz, $CDCl_3$): δ 7.89–7.84 (AA' of AA'BB', 2H, C(14)H and C(15)H), 7.62–7.58 (AA' of AA'BB', 2H, C(4)H and C(5)H), 7.42–7.35 (stack, 4H, C(6)H and C(7)H and C(16)H and C(17)H), 5.53 (s, 1H, C(9)H), 4.31–4.25 (m, 2H, C(10)H_aH_b and C(11)H_aH_b), 4.04–3.96 (m, 2H, C(10)H_aH_b and C(11)H_aH_b), 2.47 (s, 3H, C(19)H_3), 2.29–2.15 (m, 2H, C(12)H_2); ^{19}F NMR (376 MHz, $CDCl_3$) δ −66.79 (C(1)F_3);

^{13}C NMR (101 MHz, $CDCl_3$): δ 178.4 (q, $^2J_{C-F}$ = 33, C, C(2)), 146.3 (C, C(13)), 144.1 (C, C(3)), 131.7 (C, C(18)), 131.2 (CH, C(4) and C(5)), 129.9 (CH, C(14) and C(15)), 129.5 (C, C(8)), 129.3 (CH, C(16) and C(17)), 127.6 (CH, C(6) and C(7)), 116.8 (q, $^1J_{C-F}$ = 282, C, C(1)), 100.4 (CH, C(9)), 68.1 (CH_2, C(10) and C(11)), 25.2 (CH_2, C(12)), 21.6 (CH_3, C(15)); MS (TOF–ES+) *m/z* 430.5 ($[M + H]^+$, 100%).

Data are in agreement with those reported in the literature.[75]

3–(4–(1,3–dioxan–2–yl)phenyl)–3–(trifluoromethyl)diaziridine (**99**)[75]

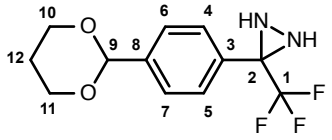

NH_3 was bubbled through a solution of tosyl oxime **98** (1.25 g, 2.92 mmol) in CH_2Cl_2 (5 mL) for 4 h at −78 ℃. The cooling bath was removed and the mixture was allowed to warm to r.t. After 18 h, the excess NH_3 and CH_2Cl_2 were evaporated under reduced pressure and the residue partitioned between CH_2Cl_2 (10 mL) and H_2O (10 mL). The organic layer was separated, washed with brine (10 mL), dried (anh. Na_2SO_4) and concentrated under reduced pressure. The residue was purified by flash column chromatography (2% EtOAc in cyclohexane to 20% EtOAc in cyclohexane) to provide diaziridine **99** as white crystals (408 mg, 51%): m.p. 65–68 ℃; R_f = 0.5 (20% EtOAc in cyclohexane); IR (neat) ν_{max} = 3220br (N–H), 2933w, 2879w, 1466m, 1382m, 1280m cm^{-1}; ^1H NMR (400 MHz, $CDCl_3$): δ 7.64–7.59 (AA' of AA'BB', 2H, C(4)H and C(5)H), 7.54–7.41 (BB' of AA'BB', 2H, C(6)H and C(7)H), 5.54 (s, 1H, C(9)H), 4.33–4.28 (m, 2H, C(10)H_aH_b and C(11)H_aH_b), 4.08–3.99 (m, 2H, C(10)H_aH_b and C(11)H_aH_b), 2.80 (d, J = 8.8, 1H, NH), 2.32 (d, J = 8.8, 1H, NH), 2.28–2.16 (m, 2H, C(12)H_2); ^{19}F NMR (376 MHz, $CDCl_3$) δ −75.2 (C(1)F_3); ^{13}C NMR (101 MHz, $CDCl_3$:): δ 130.8 (C, C(3)), 129.1 (CH, C(4) and C(5)), 128.8 (C, C(8)), 128.2 (CH, C(6) and C(7)), 118.6 (q, $^1J_{C-F}$ = 280, C, C(1)), 100.7 (CH, C(9)), 68.8 (CH_2, C(10) and C(11)), 58.2 (q, $^2J_{C-F}$ = 37, C, C(2)), 25.2 (CH_2, C(12)); MS (TOF–ES+) m/z 275.3 ($[M + H]^+$, 100%).

Data are in agreement with those reported in the literature.[75]

4–(3–(trifluoromethyl)–3*H*–diazirin–3–yl)benzaldehyde (**100**)

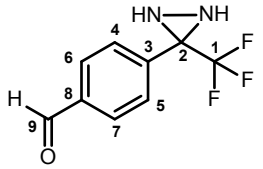

PPTS (0.2 g, 0.75 mmol) was added to a solution of acetal **99** (0.4 g, 1.49 mmol) in a mixture of H_2O/acetone 1:2 (20 mL). The solution was heated to reflux for 16 h. After this time the reaction mixture was cooled to r.t. and diluted with Et_2O (20 mL) and H_2O (20 mL). The organic layer was separated, washed with brine (20 mL), dried (anh. Na_2SO_4) and concentrated under reduced pressure. The residue was purified by flash column chromatography (1% EtOAc in cyclohexane to 20% EtOAc in cyclohexane) to provide aldehyde **100** as an orange solid (0.3 g, 97%): m.p. 102–105 °C; R_f = 0.3 (5% EtOAc in cyclohexane); IR (neat) ν_{max} = 1918w, 1694s (C=O), 1584m, 1377m cm^{-1}; ^{1}H NMR (400 MHz, $CDCl_3$): δ 10.05 (s, 1H, C(9)H), 7.92 (AA' of AA'BB', J = 7.8, 2H, C(6)H and C(7)H), 7.35 (BB' of AA'BB', J = 7.3, 2H, C(4)H and C(5)H), 2.84 (d, J = 8.8, 1H, NH), 2.37 (d, J = 8.8, 1H, NH); ^{19}F NMR (376 MHz, $CDCl_3$) δ −65.1 (C(1)F_3); ^{13}C NMR (101 MHz, $CDCl_3$:): δ 191.4 (CH, C(9)), 137.9 (C, C(8)), 131.8 (C, C(3)), 130.8 (CH, C(6) and C(7)), 127.9 (CH, C(4) and C(5)), 122.6 (q, $^1J_{C-F}$ = 276, C, C(1)), 72.4 (q, $^2J_{C-F}$ = 34, C, C(2)); MS (TOF–ES+) m/z 215.2 ([M + H]$^+$, 100%); HRMS (TOF–ES+) calcd for $C_9H_6F_3N_2O$ [M + H]$^+$ 215.0427, found 215.0418.

4–(3–(trifluoromethyl)–3*H*–diazirin–3–yl)benzaldehyde (**101**)

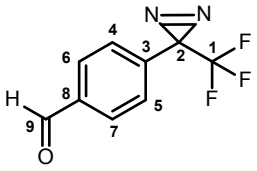

Et_3N (1 mL) was added to a solution of diaziridine **100** (0.242 g, 1.286 mmol) in MeOH (5 mL). After 5 min. a solution of iodine (2 mL, 30 mg/mL soln. in MeOH) was added dropwise at r.t. until the orange–red color of iodine persisted for more than 1 min. The reaction mixture was then stirred for 1 h in the dark at r.t. After this time, the solvent was removed under reduced pressure and the residue was diluted with Et_2O (5 mL). The product was extracted from the organic phase with NaOH (1 M aq. soln.) (3 × 5 mL). The combined aqueous phases were acidified with 6M HCl to approximately pH=1, and the product was extracted with Et_2O (20 mL). The combined organic phases were sequentially washed with H_2O (10 mL), brine (10 mL) and the solvent was evaporated under reduced pressure. The yellow oil obtained as residue was protected from light and used without further purification (0.148 g, 62%): R_f = 0.4 (10% EtOAc in cyclohexane); IR (neat) $\nu_{\max}$ = 1925w, 1692s (C=O), 1577m, 1364m cm^{-1}; ^1H NMR (400 MHz, $CDCl_3$): δ 10.08 (s, 1H, C(9)H), 7.94 (AA' of AA'BB', J = 7.8, 2H, C(6)H and C(7)H), 7.38 (BB' of AA'BB', J = 7.3, 2H, C(4)H and C(5)H); ^{19}F NMR (376 MHz, $CDCl_3$) δ −64.1 ($C(1)F_3$); ^{13}C NMR (101 MHz, $CDCl_3$:): δ 191.7 (CH, C(9)), 137.5 (C, C(8)), 132.2 (C, C(3)), 131.4 (CH, C(6) and C(7)), 128.1 (CH, C(4) and C(5)), 122.8 (q, $^1J_{C-F}$ = 274, C, C(1)), 72.7 (q, $^2J_{C-F}$ = 32, C, C(2)); MS (TOF–ES+) m/z 214.1 ($[M + H]^+$, 100%); HRMS (TOF–ES+) calcd for $C_9H_4F_3N_2O$ $[M + H]^+$ 214.0354, found 214.0358.

(*Z*)–1–(4-oxo–5–(4–(3–(trifluoromethyl)–3*H*–diazirin–3–yl)benzylidene)–4,5–dihydrothiazol–2–yl)piperidine–4–carboxamide (**102**)

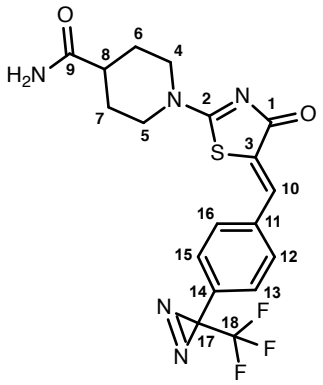

A solution of rhodanine derivative **29** (0.100 g, 0.440 mmol) in KOH solution (1 mL of a 1 M solution in MeOH) was cooled to 0 ℃. In the absence of light, aldehyde **101** (0.094 g, 0.440 mmol) was added and the mixture was stirred at r.t. After 4 h, the solvent was evaporated under reduced pressure and the residue purified by flash column chromatography (5% EtOAc in cyclohexane to 40% EtOAc in cyclohexane) to provide Knoevenagel product **102** as a yellow powder (0.123 g, 66%): m.p. 174–177 ℃; IR (neat) ν_{max} = 3358br (N–H), 3118w, 2926w, 1619m (C=O), 1546s (C=O), 1358m cm^{-1}; ^{1}H NMR (400 MHz, 1:1 $CDCl_3$:CD_3OD): δ 7.68 (s, 1H, C(10)H), 7.56–7.50 (AA' of AA'BB', 2H, C(12)H and C(16)H), 7.17–7.10 (BB' of AA'BB', 2H, C(13)H and C(15)H), 4.73 (d with unresolved fine coupling, J = 13.4, 1H, C(4)H_aH_b), 3.91 (d with unresolved fine coupling, J = 13.6, 1H, C(5)H_aH_b), 3.52–3.33 (stack, 2H, C(4)H_aH_b and C(5)H_aH_b), 2.66–2.56 (m, 1H, C(8)H), 2.08–1.95 (stack, 2H, C(6)H_aH_b and C(7)H_aH_b), 1.93–1.74 (stack, 2H, C(6)H_aH_b and C(7)H_aH_b), NH_2 not observed; ^{19}F NMR (376 MHz, $CDCl_3$) δ −65.9 (C(16)F_3);

^{13}C NMR (101 MHz, $CDCl_3$): δ 182.1 (C, C(2)), 177.8 (C, C(1)), 175.7 (C, C(9)), 131.8 (C, C(14)), 131.4 (CH, C(10)), 131.2, (CH, C(12) and C(16)), 130.6 (C, C(11)), 128.1 (C, C(3)), 127.1 (CH, C(13) and C(15)), 122.6 (q, $^1J_{C-F}$ = 281, C, C(18)), 65.8 (q, $^2J_{C-F}$ = 36, C, C(17)), 49.3 (CH_2, C(5)), 48.5 (CH_2, C(4)), 41.6 (CH, C(8)), 28.9 (CH_2, C(6)), 28.7 (CH_2, C(7)); MS (TOF–ES+) *m/z* 424.4 ($[M + H]^+$, 100%); HRMS (TOF–ES+) calcd for $C_{18}H_{17}F_3N_5O_2S$ $[M + H]^+$ 424.1050, found 424.1044.

3–chloro–*N*–(4–methoxybenzyl)isoquinolin–1–amine (**110**)

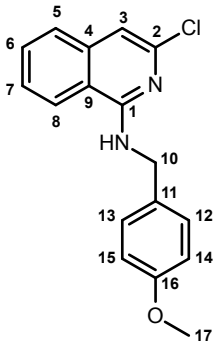

K_2CO_3 (1.3 g, 9.0 mmol) was added to a solution of 1,3–dichloroisoquinoline (**108**) (5.0 g, 25 mmol) in 1,4–dioxane (50 mL). After stirring at r.t. for 5 min *p*–methoxybenzylamine (3.9 mL, 30 mmol) was added and the mixture was heated at reflux. After 16 h, the reaction mixture was cooled to r.t., diluted with $NaHCO_3$ solution (100 mL) and extracted with EtOAc (3 × 100 mL). The organic phases were combined, dried (Na_2SO_4) and concentrated under reduced pressure. The residue was purified by flash column chromatography (2% EtOAc in cyclohexane to 10% EtOAc in cyclohexane) to obtain amine **110** as a yellow oil (6.1 g, 82%). R_f = 0.2 (20% EtOAc in cyclohexane); IR (neat) ν_{max} = 3454br w (N–H), 2962w, 2932w, 2832w, 1587m, 1510m, 1249m cm^{-1}; ^1H NMR (400 MHz, $CDCl_3$): δ 7.66 (dd, J = 8.4, 0.9, 1H, C(8)H), 7.62–7.53 (stack, 2H, C(5)H and C(6)H), 7.42–7.39 (m, 1H, C(7)H), 7.39–7.34 (AA' of AA'BB', 2H, C(14)H and C(15)H), 6.98 (d, J = 0.9, 1H, C(3)H), 6.94–6.88 (BB' of AA'BB', 2H, C(12)H and C(13)H), 5.47 (br s, 1H, NH), 4.73 (d, J = 4.9, 2H, C(10)H_2), 3.82 (s, 3H, C(17)H_3); ^{13}C NMR (101 MHz, $CDCl_3$): δ 159.3 (C, C(1)), 155.0 (C, C(16)), 144.6 (C, C(2)), 138.9 (C, C(4)), 130.9 (C, C(11)), 130.6 (CH, C(6)), 129.8 (CH, C(12) and C(13)), 126.6 (CH, C(7)), 125.9 (CH, C(5)), 121.6 (CH, C(8)), 116.5 (C, C(9)), 114.3 (CH, C(3)), 108.8 (CH, C(14) and C(15)), 55.5 (CH_3, C(17)), 45.8 (CH_2, C(10)); MS (TOF–ES+) m/z 299.7 ($[M + H]^+$, 100%); HRMS (TOF–ES+) calcd for $C_{17}H_{16}{}^{35}ClN_3O$ $[M + H]^+$ 299.0946, found 299.0938.

N–(4–methoxybenzyl)–3–(pyridin–2–yl)isoquinolin–1–amine (**111**)

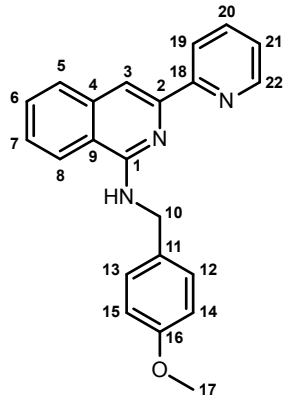

X–Phos (114.87 mg, 0.24 mmol) and $Pd_2(dba)_3$ (55.16 mg, 0.06 mmol) were dissolved in dry DMF (10 mL). The mixture was heated at 100 ℃ under a N_2 atmosphere for 5 min. After cooling to 40 ℃, amine **110** (1.20 g, 4.02 mmol), 2–pyridyl MIDA boronate (1.41 g, 6.02 mmol), K_2CO_3 (2.7 g, 20.08 mmol) and $Cu(OAc)_2$ (364.70 mg, 2.01 mmol) were sequentially added to the solution. The reaction mixture was heated at 100 ℃ for 1 h under MW radiation. The mixture was then cooled to r.t. and transferred to a separating funnel. NaOH solution (10 mL of a 1 M solution) was added and the mixture was extracted with Et_2O (3 × 10 mL). The organic phases were combined, dried ($MgSO_4$), filtered and concentrated under reduced pressure. The residue was purified by flash column chromatography (2% EtOAc in cyclohexane to 20% EtOAc in cyclohexane) to provide amine **111** as a dark yellow viscous oil (0.74 g, 54%): R_f = 0.3 (20% EtOAc in cyclohexane); IR (neat) ν_{max} = 3451br (N–H), 3063w, 2924m, 1567m, 1507s, 1420m, 1246m cm^{-1};

^{1}H NMR (400 MHz, $CDCl_3$): δ 8.69 (ddd, J = 4.8, 1.8, 0.9, 1H, C(22)H), 8.52 (dt, J = 8.0, 1.2, 1H, C(19)H), 8.18 (d, J = 0.9, 1H, C(3)H), 7.84 (d with unresolved fine coupling, J = 8.2, 1H, C(5)H), 7.79 (ddd, J = 8.2, 7.2, 1.8, 1H, C(6)H), 7.73 (d with unresolved fine coupling, J = 8.3, 1H, C(8)H), 7.58 (ddd, J = 8.3, 7.2, 1.1, 1H, C(7)H), 7.46–7.39 (stack, 3H, C(14)H and C(15)H and C(20)H), 7.25 (ddd, J = 7.5, 4.8, 1.2, 1H, C(21)H), 6.93–6.87 (BB' of AA'BB', 2H, C(12)H and C(13)H), 5.40 (br d, J = 5.1, 1H, NH), 4.90 (d, J = 5.1, 2H, C(10)H_2), 3.80 (s, 3H, C(17)H_3); ^{13}C NMR (101 MHz, $CDCl_3$): δ 158.9 (C, C(1)), 155.3 (C, C(16)), 154.9 (C, C(18)), 149.1 (C, C(2)), 148.7 (CH, C(22)), 139.8 (C, C(4)), 136.4 (CH, C(20)), 130.8 (C, C(11)), 129.9 (CH, C(6)), 129.1 (CH, C(12) and C(13)), 127.7 (CH, C(7)), 125.6 (CH, C(5)), 124.2 (CH, C(21)), 122.1 (CH, C(8)), 117.9 (C, C(9)), 115.2 (CH, C(19)), 114.3 (CH, C(3)), 110.4 (CH, C(14) and C(15)), 55.4 (CH_3, C(17)), 44.2 (CH_2, C(10)); MS (TOF–ES+) m/z 342.4 ($[M + H]^+$, 100%); HRMS (TOF–ES+) calcd for $C_{22}H_{20}N_3O$ $[M + H]^+$ 342.1601, found 342.1612.

3–(pyridin–2–yl)isoquinolin–1–amine (**112**)

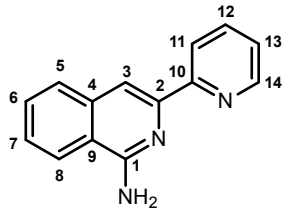

TFA (10 mL) was added to a solution of amine **111** (466 mg, 1.36 mmol) in CH_2Cl_2 (5 mL). After stirring at r.t. for 16 h, the solvent was removed under reduced pressure. The residue was dissolved in CH_2Cl_2 (20 mL) and the solution was washed with a $NaHCO_3$ solution (150 mL) until no effervescence was observed. After partitioning, the organic phase was washed with brine (25 mL), dried (Na_2SO_4) and concentrated under reduced pressure. The crude product was purified by flash column chromatography (5% EtOAc in cyclohexane to 30% EtOAc in cyclohexane) to provide amine **112** as a thick orange oil (276 mg, 92%): $R_f = 0.2$ (40% EtOAc in cyclohexane); IR (neat) $\nu_{max} = 3327$br (N–H), 3200br w, 3053w, 1624m, 1567m, 1493m, 1426s cm^{-1}; ^{1}H NMR (400 MHz, $CDCl_3$): δ 8.70 (ddd, J = 4.7, 1.5, 1.0, 1H, C(14)H), 8.37 (d with unresolved fine coupling, J = 8.1, 1H, C(11)H), 8.16 (d, J = 1.0, 1H, C(3)H), 7.89–7.76 (stack, 3H, C(5)H and C(6)H and C(8)H), 7.63 (ddd, J = 8.1, 6.9, 1.5, 1H, C(12)H), 7.50 (ddd, J = 8.2, 6.9, 1.2, 1H, C(7)H), 7.30–7.23 (m, 1H, C(13)H), 5.29 (br s, 2H, NH_2); ^{13}C NMR (101 MHz, $CDCl_3$): δ 156.7 (C, C(1)), 155.9 (C, C(10)), 149.4 (CH, C(14)), 147.9 (C, C(2)), 138.3 (C, C(4)), 136.9 (CH, C(12)), 130.5 (CH, C(6)), 128.5 (CH, C(7)), 126.7 (CH, C(5)), 123.1 (CH, C(13)), 122.8 (CH, C(8)), 121.2 (CH, C(11)), 118.1 (C, C(9)), 110.3 (CH, C(3)); MS (TOF–ES+) m/z 222.3 ([M + H]$^+$, 100%); HRMS (TOF–ES+) calcd for $C_{14}H_{12}N_3$ [M + H]$^+$ 222.1026, found 222.1031.

3-chloro-*N*-(3-(pyridin-2-yl)isoquinolin-1-yl)benzamide (**113**)

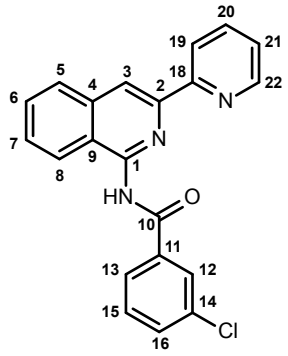

n–BuLi (0.21 mL of a 1.6 M solution in hexanes, 0.36 mmol) was added dropwise over 2 min to a solution of amine **112** (80 mg, 0.36 mmol) in anhydrous THF (2 mL) under a N_2 atmosphere at −10 ℃. After 10 min, a solution of 3–chlorobenzoyl chloride (46 μL, 0.36 mmol) in anhydrous THF (0.5 mL) was added. After stirring −10 ℃ for 1 h, the cooling bath was removed and when the mixture had reached r.t. H_2O (10 mL) was added. The reaction mixture was washed with $CHCl_3$ (3 × 10 mL). The combined organic phases were washed with $NaHCO_3$ solution (30 mL of a 1 M solution), dried (Na_2SO_4), and concentrated under reduced pressure. The residue was purified by flash column chromatography (1% EtOAc in cyclohexane to 10% EtOAc in cyclohexane) to provide amide **113** as a red viscous oil (31 mg, 24%): R_f = 0.4 (5% EtOAc in cyclohexane); IR (neat) ν_{max} = 3374br (N–H), 3044w, 2941w, 1658s (C=O), 1512m, 1472m, 1324m cm^{-1}; ^{1}H NMR (400 MHz, d_4–MeOH): δ 9.00 (app. d, J = 8.2, 1H, C(19)H), 8.86 (app. d, J = 4.8, 1H, C(22)H), 8.52 (s, 1H, C(3)H), 8.39 (d, J = 7.6, 1H, C(13)H), 7.97 (d, J = 7.6, 1H, C(16)H), 7.83 (td, J = 7.8, 1.5, 1H, C(5)H), 7.80–7.70 (stack, 2H, C(6)H and C(8)H), 7.66 (ddd, J = 8.2, 7.1, 1.6, 1H, C(20)H), 7.61 (s, 1H, C(12)H), 7.48 (ddd, J = 7.8, 7.2, 1.5, 1H, C(7)H), 7.42 (app. t, J = 7.6, 1H, C(15)H), 7.36 (ddd, J = 7.1, 4.8, 1.1, 1H, C(21)H), NH not observed;

^{13}C NMR (101 MHz, $CDCl_3$): δ 165.8 (C, C(10)), 155.4 (C, C(1)), 149.6 (C, C(18)), 149.2 (C, C(2)), 148.8 (CH, C(22)), 139.8 (CH, C(20)), 136.6 (C, C(4)), 134.4 (C, C(14)), 133.9 (C, C(11)), 130.9 (CH, C(16)), 130.3 (CH, C(7)), 130.1 (CH, C(5)), 129.4 (CH, C(6)), 127.6 (CH, C(12)), 126.1 (CH, C(8)), 125.3 (CH, C(13)), 124.1 (CH, C(15)), 121.4 (CH, C(21)), 119.3 (CH, C(19)), 118.4 (C, C(9)), 116.7 (CH, C(3)); MS (TOF–ES+) *m/z* 361.1 ($[M + H]^+$, 100%); HRMS (TOF–ES+) calcd for $C_{21}H_{15}{}^{35}ClN_3O$ $[M + H]^+$ 360.0898, found 360.0911.

3-chloro-*N'*-(3-(pyridin-2-yl)isoquinolin-1-yl)benzimidamide (**103**)

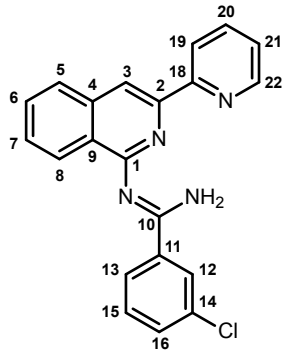

A solution of amide **113** (43 mg, 0.12 mmol) in dry $CHCl_3$ (2 mL) was added dropwise over 2 min to a solution of PCl_5 (50 mg, 0.24 mmol) in $CHCl_3$ (1 mL) under a N_2 atmosphere. The reaction mixture was heated at reflux for 1 h and then cooled in an ice bath. Anhydrous NH_3 gas was then bubbled through the mixture. After 1 h, an ice–cold $NaHCO_3$ solution (5 mL) was cautiously added. The phases were separated and the organic phase was washed with H_2O (3×5 mL), dried (Na_2SO_4) and concentrated under reduced pressure. The residue was purified by flash column chromatography (1% EtOAc in cyclohexane to 10% EtOAc in cyclohexane) to provide amidine **103** as a red oil (4.4 mg, 10%): $R_f = 0.4$ (5% EtOAc in cyclohexane); IR (neat) $\nu_{\max} =$ 3380br (N–H), 3028w, 2924w, 1655s (C=N), 1530m, 1418m cm^{-1}; ^1H NMR (400 MHz, d_4–MeOH): δ 8.97 (d with unresolved fine coupling, $J = 8.2$, 1H, C(19)H), 8.76 (ddd, $J = 4.8, 1.7, 0.9$, 1H, C(22)H), 8.41 (d, $J = 1.0$, 1H, C(3)H), 8.19 (app. dt, $J = 7.8, 1.4$, 1H, C(13)H), 8.17 (app. t, $J = 1.4$, 1H, C(12)H), 7.99 (app. dt, $J = 7.8, 1.4$, 1H, C(16)H), 7.89 (dt, $J = 7.5, 1.0$, 1H, C(5)H), 7.84 (td, $J = 7.5, 2.0$, 1H, C(6)H), 7.70 (ddd, $J = 8.1, 7.5, 1.0$, 1H, C(7)H), 7.63 (ddd, $J = 8.2, 7.5, 1.7$, 1H, C(20)H), 7.52 (ddd, $J = 8.1$, 2.0, 1.2, 1H, C(8)H), 7.47 (app. t, $J = 7.8$, 1H, C(15)H), 7.32 (ddd, $J = 7.5$, 4.8, 0.9, 1H, C(21)H), NH_2 not observed;

^{13}C NMR (101 MHz, $CDCl_3$): δ 169.3 (C, C(10)), 155.9 (C, C(1)), 153.5 (C, C(18)), 151.6 (C, C(2)), 149.1 (CH, C(22)), 136.7 (CH, C(20)), 135.8 (C, C(4)), 134.1 (C, C(14)), 131.5 (C, C(11)), 130.5 (CH, C(16)), 130.4 (CH, C(7)), 129.8 (CH, C(5)), 128.5 (CH, C(6)), 128.1 (CH, C(12)), 127.8 (CH, C(8)), 127.1 (CH, C(13)), 125.6 (CH, C(15)), 124.1 (CH, C(21)), 122.0 (CH, C(19)), 120.7 (C, C(9)), 116.4 (CH, C(3)); MS (TOF–ES+) *m/z* 360.1 ([M + H]$^+$, 100%); HRMS (TOF–ES+) calcd for $C_{21}H_{16}{}^{35}ClN_4$ [M + H]$^+$ 359.1058, found 359.1052.

6.3 Biology Protocols

6.3.1 AspRS Protein Purification Protocol

Materials

- *E. coli* CL21 competent cells (One Shot ™ BL21(DE3) Chemically Competent *E. coli*, Thermo Fischer Scientific, C600003)
- pET28b::AspRS (His–tagged at the C–terminus) plasmid
- Prepacked 1 mL Ni^{2+} Sepharose Column (GE Healthcare)
- Standard peristaltic pump
- 0.2 M Tris–HCl buffer pH=8
- 100% Glycerol
- 1 M NaCl
- Imidazole
- SOC medium (provided with One Shot™ BL21(DE3) Chemically Competent *E. coli*, Thermo Fischer Scientific, C600003)
- Protease inhibitor tablets (Roche)
- Lysozyme
- Sonicator probe
- Amicon Ultrafiltration Unit 10 KDa cutoff
- BCA Protein Quantification Kit

Method

1 μL of pET28b–Mt–aspS construct with the C–terminal His6–tagged thawed in an ice bath was added to 50 µL of *E. coli* CL21 (DE3) cells thawed the same way. The mixture was left on ice for 20 min. To transform the construct into the CL21 cells for protein expression the mixture was submitted to a thermal shock at 42 ℃ for 2 min. After this, 500 μL of SOC medium were added to the mixture, which was incubated at 37 ℃ for 1 h. In parallel, the same protocol (except adding 1 μL of plasmid) was followed to obtain a control strain of CL21 cells submitted to the same process.

25 μL (and 100 μL) of both the transformed mixture and the control experiment were spread on LB–agar plates (25 mL of LB–agar per plate) containing 25 μg/mL kanamycin. The plates were left incubating for 16 h at 37 ℃. After this time 2 colonies were observed on both the plate with 25 μL and 100 μL of transformed culture. No colonies were observed in the control experiment.

An overnight starter culture was prepared by inoculating a single colony from the freshly transformed plates (the 100 μL plate) into LB broth (50 mL) containing kanamycin (25 mug/mL). A 1% inoculum of the starter culture was used to inoculate LB broth (4×1 L) containing kanamycin (25 μg/mL), which was grown at 37 ℃ until an OD_{600} of 0.6 was attained. The cultures were then induced with 1 mM isopropyl–b–D–thiogalactopyranoside (IPTG) and cultured at 16 ℃ for 18 hours. The cultures were then centrifuged at 3.750 rpm for 15 min at 4 ℃. The pellets obtained were washed with 15 mL of cold PBS solution and after centrifugation at 3.750 rpm for 15 min at 4 ℃ were frozen at −80 ℃.

The harvested cells (pellets) were resuspended in lysis buffer (30 mL) containing 20 mM Tris–HCl pH 8.0, 500 mM NaCl, 10% glycerol, 40 mM imidazole and a protease inhibitor tablet and disrupted by sonication with 10 cycles of 30 s pulses at 60 s intervals using 50% amplitude. The crude lysate was clarified by centrifugation at 15.000 rpm for 50 minutes at 4 ℃. The supernatant separated from the pellet and loaded onto a pre–packed Ni^{2+} Sepharose HisTrap high performance column, which was equilibrated with buffer A (lysis buffer without lysozyme and protease inhibitor). The column was washed with buffer A and eluted with a stepwise gradient of imidazole (50, 75, 100, 200, 300 and 500 mM) in Buffer A (10 mL). At the end the column is washed with H_2O and 20% EtOH. The purified fractions were analysed by SDS–PAGE gel and the relevant fractions (100 and 200 mM) containing AspRS were pooled and dialysed against Buffer B (20 mM Tris–HCl pH 8.0, 50 mM NaCl, 10% glycerol, 1 mM DTT and 100 mM EDTA) and concentrated with an Amicon ultrafiltration unit containing a 10 kDa cutoff membrane. Protein concentration was measured with the BCA protein reagent kit using BSA as a standard.

6.3.2 Preparation of cell lysate from *M. bovis* BCG grown in Middlebrook 7H9 media with glucose as carbon source

Bacterial culture preparation

1. Culture *M. bovis* BCG in glucose medium at 37 ℃ for 8–10 days until reaching an optical density between 0.8–1 (λ=600 nm).

2. Centrifuge the culture at 3.500 rpm and wash the pellets twice with a solution of PBS/tyloxapol 0.025% (10 mL). Keep samples on ice and use a cool PBS/tyloxapol solution for the washing steps.

3. Store the pellets at −80 ℃ until use.

Lysate preparation

Samples to be kept on ice during the whole process.

- Add 2 volumes of cold 1X lysis buffer to the cell pellet and re–suspend the cells (x wet grams of cell pellet are resuspended in 2x mL of lysis buffer).

- Transfer the suspension into 15 mL tubes (3 mL/ tube approximately).

- Sonicate each tube three cycles at 50% amplitude for 30 seconds (perform sonication cycles on ice). Keep samples at least 60 seconds on ice after each sonication cycle.

- Transfer the same volume of lysate into ultracentrifuge tubes and weigh them. On the rotor, distribute the tubes which have the same weight in pairs.

- Centrifuge at 140000xG and 4 ℃ for 60–90 minutes.

- Transfer the supernatant into a new tube and discard cellular debris.

- Perform protein quantitation by Bradford assay.

6.3.3 Protocol for Capturing and Eluting Biotinylated Proteins

1. Preparing the Mag Sepharose beads

1. Mix the beads medium slurry thoroughly by vortexing. Dispense 100 μL of the homogenous medium slurry into an Eppendorf tube.
2. Place the Eppendorf tube in the magnetic rack.
3. Remove the storage solution.

2. Equilibrating

1. Add 500 μL of binding buffer and re–suspend the beads in the medium.
2. Remove the liquid.

3. Applying the Sample

1. Add 300 μL of sample. If the sample volume is less than 300 μL, dilute to 300 μL with binding buffer.
2. Re–suspend the medium and incubate for 30 minutes with slow end–over–end mixing or by using a benchtop shaker.
3. Remove the sample.

4. Washing

Perform this step three times.

1. Add 500 μL of washing buffer and re–suspend the medium.
2. Remove the liquid.

5. Eluting Biotinylated Proteins

1. Add 100 μL of elution buffer.
2. Re–suspend the medium and incubate at 95 ℃ to 100 ℃ for five minutes.
3. Remove and collect the eluted fraction.

The eluted fraction can be loaded directly into gels for SDS–PAGE analysis.

6.3.4 General Procedures

Stock Buffer for Enzyme

The buffer used to store pure the AspRS stock over time is a solution of the following composition: 20 mM TRIS pH = 8, 50 mM NaCl and 10% gfflycerol.

Preparation of Membranes for Dialysis

Materials

- 500 mL of 2% $NaHCO_3$ and 1 mM EDTA solution
- 1 L H_2O (de–ionised)
- 2×500 mL 1 mM EDTA (1 Filter Sterilized)

The membranes are boiled under MW radiation for 10 min. in the $NaHCO_3$ solution. They are then washed with H_2O, boiled in 500 mL of 1 mM EDTA solution and kept refrigerated (−4 ℃) in the sterilized 1 mM EDTA solution.

Preparation of 5X Lysis Buffer

Materials

- TRIS/HCl pH=7.5 solution (Sigma–Aldrich, T–2663)
- 87% glycerol (Merck, Cat. No. 04091.2500)
- $MgCl_2$ 1 M solution (Sigma–Aldrich, M–1028)
- NaCl 5 M solution (Sigma–Aldrich, S–5150)
- Na_3VO_4 100 mM solution

The 5X lysis buffer is prepared by mixing 250 mL of TRIS/HCl 1 M stock solution, 288 mL of glycerol, 7.5 mL of $MgCl_2$ 1 M solution, 150 mL of NaCl

5 M solution and 50 mL of Na_3VO_4 100 mM solution. De–ionised water is added until reaching a 1 L volume of solution. After preparation the 5X lysis buffer is filtered through a 0.22 μm filter and stored in 40 mL aliquots at -80 ℃.

Preparation of 1X Lysis Buffer

The 1X lysis buffer is prepared in volumes of 100 mL by mixing 20 mL of 5X lysis buffer, 60 mL of de–ionised water, 5 mL of NaF 0.5 M solution and 4 mL NP40 20% solution. De–ionised water is added until reaching a final volume of 100 mL. Finally, 4 EDTA–free protease inhibitor cocktail (Roche 1–873–580) are added and the solution is stirred at -4 ℃ until the tablets are dissolved. Prior to use, 100 μL of DDT 1 M solution are added.

Bibliography

[1] Licker, M. D., Ed. *McGraw–Hill Dictionary of Bioscience*, 2nd ed.; McGraw–Hill Professional: New York, 2003.

[2] Berg, J. M., Tymoczko, J. L., Stryer, L., Eds. *Biochemistry*, 5th ed.; W. H. Freeman and Company: New York, 2002.

[3] Cox, M., Nelson, D. L., Eds. *Lehninger Principles of Biochemistry*, 4th ed.; W. H. Freeman and Company: New York, 2008.

[4] Laursen, B. S.; Sørensen, H. P.; Mortensen, K. K.; Sperling-Petersen, H. U. *Microbiol. Mol. Biol. Rev.* **2005**, *69*, 101–123.

[5] Fujiwara, S.; Lee, S.; Haruki, M.; Kanaya, S.; Takagi, M.; Imanaka, T. *FEBS Lett.* **1996**, *394*, 66–70.

[6] Rogers, M. J.; Weygand-Durašević, I.; Schwob, E.; Sherman, J. M.; Rogers, K. C.; Adachi, T.; Inokuchi, H.; Söll, D. *Biochimie* **1993**, *75*, 1083–1090.

[7] Landès, C.; Perona, J. J.; Brunie, S.; Rould, M. A.; Zelwer, C.; Steitz, T. A.; Risler, J. L. *Biochimie* **1995**, *77*, 194–203.

[8] Ribas de Pouplana, L.; Schimmel, P. *Cell* **2001**, *104*, 191–193.

[9] Cusack, S. *Curr. Opin. Struc. Biol.* **1997**, *7*, 881–889.

[10] Hurdle, J. G.; O'Neill, A. J.; Chopra, I. *Antimicrob. Agents Ch.* **2005**, *49*, 4821–4833.

[11] Ruff, M.; Krishnaswamy, S.; Boeglin, M.; Poterszman, A.; Mitschler, A.; Podjarny, A.; Rees, B.; Thierry, J. C.; Moras, D. *Science* **1991**, *252*, 1682–1689.

[12] Bonnefond, L.; Fender, A.; Rudinger-Thirion, J.; Giegé, R.; Florentz, C.; Sissler, M. *Biochemistry* **2005**, *44*, 4805–4816.

[13] Moras, D. *Trends Biochem. Sci.* **1992**, *17*, 159–164.

[14] Eriani, G.; Delarue, M.; Poch, O.; Gangloff, J.; Moras, D. *Nature* **1990**, *347*, 203–206.

[15] Cavarelli, J.; Eriani, G.; Rees, B.; Ruff, M.; Boeglin, M.; Mitschler, A.; Martin, F.; Gangloff, J.; Thierry, J. C.; Moras, D. *EMBO J.* **1994**, *13*, 327–337.

[16] Archontis, G.; Simonson, T.; Moras, D.; Karplus, M. *J. Mol. Biol.* **1998**, *275*, 823–846.

[17] Gurcha, S. S. et al. *PLoS ONE* **2014**, *9*, e113568.

[18] Ioerger, T. R.; O'Malley, T.; Liao, R.; Guinn, K. M.; Hickey, M. J.; Mohaideen, N.; Murphy, K. C.; Boshoff, H. I. M.; Mizrahi, V.; Rubin, E. J.; Sassetti, C. M.; Barry, I., Clifton E.; Sherman, D. R.; Parish, T.; Sacchettini, J. C. *PLoS ONE* **2013**, *8*, e75245.

[19] Agarwal, V.; Nair, S. K. *Med. Chem. Commun.* **2012**, *3*, 887–898.

[20] Saks, M. E.; Sampson, J. R.; Abelson, J. N. *Science* **1994**, *263*, 191–197.

[21] Imanaka, T.; Lee, S.; Takagi, M.; Fujiwara, S. *Gene* **1995**, *164*, 153–156.

[22] Messmer, M.; Blais, S. P.; Balg, C.; Chênevert, R.; Grenier, L.; Lagüe, P.; Sauter, C.; Sissler, M.; Giegé, R.; Lapointe, J.; Florentz, C. *Biochimie* **2009**, *91*, 596–603.

[23] Moras, D. *Biochimie* **1993**, *75*, 651–657.

[24] Pütz, J.; Giegé, R.; Florentz, C. *FEBS Lett.* **2010**, *584*, 350–358.

[25] Werner, R. G. *Antimicrob. Agents Ch.* **1980**, *18*, 858–862.

[26] Heacock, D.; Forsyth, C. J.; Shiba, K.; Musier-Forsyth, K. *Bioorg. Chem.* **1996**, *24*, 273–289.

[27] Kim, S.; Lee, S. W.; Choi, E. C.; Choi, S. Y. *Appl. Microbiol. Biotechnol.* **2003**, *61*, 278–288.

[28] Reader, J. S.; Ordoukhanian, P. T.; Kim, J.-G.; de Crécy-Lagard, V.; Hwang, I.; Farrand, S.; Schimmel, P. *Science* **2005**, *309*, 1533.

[29] Stefanska, A. L.; Fulston, M.; Houge-Frydrych, C. S.; Jones, J. J.; Warr, S. R. *J. Antibiot.* **2000**, *53*, 1346–1353.

[30] Metlitskaya, A.; Kazakov, T.; Kommer, A.; Pavlova, O.; Praetorius-Ibba, M.; Ibba, M.; Krasheninnikov, I.; Kolb, V.; Khmel, I.; Severinov, K. *J. Biol. Chem.* **2006**, *281*, 18033–18042.

[31] Gentry, D. R.; Ingraham, K. A.; Stanhope, M. J.; Rittenhouse, S.; Jarvest, R. L.; O'Hanlon, P. J.; Brown, J. R.; Holmes, D. J. *Antimicrob. Agents Ch.* **2003**, *47*, 1784–1789.

[32] Zumla, A.; Raviglione, M.; Hafner, R.; Fordham von Reyn, C. *New Engl. J. Med.* **2013**, *368*, 745–755.

[33] Caws, M. et al. *PLoS Pathog.* **2008**, *4*, e1000034.

[34] WHO Global Tuberculosis Report 2017.

[35] Abdool Karim, S. S.; Naidoo, K.; Grobler, A.; Padayatchi, N.; Baxter, C.; Gray, A. L.; Gengiah, T.; Gengiah, S.; Naidoo, A.; Jithoo, N.; Nair, G.; El-Sadr, W. M.; Friedland, G.; Abdool Karim, Q. *New Engl. J. Med.* **2011**, *365*, 1492–1501.

[36] Gandhi, N. R.; Nunn, P.; Dheda, K.; Schaaf, H. S.; Zignol, M.; van Soolingen, D.; Jensen, P.; Bayona, J. *Lancet* **2010**, *375*, 1830–1843.

[37] Lönnroth, K.; Castro, K. G.; Chakaya, J. M.; Chauhan, L. S.; Floyd, K.; Glaziou, P.; Raviglione, M. C. *Lancet* **2010**, *375*, 1814–1829.

[38] Jenkins, H. E.; Tolman, A. W.; Yuen, C. M.; Parr, J. B.; Keshavjee, S.; Perez-Valez, C. M.; Pagano, M.; Becerra, M. C.; Cohen, T. *Lancet* **2014**, *383*, 1572–1579.

[39] Olaru, I. D.; von Groote-Bidlingmaier, F.; Heyckendorf, J.; Yew, W. W.; Lange, C.; Chang, K. C. *Eur. Respir. J.* **2015**, *45*, 1119–1131.

[40] Maddry, J. A.; Ananthan, S.; Goldman, R. C.; Hobrath, J. V.; Kwong, C. D.; Maddox, C.; Rasmussen, L.; Reynolds, R. C.; Secrist III, J. A.; Sosa, M. I.; White, E. L.; Zhang, W. *Tuberculosis* **2009**, *89*, 354–363.

[41] King, G. M. *Appl. Environ. Microb.* **2003**, *69*, 7266–7272.

[42] Baell, J. B.; Holloway, G. A. *J. Med. Chem.* **2010**, *53*, 2719–2740.

[43] Pansare, D. N.; Shinde, D. B. *Tetrahedron Lett.* **2014**, *55*, 1107–1110.

[44] Bourahla, K.; Derdour, A.; Rahmouni, M.; Carreaux, F.; Bazureau, J. P. *Tetrahedron Lett.* **2007**, *48*, 5785–5789.

[45] Mendgen, T.; Steuer, C.; Klein, C. D. *J. Med. Chem.* **2012**, *55*, 743–753.

[46] Khodair, A. I. *J. Heterocyclic Chem.* **2002**, *39*, 1943–5193.

[47] Bignan, G.; Gaul, M.; Xu, G.; Zhao, B. P. Aminothiazolones as estrogen related receptor–alpha modulators. `http://www.google.com/patents/US20110200586`, U.S. Pat. Appl. 13/028,266, Aug. 18, 2011.

[48] Min, G.; Lee, S.-K.; Kim, H.-N.; Han, Y.-M.; Lee, R.-H.; Jeong, D. G.; Han, D. C.; Kwon, B.-M. *Bioorg. Med. Chem. Lett.* **2013**, *23*, 3769–3774.

[49] Ohishi, Y.; Mukai, T.; Nagahara, M.; Yajima, M.; Kajikawa, N.; Miyahara, K.; Takano, T. *Chem. Pharm. Bull.* **1990**, *38*, 1911–1919.

[50] Vogeli, U.; von Philipsborn, W.; Nagarajan, K.; Nair, M. D. *Helv. Chim. Acta* **1978**, *61*, 607–617.

[51] Momose, Y.; Meguro, K.; Ikeda, H.; Hatanaka, C.; Oi, S.; Sohda, T. *Chem. Pharm. Bull.* **1991**, *39*, 1440–1445.

[52] Granacher, C.; Gero, M.; Ofner, A.; Klopfenstein, A.; Schlatter, E. *Helv. Chim. Acta* **1923**, *6*, 458–467.

[53] Danilchanka, O.; Pires, D.; Anes, E.; Niederweis, M. *Antimicrob. Agents Ch.* **2015**, *59*, 2328–2336.

[54] Ishikawa, M.; Hashimoto, Y. *J. Med. Chem.* **2011**, *54*, 1539–1554.

[55] Sanghvi, T.; Jain, N.; Yang, G.; Yalkowsky, S. *QSAR & Comb. Sci.* **2003**, *22*, 258–262.

[56] Lovering, F.; Bikker, J.; Humblet, C. *J. Med. Chem.* **2009**, *52*, 6752–6756.

[57] Polepally, P. R.; Huben, K.; Vardy, E.; Setola, V.; Mosier, P. D.; Roth, B. L.; Zjawiony, J. K. *Eur. J. Med. Chem.* **2014**, *85*, 818–829.

[58] Bethge, L.; Jarikote, D. V.; Seitz, O. *Bioorg. Med. Chem.* **2008**, *16*, 114–125.

[59] Shuttleworth, S. J.; Folkes, A. J.; Wan, N. C.; Hancox, T. C.; Baker, S. J. 1–Cyclyl–3–substituted– –benzenes and –azines as inhibitors of phosphatidylinositol 3–kinase. U.K. Pat. Appl. 2 431 156, April 18, 2007.

[60] Zhao, N.; Sun, M.; Burns-Huang, K.; Jiang, X.; Ling, Y.; Darby, C.; Ehrt, S.; Liu, G.; Nathan, C. *PLoS ONE* **2015**, *10*, 1–16.

[61] Liu, Y.; Patricelli, M. P.; Cravatt, B. F. *P. Natl. Acad. Sci. USA* **1999**, *96*, 14694–14699.

[62] Thompson, D. A.; Ng, R.; Dawson, P. E. *J. Pept. Sci.* **2016**, *22*, 311–319.

[63] Drewes, G., Bantscheff, M., Eds. *Chemical Proteomics: Methods and Protocols*, 1st ed.; Humana Press: New York, 2012.

[64] Sorenson, A. E.; Askin, S. P.; Schaeffer, P. M. *Anal. Methods* **2015**, *7*, 2087–2092.

[65] Green, N. M. *Methods Enzymol.* **1990**, 51–67.

[66] Hyre, D. E.; Le Trong, I.; Merritt, E. A.; Eccleston, J. F.; Green, N. M.; Stenkamp, R. E.; Stayton, P. S. *Protein Sci.* **2009**, *15*, 459–467.

[67] Ju, W. et al. *Am. J. Pathol.* **2009**, *174*, 2073–2085.

[68] Jervis, P. J.; Polzella, P.; Wojno, J.; Jukes, J.-P.; Ghadbane, H.; Diaz, Y. R. G.; Besra, G. S.; Cerundolo, V.; Cox, L. R. *Bioconjugate Chem.* **2013**, *24*, 586–594.

[69] Kotzyba-Hibert, F.; Kapfer, I.; Goeldner, M. *Angew. Chem. Int. Ed.* **1995**, *34*, 1296–1312.

[70] Smith, E.; Collins, I. *Future Med. Chem.* **2015**, *7*, 159–183.

[71] Hashimoto, M.; Hatanaka, Y. *Eur. J. Org. Chem.* **2008**, *115*, 2513–2523.

[72] Zhang, L.; Zhang, Y.; Dong, J.; Liu, J.; Zhang, L.; Sun, S. *Bioorg. Med. Chem. Lett.* **2012**, *22*, 1036–1039.

[73] Kotake, Y.; Sagane, K.; Owa, T.; Mimori-Kiyosue, Y.; Shimizu, H.; Uesugi, M.; Ishihama, Y.; Iwata, M.; Mizui, Y. *Nat. Chem. Biol.* **2007**, *3*, 570–575.

[74] Jessen, K. A.; English, N. M.; Wang, J. Y.; Maliartchouk, S.; Archer, S. P.; Qiu, L.; Brand, R.; Kuemmerle, J.; Zhang, H.-Z.; Gehlsen, K.; Drewe, J.; Tseng, B.; Cai, S. X.; Kasibhatla, S. *Mol. Cancer Ther.* **2005**, *4*, 761–771.

[75] Delfino, J. M.; Schreiber, S. L.; Richards, F. M. *J. Am. Chem. Soc.* **1993**, *115*, 3458–3474.

[76] Masukawa, T.; Kato, H.; Kakiuchi, T.; Jayasundera, K. P.; Kinoshita, H.; Inomata, K. *Chem. Lett.* **1998**, *27*, 455–456.

[77] Ballell, L. et al. *ChemMedChem* **2013**, *8*, 1860–7187.

[78] Hennigan, S. L.; Driskell, J. D.; Ferguson-Noel, N.; Dluhy, R. A.; Zhao, Y.; Tripp, R. A.; Krause, D. C. *Appl. Environ. Microb.* **2012**, *78*, 1930–1935.

[79] De Zwart, M. A. H.; Van der Goot, H.; Timmerman, H. *J. Med. Chem.* **1989**, *32*, 487–493.

[80] Cho, W.-J.; Min, S. Y.; Le, T. N.; Kim, T. S. *Bioorg. Med. Chem. Lett.* **2003**, *13*, 4451–4454.

[81] Khadka, D. B.; Woo, H.; Yang, S. H.; Zhao, C.; Jin, Y.; Le, T. N.; Kwon, Y.; Cho, W.-J. *Eur. J. Med. Chem.* **2015**, *92*, 583–607.

[82] Yang, S. H.; Van, H. T. M.; Le, T. N.; Khadka, D. B.; Cho, S. H.; Lee, K.-T.; Lee, E.-S.; Lee, Y. B.; Ahn, C.-H.; Cho, W.-J. *Eur. J. Med. Chem.* **2010**, *45*, 5493–5497.

[83] Hodgson, P. B.; Salingue, F. H. *Tetrahedron Lett.* **2004**, *45*, 685–687.

[84] Lennox, A. J. J.; Lloyd-Jones, G. C. *Chem. Soc. Rev.* **2014**, *43*, 412–443.

[85] Knapp, D. M.; Gillis, E. P.; Burke, M. D. *J. Am. Chem. Soc.* **2009**, *131*, 6961–6963.

[86] Soto, R.; Perez-Herran, E.; Rodriguez, B.; Duma, B. M.; Cacho-Izquierdo, M.; Mendoza-Losana, A.; Lelievre, J.; Aguirre, D. B.; Ballell, L.; Cox, L. R.; Alderwick, L. J.; Besra, G. S. *Sci. Rep.* **2018**, *8*, 2045–2322.

[87] Matuszak, N.; Muccioli, G. G.; Labar, G.; Lambert, D. M. *J. Med. Chem.* **2009**, *52*, 7410–7420.

[88] Routasalo, T.; Helaja, J.; Kavakka, J.; Koskinen, A. M. P. *Eur. J. Org. Chem.* **2008**, *2008*, 3190–3199.

[89] Malkoch, M.; Schleicher, K.; Drockenmuller, E.; Hawker, C. J.; Russell, T. P.; Wu, P.; Fokin, V. V. *Macromolecules* **2005**, *38*, 3663–3678.

[90] Zhang, C.-J.; Li, L.; Chen, G. Y. J.; Xu, Q.-H.; Yao, S. Q. *Org. Lett.* **2011**, *13*, 4160–4163.

[91] Barbe, J.-M.; Canard, G.; Brandes, S.; Guilard, R. *Eur. J. Org. Chem.* **2005**, *21*, 4601–4611.

[92] Saitton, S.; Del Tredici, A. L.; Saxin, M.; Stenstrom, T.; Kihlberg, J.; Luthman, K. *Org. Biomol. Chem.* **2008**, *6*, 1647–1654.

[93] Zampieri, D.; Mamolo, M. G.; Laurini, E.; Zanette, C.; Florio, C.; Collina, S.; Rossi, D.; Azzolina, O.; Vio, L. *Eur. J. Med. Chem.* **2009**, *44*, 124–130.

[94] Loudet, A.; Han, J.; Barhoumi, R.; Pellois, J.-P.; Burghardt, R. C.; Burgess, K. *Org. Biomol. Chem.* **2008**, *6*, 4516–4522.

[95] Pelletier, J. C.; de Araujo Felix, L.; Green, D. M.; Hauze, D. B.; Lundquist, J. T.; Mann, C. W.; Mehlmann, J. F.; Rogers, J., John Francis; Vera, M. D.; Molinari, A. J. Preparation of naphthylpyrimidine, naphthylpyrazine and naphthylpyridazine analogs and their use as agonists of the Wnt–β–catenin cellular messaging system. WO Pat. Appl. 2009026326, Feb. 26, 2009.